Turkish Journal of Earth Sciences (Turkish J. Earth Sci.), Vol. 19, 2010, pp. 185–238. Copyright ©TÜBİTAK
doi:10.3906/yer-0901-6 First published online 14 August 2009

Statistical Evaluation of Bivariate, Ternary and Discriminant Function Tectonomagmatic Discrimination Diagrams

SURENDRA P. VERMA

Departamento de Sistemas Energéticos, Centro de Investigación en Energía,
Universidad Nacional Autónoma de México, Priv. Xochicalco s/no., Col. Centro, Temixco, Mor. 62580, Mexico
(E-mail: spv@cie.unam.mx)

Received 06 January 2009; revised typescript received 27 April 2009; accepted 30 April 2009

Abstract: This work applies a statistical methodology involving the calculation of success rates to evaluate a total of 28 tectonomagmatic discrimination diagrams: four bivariate (Ti/Y-Zr/Y; Zr-Zr/Y; Ti/1000-V; and Nb/Y-Ti/Y); six ternary (Zr-3Y-Ti/1000; MgO-Al_2O_3-FeO^t, Th-Ta-Hf/3; 10MnO-15P_2O_5-TiO_2; Zr/4-Y-2Nb; and La/10-Nb/8-Y/15); and three old ($Score_1$-$Score_2$; F_1-F_2; and F_2-F_3) and three sets of new discriminant function diagrams (each set consisting of five DF1-DF2 type diagrams proposed during 2004–2008). I established and used extensive geochemical databases of Miocene to Recent fresh rocks from island arcs, back arcs, continental rifts, ocean-islands, and mid-ocean ridges. Rock and magma types were inferred from a SINCLAS computer program. Although some of the existing bivariate and ternary diagrams did provide some useful information, none was found to be totally satisfactory, because success rates for pure individual tectonic settings typically varied from very low (1.1–41.6%) to only moderately high values (63.6–78.1%) and seldom exceeded them. Additionally, only 'combined' tectonic settings were discriminated, or numerous samples plotted in overlap regions designated for two or more tectonic settings or even in areas outside any field. Furthermore, these old diagrams are generally characterized by erroneous statistical basis of closure problems or constant sum constraints in compositional data and by subjective boundaries drawn by eye. All such diagrams, therefore, should be abandoned and replaced by the new sets of discriminant function diagrams proposed during 2004–2010. These diagrams, especially those of 2006–2010 based on the correct statistical methodology and the boundaries drawn from probabilities, showed very high success rates (mostly between 83.4% and 99.2%) for basic and ultrabasic rocks from four tectonic settings and should consequently be adopted as the best sets of tectonomagmatic discrimination diagrams at present available for this purpose. Three case studies from Turkey (Kula, Eastern Pontides, and Lycian-Tauride) were also provided to illustrate the use of two new sets of discriminant function diagrams (2006–2008). For the Kula area, both sets of major- and trace-element based diagrams provided results consistent with a rift setting. For the Pontides area, trace-element based diagrams suggested an arc setting to be more likely, according to both basic and intermediate rocks. For the Lycian ophiolites, however, only the major-element based set of diagrams could be applied, and because of alteration effects, the tectonic inference between an arc or a MORB setting could not be decisive. A newer set of immobile element based, highly successful diagrams currently under preparation (2010) should provide a complementary set to the existing diagrams (2006–2008) for a better application of this important geochemical tool. Further work on these lines is still necessary to propose discrimination diagrams for other types of magmas such as those of intermediate silica compositions.

Key Words: volcanic rocks, basalts, geochemistry, igneous rocks, mathematical geology

İki ve Üç Değişkenli Tektonomagmatik Ayırtman Diyagramlarının İstatistiksel Değerlendirmesi

Özet: Bu çalışmada, dört adet iki değişkenli (Ti/Y-Zr/Y; Zr-Zr/Y; Ti/1000-V; ve Nb/Y-Ti/Y), altı adet üç değişkenli (Zr-3Y-Ti/1000; MgO-Al_2O_3-FeO^t; Th-Ta-Hf/3; 10MnO-15P_2O_5-TiO_2; Zr/4-Y-2Nb; ve La/10-Nb/8-Y/15), üç adet eski ($Score_1$-$Score_2$; F_1-F_2; and F_2-F_3) ve her biri 2004–2008 arasında önerilmiş beş DF1-DF2 tipi diyagram içeren üç adet yeni olmak üzere toplam 28 tektonomagmatik ayırtman diyagramını değerlendirmek üzere doğruluk oranı hesaplarını

içeren istatistiksel bir yöntem uygulanmıştır. Bunun için, ada yaylarından, yay-ardı ortamlarından, kıtasal riftlerden, okyanus adalarından ve okyanus ortası sırtlarından alınan Miyosen–Güncel yaşlı altere olmamış volkanik kayalara ait jeokimyasal veri tabanı kullanılmıştır. Kaya ve magma tipleri SINCLAS bilgisayar programı yardımıyla elde edilmiştir. Mevcut iki ve üç bileşenli diyagramların bazıları kullanışlı bilgiler vermiş olmasına rağmen, diyagramlar tek bir tektonik ortam için doğruluk oranları çok düşük (%1.1–41.6) ve orta-yüksek değerler (%63.6–78.1) arasında veya bu değerleri nadiren geçtiği için tam anlamıyla yeterli değildir. Sonuçta yalnızca kombine tektonik ortamlar ayırtlanmış ve örneklerin birçoğu ya iki veya daha fazla tektonik ortam alanlarında aşmalar yapmış ya da herhangi bir alanın dışında kalmıştır. Ayrıca, hatalı istatistiksel kapanma problemleri veya bileşimsel verilerde sabit toplam sınırlamaları içeren bu eski diyagramların alan sınırları genelde sübjektif olarak gözle belirlenmiştir. Bu nedenle tüm bu ve benzer diyagramların yerine 2004–2010 yıllarında önerilmiş yeni ayırtman diyagramları kullanılmalıdır. Özellikle 2006–2010 yıllarında önerilenler olmak üzere bu diyagramlar doğru istatistiksel yöntemlere dayalıdır. Alan sınırları olasılıklara göre çizilmiştir ve dört farklı tektonik ortamdan bazik ve ultrabazik kayalar için çok yüksek doğruluk oranları (genelde %83.4 ve %99.2 arasında) gösterirler. Bu çalışmada ayrıca iki yeni ayırtman diyagramı setinin (2006–2008) kullanımını göstermek amacıyla Türkiye'den üç çalışma (Kula, Doğu Pontidler ve Likya-Torid) örneklendirilmiştir. Kula bölgesi için hem ana hem de iz element diyagramları rift ortamları ile uyumlu sonuçlar vermiştir. Pontidler için iz element diyagramları hem bazik hem de ortaç bileşimli kayalar için yay ortamını önermiştir. Likya ofiyolitleri için yalnızca ana element diyagramları uygulanabilir ve alterasyon etkileri nedeniyle yay ve MORB ortamları arasında tektonik seçim kesin değildir. Bu önemli jeokimyasal aracın daha iyi uygulanabilmesi amacıyla şu an hazırlanmakta olan (2009) ve hareketsiz (*immobile*) elementleri kullanıp daha başarılı sonuçlar veren yeni diyagramlar (2010), mevcut diyagramlara (2006–2008) tamamlayıcı bir set oluşturacaktır. Ortaç silisli gibi farklı tipteki magmaların ayırtlama diyagramları için bu yönde çalışmaların arttırılması şarttır.

Anahtar Sözcükler: volkanik kayalar, bazaltlar, jeokimya, magmatik kayalar, matematiksel jeoloji

Introduction

Discrimination diagrams have been in use now for nearly four decades since the advent of the plate tectonics theory. The main tectonic settings are: island arc, continental rift, ocean-island, and mid-ocean ridge. Pearce & Cann (1971, 1973) pioneered the idea that the magmas from different tectonic settings might be distinguishable in their chemistry. Interestingly, well before them, Chayes & Velde (1965) attempted to distinguish two basalt types (today recognised as island arc and ocean-island) from discriminant functions of major-elements that necessarily involved TiO_2 as one of the discriminating elements, although these authors did not propose any diagrams to use their findings.

Since the early seventies, a plethora of tectonomagmatic discrimination diagrams have been proposed (see for reviews, e.g., Wang & Golver III 1992; Rollinson 1993; Verma 1996, 1997, 2000, 2006, 2008; Vasconcelos-F. *et al.* 1998, 2001; Gorton & Schandl 2000; Agrawal *et al.* 2004, 2008; Verma *et al.* 2006). These diagrams were mostly meant for use with basic igneous rocks. A few diagrams for granitic or felsic rocks were also proposed (Pearce *et al.* 1984). The functioning of one such diagram –Rb versus Y+Nb– was evaluated by Förster *et al.* (1997); these authors concluded that for felsic rocks this discrimination diagram does not work well and should be used in combination with radiometric dating and geologic assessment. Discrimination diagrams are widely used for sedimentary rocks as well (e.g., Bhatia 1983; Roser & Korsch 1986), which were evaluated by Armstrong-Altrin & Verma (2005), using published data from Miocene to Recent sand and sandstone rocks from all around the world. These authors concluded that there exists a need for newer discriminant function diagrams because the existing ones did not work well.

For this work, I selected examples from three major categories of tectonomagmatic discrimination diagrams and performed their statistical evaluation. The first set included four simple bivariate diagrams (viz., element-element, element-element ratio, or ratio-ratio): (1) Ti/Y-Zr/Y of Pearce & Gale (1977); (2) Zr-Zr/Y of Pearce & Norry (1979); (3) Ti/1000-V of Shervais (1982); and (4) Nb/Y-Ti/Y of Pearce (1982). The second set consisted of ternary diagrams. These were: (5) Zr-3Y-Ti/1000 of Pearce & Cann (1973); (6) MgO-Al_2O_3-FeO^t of Pearce *et al.* (1977); (7) Th-Ta-Hf/3 of Wood (1980); (8) $10MnO$-$15P_2O_5$-TiO_2 of Mullen (1983); (9) Zr/4-Y-2Nb of

Meschede (1986); and (10) La/10-Nb/8-Y/15 of Cabanis & Lecolle (1989). The third and final set included several old and new discriminant function diagrams: (11) $Score_1$-$Score_2$ of Butler & Woronow (1986); (12) F_1-F_2 of Pearce (1976); (13) F_2-F_3 of Pearce (1976); (14) set of five discriminant function diagrams based on major-elements (Agrawal *et al.* 2004); (15) set of five discriminant function diagrams based on log-transformed ratios of major-elements (Verma *et al.* 2006); and (16) set of five discriminant function diagrams based on log-transformed ratios of five relatively immobile trace-elements (La, Sm, Yb, Nb and Th; Agrawal *et al.* 2008).

Given such a diversity of diagrams available for basic igneous rocks, it is instructive to evaluate their discriminating power, which could provide constraints on their use. Earlier evaluations of a total of 14 discrimination diagrams for igneous rocks were carried out by Wang & Golver III (1992), using geochemical data (some of them being average values of a larger dataset) for 196 samples of Jurassic basalts from eastern North America. These authors concluded that none of the evaluated diagrams worked well for discriminating the tectonic setting of their compiled rocks. However, this evaluation was rather limited or even probably biased, because samples from only one part of the world (eastern North America) were used, which is certainly not representative of the entire Earth. Furthermore, these samples were old (altered) rocks and their tectonic setting was assumed from plate tectonic reconstructions.

For the present paper, the following methodology was used to provide an unbiased evaluation: (a) establish representative databases for different tectonic settings from all around the world; (b) plot samples in the various diagrams to be evaluated and obtain statistical information from each diagram; and (c) report the implications of this evaluation in terms of the utility of the diagrams, whether or not they should be continued to be used. In addition to evaluating the newer (2004–2008) diagrams, I also compared the results with the statistical evaluation done by the original authors (Agrawal *et al.* 2004, 2008; Verma *et al.* 2006). Finally, to illustrate the application of discrimination diagrams I applied the newest diagrams (2006–2008) obtained from the correct statistical methodology of log-ratio transformation and linear discriminant analysis (LDA), to magmas from three areas of Turkey. Still newer highly successful, natural logarithm-ratio based, discriminant function discrimination diagrams (a set of five diagrams) currently (2009) under preparation by Verma & Agrawal, were also mentioned, which should complement the new (2006–2008) statistically correct diagrams.

Databases

Six extensive databases (B stands for basic magmas) were prepared: (i) island arc (IAB); (ii) island back arc; (iii) continental rift (CRB); (iv) ocean-island (OIB); (v) 'normal' mid-ocean ridge (MORB); and (vi) 'enriched' mid-ocean ridge (E-MORB).

Geochemical data were compiled for Miocene to Recent rocks from different tectonic settings from all over the world. For each database, samples from only those areas with a known, uncontroversial tectonic setting were compiled. Initially, databases for basic and ultrabasic rocks from island arcs, continental rifts, ocean-islands, and mid-ocean ridges were established by Verma (2000, 2002, 2006), Agrawal *et al.* (2004, 2008) and Verma *et al.* (2006). Later, I included data for all types of rocks available from the papers compiled in the above references as well as some other more recent ones. This updated version of these databases was used for the present work although only those rock types, for which the diagrams were initially proposed, were considered. Their brief description is presented below.

The compiled island arcs (and the literature sources) were: Aegean (Zellmer *et al.* 2000); Aleutian (Kay *et al.* 1982; Myers *et al.* 1985, 2002; Brophy 1986; Nye & Reid 1986; Romick *et al.* 1990; Singer *et al.* 1992a; Kay & Kay 1994); Barren Island (Alam *et al.* 2004; Luhr & Haldar 2006); Burma (Stephenson & Marshall 1984); Izu-Bonin (Tatsumi *et al.* 1992; Taylor & Nesbitt 1998); Japan (Sakuyama & Nesbitt 1986; Togashi *et al.* 1992; Tamura 1994; Kita *et al.* 2001; Sano *et al.* 2001; Kimura *et al.* 2002; Moriguti *et al.* 2004; Kimura & Yoshida 2006); Kamchatka (Kepezhinskas *et al.* 1997; Churikova *et al.* 2001); Kermadec (Gamble *et al.* 1993, 1995; Smith

et al. 2003; Wright *et al.* 2006); Kermadec-Havre (Haase *et al.* 2002); Kuril (Zhuravlev *et al.* 1987; Nakagawa *et al.* 2002); Lesser Antilles (Shimizu & Arculus 1975; Arculus 1976; Brown *et al.* 1977; Thirlwall & Graham 1984; Devine 1995; Smith *et al.* 1996; Thirlwall *et al.* 1997; Defant *et al.* 2001; Zellmer *et al.* 2003; Lindsay *et al.* 2005); Luzon (Defant *et al.* 1991; Castillo & Newhall 2004); Mariana (Hole *et al.* 1984; Woodhead 1988; Bloomer *et al.* 1989; Elliott *et al.* 1997; Wade *et al.* 2005); New Hebrides (Dupuy *et al.* 1982; Monzier *et al.* 1997); Papua New Guinea (Hegner & Smith 1992; Woodhead & Johnson 1993); Philippines (Defant *et al.* 1989; Knittel *et al.* 1997); Ryukyu (Shinjo *et al.* 2000); South Shetland (Smellie 1983); Sua (Turner & Foden 2001); Sunda-Banda (Whitford *et al.* 1979; Foden & Varne 1980; Wheller *et al.* 1987; Stolz *et al.* 1990; Hoogewerff *et al.* 1997); Taupo (Cole 1981; Gamble *et al.* 1993); Tonga-Kermadec (Bryan *et al.* 1972; Ewart & Bryan 1972; Ewart *et al.* 1977); Vanuatu (Barsdell 1988; Barsdell & Berry 1990; Peate *et al.* 1997; Raos & Crawford 2004); and Yap system (Ohara *et al.* 2002).

Back arc magmas from island arcs were separately compiled; these were from: Alaska Peninsula (Hildreth *et al.* 2004); Izu-Bonin (Tatsumi *et al.* 1992; Taylor & Nesbitt 1998; Ishizuka *et al.* 2006); Japan (Sakuyama & Nesbitt 1986; Ujike & Stix 2000; Moriguti *et al.* 2004; Shuto *et al.* 2004; Kimura & Yoshida 2006); Java (Edwards *et al.* 1994); Kamchatka (Dorendorf *et al.* 2000; Churikova *et al.* 2001; Ishikawa *et al.* 2001); Kermadec (Gamble *et al.* 1995); Kermadec-Havre (Haase *et al.* 2002); Kuril (Zhuravlev *et al.* 1987); Luzon (Defant *et al.* 1991); Mariana Trough (Gribble *et al.* 1998); Papua New Guinea (Woodhead & Johnson 1993); Philippines (Bau & Knittel 1993); Ryukyu-Okinawa Trough (Shinjo 1998, 1999; Shinjo *et al.* 2000); Sangihe (Tatsumi *et al.* 1991); Sunda-Banda (Wheller *et al.* 1987; Stolz *et al.* 1988; Van Bergen *et al.* 1992; Turner *et al.* 2003); and Taupo (Gamble *et al.* 1993).

The continental rifts compiled were: Abu Gabra (Davidson & Wilson 1989); Africa–North West (Bertrand 1991; Dautria & Girod 1991); Africa-West (Kampunzu & Mohr 1991); Antarctica (Panter *et al.* 2000); Basin and Range (Singer & Kudo 1986; Lum *et al.* 1989; Moyer & Esperança 1989; Perry *et al.* 1990; Fitton *et al.* 1991; Feuerbach *et al.* 1993); Central European Volcanic Province (Haase *et al.* 2004); China-East (Peng *et al.* 1986; Zhi *et al.* 1990; Basu *et al.* 1991; Fan & Hooper 1991; Liu *et al.* 1994); China-North (Han *et al.* 1999); China-North East (Liu *et al.* 1992; Zhang *et al.* 1995; Hsu *et al.* 2000; Zou *et al.* 2003); China-Leiqiong area (Ho *et al.* 2000); China-South East (Zou *et al.* 2000); Colorado Plateau Transition to Basin and Range (Smith *et al.* 1999); Columbia River Basalt (Maldonado *et al.* 2006); East Africa (Aoki *et al.* 1985; De Mulder *et al.* 1986; Auchapt *et al.* 1987; Kampunzu & Mohr 1991; Class *et al.* 1994; Paslick *et al.* 1995; Le Roex *et al.* 2001); Ethiopia (Hart *et al.* 1989; Deniel *et al.* 1994; Trua *et al.* 1999; Barrat *et al.* 2003; Peccerillo *et al.* 2003); Harney Basin (Streck & Grunder 1999; Streck 2002); Kenya (Bell & Peterson 1991; MacDonald *et al.* 1995, 2001; Kabeto *et al.* 2001; Furman *et al.* 2004); Massif Central (Chauvel & Jahn 1984; Pilet *et al.* 2005); Newer Volcanic Province, Australia (Price *et al.* 1997); Rio Grande (Johnson & Lipman 1988; Duncker *et al.* 1991; Gibson *et al.* 1992; McMillan *et al.* 2000; Maldonado *et al.* 2006); San Quintín Volcanic Field (Storey *et al.* 1989; Luhr *et al.* 1995); Saudi Arabia (Camp *et al.* 1991); Spain-South East (Benito *et al.* 1999); Taiwan-North West (Chung *et al.* 1995); Taiwan Strait (Chung *et al.* 1994); Turkey (Buket & Temel 1998; Aldanmaz *et al.* 2000; Alici *et al.* 2002); Uganda-South West (Llyod *et al.* 1991); U.S.A.-West (Leat *et al.* 1989; Kempton *et al.* 1991); and West Antarctica (Hart *et al.* 1995).

Ocean-islands away from mid-ocean ridges were compiled separately as OIB magmas from the following localities: Atlantic (Blum *et al.* 1996; Praegel & Holm 2006); Austral Chain, South Pacific Ocean (Hémond *et al.* 1994); oceanic part of the Camaroon Line (Deruelle *et al.* 1991; Lee *et al.* 1994); Cape Verde Islands (Jørgensen & Holm 2002; Doucelance *et al.* 2003; Holm *et al.* 2006); Cook-Austral Islands (Palacz & Saunders 1986); French Polynesia (Liotard *et al.* 1986; Dupuy *et al.* 1988; Dupuy *et al.* 1989; Cheng *et al.* 1993; Lassiter *et al.* 2003); Grande Comore Island (Class *et al.* 1998; Class & Goldstein 1997; Claude-Ivanaj *et al.* 1998); Hawaiian Islands (Chen *et al.* 1990; Lipman *et al.* 1990; Chen *et al.* 1991; Garcia *et al.* 1992; Maaløe *et al.* 1992; West *et al.* 1992; Frey *et al.* 1994; Bergmanis

et al. 2000; Ren *et al.* 2004); Heard Islands (Barling *et al.* 1994); Kerguelen Archipelago (Storey *et al.* 1988; Weis *et al.* 1993; Borisova *et al.* 2002); Madeira Archipelago (Geldmacher & Hoernle 2000; Schwarz *et al.* 2005); South Pacific (Hauri & Hart 1997; Hekinian *et al.* 2003); Ponape Island (Dixon *et al.* 1984); Reunion Islands (Fretzdorf & Haase 2002); Samoa Seamount (Hart *et al.* 2004); Society Chain (Binard *et al.* 1993; Hémond *et al.* 1994); and Socorro Islands (Bohrson & Reid 1995).

MORB data were compiled from the following ridges: America-Antarctica (Le Roex & Dick 1981); Chile (Bach *et al.* 1996); East Pacific Rise (Lonsdale *et al.* 1992; Bach *et al.* 1994; Hekinian *et al.* 1996; Sims *et al.* 2003); Galapagos Spreading Centre (Schilling *et al.* 1982; Verma & Schilling 1982); Genovesa (Harpp *et al.* 2003); Indian (Price *et al.* 1986; Dosso *et al.* 1988; Mahoney *et al.* 1992; Ray *et al.* 2007); Mendocino (Kela *et al.* 2007); Mid-Atlantic (Bryan *et al.* 1981; Schilling *et al.* 1983; Le Roex *et al.* 1987; Bougault *et al.* 1988; Dosso *et al.* 1993; Haase *et al.* 1996; Le Roux *et al.* 2002a, 2002b); North Fiji Basin (Monzier *et al.* 1997); Red Sea (Barrat *et al.* 2003); and Western Pacific (Park *et al.* 2006).

Finally, enriched types of MORB (E-MORB) from locations at and near the ridges were separately compiled. These were from: Amsterdam Island (Doucet *et al.* 2004); Bouvet Island (Verwoerd *et al.* 1976; Le Roex & Erlank 1982); Galápagos Islands (Geist *et al.* 1986; White *et al.* 1993); Iceland (Slater *et al.* 1998); North Fiji Basin (Monzier *et al.* 1997); and St. Paul Island (Doucet *et al.* 2004).

The magma types were determined from the SINCLAS computer program (Verma *et al.* 2002), which also provided standard igneous norms and rock names strictly according to the IUGS recommendations. It may be mentioned, in this context, that many workers do not correctly follow the IUGS recommendations for volcanic rock classification (Le Bas *et al.* 1986; Le Bas 2000), for which plotting the analytical data in a TAS diagram *without* proper Fe oxidation recalculations and anhydrous basis, is *not* the recommended procedure unless Fe-oxidation varieties are individually determined for all samples using classical analytical procedures. Modern analytical instruments are not generally capable of distinguishing between different Fe-oxidation states, and therefore it is not a common practice to analyse them separately. In this context, in spite of the IUGS recommendations to use the measured Fe-oxidation varieties as determined, Middlemost (1989) had suggested that they should not be used because they are highly susceptible to changes related to weathering after magma emplacement. On the other hand, because we are dealing with compositional data, both individual concentrations and sums strongly depend on the procedure of Fe-ratio (Fe_2O_3 and FeO) adjustment (e.g., Le Maitre 1976; Middlemost 1989), which would affect rock and magma types inferred from the TAS diagram. Furthermore, some rock names actually depend on the CIPW norm values, for which 'standardised' calculations are required (Verma *et al.* 2003). I therefore strongly recommend the use of a computer program, such as SINCLAS, for these purposes. SINCLAS (Verma *et al.* 2002) is freely available by request from any of the authors.

For evaluation of the MgO-Al_2O_3-FeO^t diagram of Pearce *et al.* (1977), more differentiated intermediate magmas, as inferred from SINCLAS, were also used following the recommendations of the original authors. Database compilation for the companion paper by Verma *et al.* (2010) required all kinds of magmas ranging from ultrabasic to acid types to be separated and used for evaluation. The additional literature references –besides those above– for constructing the complete databases that included all types of magmas, were as follows: Barberi *et al.* (1975); Singer *et al.* (1992b); Tamura *et al.* (2003); Izbekov *et al.* (2004); Schmitz & Smith (2004); de Moor *et al.* (2005); Nakada *et al.* (2005); Pallister *et al.* (2005); Ayalew *et al.* (2006); Hirotani & Ban (2006); and Shukuno *et al.* (2006).

I finally stress that the present compilation includes rocks from only 'pure' uncontroversial tectonic settings, and therefore, for correct discrimination, the application of discrimination diagrams should result in unique tectonic settings. Therefore, if a diagram designated an overlap region of two different tectonic settings, a significant number of samples should not plot there if that particular diagram is to be determined as an efficient one for rock discrimination.

Results

All six databases (island arc, island back arc, continental rift, ocean-island, normal mid-ocean ridge, and enriched mid-ocean ridge) were used to statistically evaluate four bivariate, six ternary, and three old and three sets (each consisting of five diagrams) of new discriminant function discrimination diagrams (a total of 28 diagrams). For some of these diagrams, Rickwood (1989) reported boundary line coordinates, which have been useful in reproducing the corresponding boundaries in them.

The efficiency of a plot for a given tectonic setting, also called 'success rate', is the ratio of the correctly discriminated samples to the total number of samples, expressed as the percentage of this ratio. The incorrect discrimination or mis-discrimination is the complement of the above efficiency. Thus, efficiencies were calculated for all fields in a given diagram, including those designated for overlap regions and for other areas outside any given field when this was so. The results are reported in three subheadings – I. *bivariate*, II. *ternary* and III. *discriminant function* – as follows.

Four Bivariate Diagrams

All bivariate diagrams evaluated in this paper are based on the so-called immobile or high field strength elements Ti, Zr, Nb, Y, and V (Rollinson 1993), which seems to be an advantage for application to altered samples, especially those from older terrains. Nevertheless, the problems common to all diagrams in this category are incorrect statistical handling of compositional data (Aitchison 1982, 1986; Verma *et al.* 2006; Agrawal & Verma 2007) and use of boundaries subjectively drawn by eye (Agrawal 1999). The lack of a representative sample database may be another inherent problem in the proposals of at least some of the diagrams evaluated in this work (see Verma *et al.* 2006; Agrawal *et al.* 2008). The conclusion of this statistical evaluation is that all such simple bivariate diagrams should be abandoned in favour of more complex discriminant function bivariate diagrams.

(1) Ti/Y-Zr/Y of Pearce & Gale (1977)

This element ratio-element ratio diagram has been widely used and is still in use, as demonstrated by recent references during 2007–2008; a few of them are: Birkenmajer *et al.* (2007); Shahabpour (2007); and Cassinis *et al.* (2008).

The results of this evaluation are plotted in Figure 1 and summarised in Table 1. This diagram discriminates only two grouped-tectonic settings, i.e., the combined groups of plate-margin (supposed to include arc and mid-ocean ridge settings) and within-plate (includes rift and ocean-island settings).

Numerous data plotted far beyond the dividing line proposed by these authors (Figure 1); they were discriminated by assuming a linear extension of this line. For island arc and mid-ocean ridge samples assumed to pertain to plate margin basalt (PMB) compiled in this work, the plot showed a very high efficiency of about 95.5% for main arcs, 90.3% for back arcs and 94.7% for MORB, but lower for E-MORB (58.3%). Note E-MORB compiled in this work (e.g., Iceland, Galápagos, etc.) largely come from plate margins, and therefore, should theoretically plot in the PMB field. For the combined group of within-plate basalt (WPB) samples, the efficiency of correct discrimination was also high (89.1%) for continental rifts and even increased to 98.0% for ocean-island setting. Thus, the incorrect discrimination was very low (2.0% to 10.9%).

The main limitation of this discrimination diagram is that it actually distinguishes only two tectonic settings (plate margin and within-plate), instead of at least the four settings required for a modern view of plate tectonics. Thus, the arc and mid-ocean ridge settings cannot be distinguished from one another, nor can continental rift and ocean-island settings be distinguished from each other. Furthermore, the boundary or dividing line, drawn subjectively by eye, is too short and does not provide good constraints on the discrimination of a large number of samples that have greater Zr/Y values than the dividing line (Figure 1).

Although characterised by high success rates, the restricted power of discriminating only two combined tectonic settings renders this diagram less

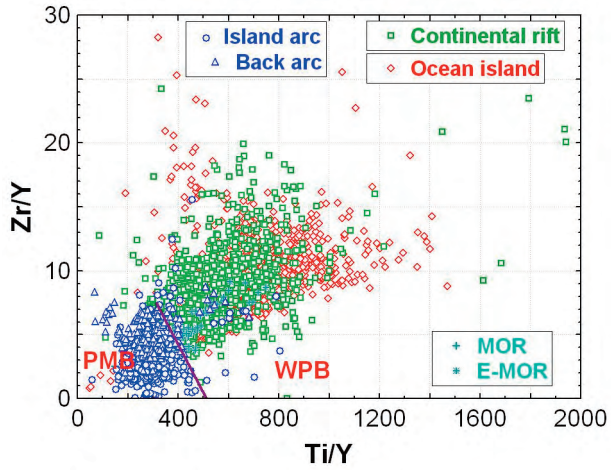

Figure 1. Statistical evaluation of the Ti/Y-Zr/Y (Pearce & Gale 1977) bivariate diagram for plate margin basalt (PMB) and within-plate basalt (WPB), using basic and ultrabasic rocks from different tectonic settings. PMB is assumed to include both arc and mid-ocean ridge (MOR) settings, whereas WPB would include both continental rift and ocean-island settings. The solid line is the boundary proposed by the original authors. The symbols used are explained as inset (E-MOR– enriched mid-ocean ridge). The same symbols are maintained throughout Figures 2–16. Statistical results are summarised in Table 1.

useful than the newer (discriminant function) diagrams discussed later in this paper.

(2) Zr-Zr/Y of Pearce & Norry (1979)

The recent papers by Srivastava & Rao (2007), Bağcı *et al.* (2008), Cassinis *et al.* (2008), Çelik & Chiaradia (2008) and Jarrar *et al.* (2008) are among the recent references of this extensively cited work of Pearce & Norry (1979). The diagram is of element-element ratio type.

The diagram has a logarithmic scale for both axes (Figure 2). The fields are totally enclosed in parallelograms or rhombuses. Consequently, samples can also plot outside any of the fields. Island arc samples were poorly discriminated, with a very low success rate of only about 39.2% plotting in the sole field of IAB, whereas back arc magmas showed an even worse efficiency (3.1%; region A in Figure 2; Table 2). A small but significant proportion of magmas (21.6% and 8.9%, respectively) plot in the overlap region of IAB+MORB. Similarly, mid-ocean ridge magmas (both MORB and E-MORB) were also very poorly discriminated (Table 2; only 26.3% and 5.5% respectively plot in the pure MORB field B in Figure 2, with 56.2% and 16.7% in the overlap region D of IAB+MORB and 3.4% and 4.2% in the overlap region E of WPB+MORB). These low success rates imply inapplicability of this diagram for IAB and MORB, because overlap regions are of no great value in such discriminations unless one is considering transitional setting or sources. As stated in the 'Databases' section, the data used in this evaluation were compiled for pure, uncontroversial tectonic settings, and therefore, overlap regions should actually be considered as mis-discriminations. The rift and ocean-island magmas, on the other hand, showed a greater efficiency; about 65.7%, and 65.6% of them plotted in the WPB field (see region C in Figure 2; Table 2).

Table 1. Statistical evaluation information of Ti/Y-Zr/Y (Pearce & Gale 1977) bivariate diagram for plate margin basalt (PMB) and within plate basalt (WPB).

Tectonic setting	Total samples	Number of discriminated samples (%)	
		PMB	WPB
Island arc	577 (100)	**551 (95.5)** *	26 (4.5)
Island back arc	259 (100)	**234 (90.3)**	25 (6.7)
Continental rift	1040 (100)	105 (10.1)	**935 (89.1)**
Ocean-island	1198 (100)	24 (2.0)	**1198 (98.0)**
MORB	696 (100)	**659 (94.7)**	37 (5.3)
E-MORB	72 (100)	**42 (58.3)**	30 (41.7)

* Correct discrimination is indicated in **bold** when the inferred setting was similar to the expected one, or the indicated setting pertained to an overlap region (for ** ***italic bold***, see **Table 2**).

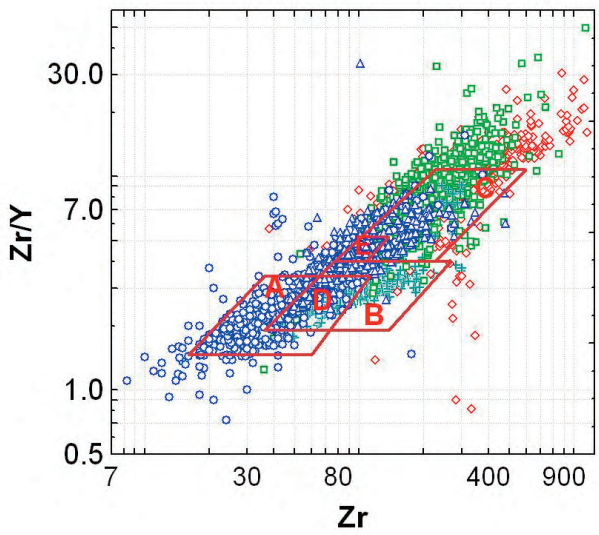

Figure 2. Statistical evaluation of the Zr-Zr/Y bivariate diagram (base 10 log-log scales; Pearce & Norry 1979) for island arc basalt (IAB; field A), within-plate basalt (WPB; field C), mid-ocean ridge basalt (MORB; field B), overlap regions of IAB and MORB (IAB+MORB; field D), and WPB and MORB (WPB+MORB; field E), using basic and ultrabasic rocks from different tectonic settings. For symbols see Figure 1. Statistical results are summarised in Table 2.

Numerous samples plotted outside all the 'closed' fields (Figure 2; 1.9% to 32.3% in Table 2), and this is a major defect of this diagram. The low success rates, combined with this problem, indicate that this diagram can only be used for within-plate magmas.

Pearce (1983) separated the fields of continental and oceanic-arc basalts on the basis of Zr/Y value of 3 with some overlap around this value; samples plotting above this value were identified as continental arc, whereas below it as oceanic (or island) arc. Nevertheless, for samples from an unknown tectonic setting, confusion would prevail if the samples with Zr/Y > 3 are truly continental arc samples, or are from MORB or within-plate settings.

In the light of the very low success rates (3.1% to 65.7%), the use of this diagram is not recommended.

(3) Ti/1000-V of Shervais (1982)

This diagram has also been extensively used and remains in use (e.g., Wiszniewska *et al.* 2007; Bruni *et al.* 2008; Dampare *et al.* 2008), even though Verma (2000) documented that the equi-Ti/V boundaries proposed by Shervais (1982) did not work well.

Table 2. Statistical evaluation information of Zr-Zr/Y bivariate diagram (base 10 log-log scales; Pearce & Norry 1979) for island arc basalt (IAB), mid-ocean ridge basalt (MORB), within plate basalt (WPB), overlap regions of IAB and MORB (IAB+MORB) and of WPB and MORB (WPB+MORB).

Tectonic setting	Total samples	Number of discriminated samples (%)					
		IAB	WPB	MORB	Overlap		Other (outside any field)
					(IAB+MORB)	(WPB+MORB)	
Island arc	561 (100)	***220 (39.2)*** **	31 (5.5)	34 (6.1)	**121 (21.6)** *	25 (4.4)	130 (23.2)
Island back arc	259 (100)	***8 (3.1)***	83 (32.0)	39 (15.1)	**23 (8.9)**	40 (15.4)	66 (25.5)
Continental rift	1040 (100)	6 (0.6)	***683 (65.7)***	19 (1.8)	14 (1.3)	**33 (3.2)**	285 (27.4)
Ocean-island	1198 (100)	0 (0.0)	***786 (65.6)***	2 (0.2)	0 (0.0)	**23 (1.9)**	387 (32.3)
MORB	696 (100)	10 (1.4)	75 (10.8)	***183 (26.3)***	**391 (56.2)**	**24 (3.4)**	13 (1.9)
E-MORB	72 (100)	27 (37.5)	23 (31.9)	***4 (5.5)***	**12 (16.7)**	**3 (4.2)**	3 (4.2)

* Correct discrimination is indicated in **bold** when the inferred setting was similar to the expected one, or the indicated setting pertained to an overlap region.

** Correct discrimination is indicated in ***italic bold*** when the inferred setting was the same as the expected one and no overlap region was indicated.

The boundaries of equi-values of Ti/1000V for 10 to 100 are shown in Figure 3. They have been drawn only up to the scale values presented by the original author. Only 63.6% of island arc magmas were correctly discriminated as IAB (Table 3). The back arc magmas mostly plotted in the MORB field (63.0%), with only 35.0% in the correct IAB field, which is a drawback of this diagram. This point is important because, in spite of the complex multi-component sources in practically all tectonic settings, the main purpose of discrimination diagrams is to attain a high success rate for a given tectonic setting, as will be seen later in newer (2004–2008) discrimination diagrams (see the section of '*old and new sets of discriminant function diagrams*').

The success rates for continental rift and ocean island were considerably greater than those for arcs (73.1% and 82.7%, respectively, as OIB; Table 3). The discrimination of MORB was excellent (92.5% plot in the MORB field; Table 3), although E-MORB were poorly discriminated (50.7%) as MORB. Few samples plot outside the acceptable range of Ti/1000V= 10–100 (0.0% to 7.7%; Table 3).

Continental rift setting was not included in the original diagram; it was implicitly assumed to belong to the ocean-island setting in the present evaluation. The diagram seems to work relatively well for IAB, OIB and MORB (63.6–92.5%), but not for back arc and E-MORB. The proposed equi-value boundaries were drawn by eye. Incorrect statistical handling of compositional data implied in this element-element diagram is another defect (Agrawal & Verma 2007)

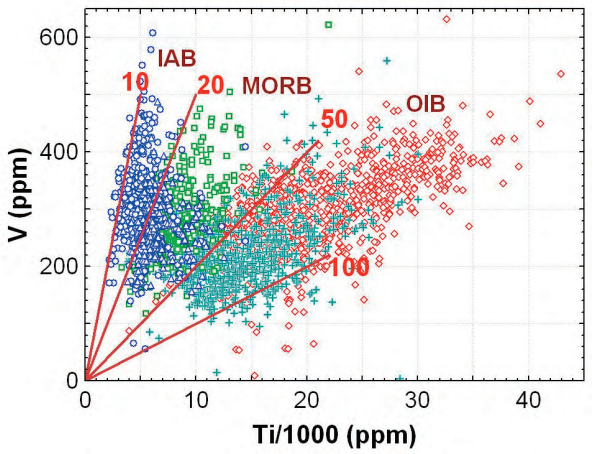

Figure 3. Statistical evaluation of the Ti/1000-V bivariate diagram (Shervais 1982) for island arc basalt (IAB; Ti/1000V equi-values of 10–20), ocean-island basalt (OIB; Ti/1000V equi-values 50-100), and mid-ocean ridge basalt (MORB; Ti/1000V equi-values are 20–50), using basic and ultrabasic rocks from different tectonic settings. For symbols see Figure 1. Statistical results are summarised in Table 3.

that should be corrected in any new proposal based on these and other immobile elements (Verma and Agrawal, in preparation). Besides, significantly better results (much greater success rates) were obtained from the newer (2004–2008) diagrams (see the section of 'discriminant function discrimination diagrams' below), and therefore this Ti-V diagram can be replaced by these newer trace-element based discriminant function diagrams.

In view of the above considerations, my conclusion is that this diagram can also be abondoned.

Table 3. Statistical evaluation information of Ti/1000-V bivariate diagram (Shervais 1982) for island arc basalt (IAB), mid-ocean ridge basalt (MORB), and ocean-island basalt (OIB).

Tectonic setting	Total samples	Number of discriminated samples (%)			
		IAB	OIB	MORB	Other (outside any field)
Island arc	450 (100)	***286 (63.6)***	3 (0.7)	142 (31.5)	19 (4.2)
Island back arc	203 (100)	**71 (35.0)**	4 (2.0)	128 (63.0)	0 (0.0)
Continental rift	769 (100)	1 (0.1)	**562 (73.1)**	155 (20.2)	51 (6.6)
Ocean-island	1015 (100)	0 (0.0)	***839 (82.7)***	98 (9.6)	78 (7.7)
MORB	532 (100)	30 (5.6)	10 (1.9)	***492 (92.5)***	0 (0.0)
E-MORB	69 (100)	15 (21.8)	19 (27.5)	**35 (50.7)**	0 (0.0)

(4) Nb/Y-Ti/Y of Pearce (1982)

This ratio-ratio diagram (Pearce 1982) also remains widely used today (e.g., Greiling *et al.* 2007; Barboza-Gudiño *et al.* 2008; Boztuğ 2008; Çelik 2008; Femenias *et al.* 2008; Xu *et al.* 2008).

The diagram uses base 10 log-log scales and the X–Y variables are characterised by a common divisor (Y). The eye-drawn fields are enclosed in closed boundaries (Figure 4). The region of solely arc field (A in Figure 4) and mid-ocean ridge (M in Figure 4) is limited; the overlap region of these two settings (A+M) is considerably larger. Continental rift and ocean-island settings are defined as a single field (W in Figure 4).

The success rates for both island arc and back arc magmas were extremely low (1.1% and 3.2%, respectively) for pure field A (Figure 4; Table 4). Similarly, very low success rates were obtained for both MORB and E-MORB (8.6% and 8.0%, respectively). Therefore, the diagram seems to be practically useless for these (arc and MORB) settings (Table 4). These (MORB and E-MORB) magmas mostly (85.9% to 46.0%, respectively) plotted in the overlap region of IAB+MORB. For continental rift and ocean-island settings as within-plate, its functioning was acceptable (success rates of 71.4% and 87.4%, respectively; Table 4). However, a serious problem recognised for arc and within-plate settings is that a large proportion of samples (11.5% to 27.7%) plot outside of any of the recognised fields (Table 4; Figure 4).

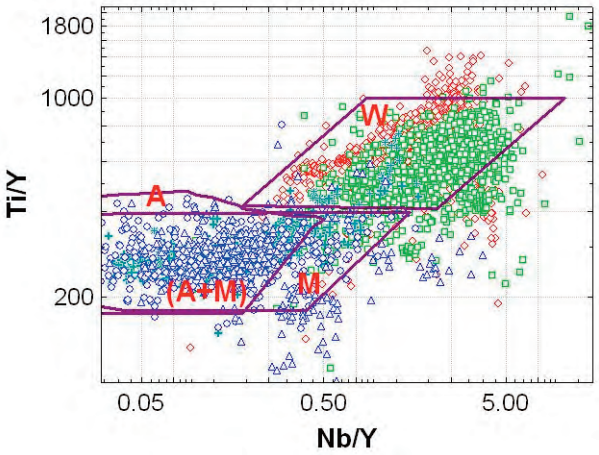

Figure 4. Statistical evaluation of the Nb/Y-Ti/Y bivariate diagram (Pearce 1982) for island arc basalt (IAB), within plate basalt (WPB), and mid-ocean ridge basalt (MORB), using basic and ultrabasic rocks from different tectonic settings. A– arc; M– MORB; A+M– overlap region of arc and MORB; and W– within-plate. For symbols see Figure 1. Statistical results are summarised in Table 4.

This diagram is not recommended to be used for arc and MORB settings, although it can effectively discriminate within-plate magmas from them. Continental rift and ocean-island cannot be discriminated. The overall conclusion is that this diagram should be abondoned.

Six Ternary Diagrams

As for bivariate diagrams, most (four out of six) ternary diagrams evaluated in this paper are based

Table 4. Statistical evaluation information of Nb/Y-Ti/Y bivariate diagram (Pearce 1982) for island arc basalt (IAB), within plate basalt (WPB), and mid-ocean ridge basalt (MORB).

Tectonic setting	Total samples	Number of discriminated samples (%)				
		IAB	WPB	MORB	Overlap (IAB+MORB)	Other (outside any field)
Island arc	438 (100)	***5 (1.1)***	0 (0.0)	52 (11.9)	**312 (71.2)**	69 (15.8)
Island back arc	249 (100)	***8 (3.2)***	13 (5.2)	21 (8.5)	**138 (55.4)**	69 (27.7)
Continental rift	974 (100)	0 (0.0)	**696 (71.4)**	70 (7.2)	24 (2.5)	184 (18.9)
Ocean-island	1197 (100)	0 (0.0)	**1046 (87.4)**	11 (0.9)	2 (0.2)	138 (11.5)
MORB	617 (100)	2 (0.3)	19 (3.1)	***53 (8.6)***	**530 (85.9)**	13 (2.1)
E-MORB	63 (100)	0 (0.0)	42 (46.0)	***5 (8.0)***	**29 (46.0)**	0 (0.0)

on the so-called immobile elements Ti, P, Zr, Hf, Nb, Y, and V (Rollinson 1993), which seems to be an advantage for application to altered samples especially from older terrains. Two diagrams are based on major elements. The major problems common to all diagrams in this category are incorrect statistical handling of compositional data (Aitchison 1982, 1986; Agrawal & Verma 2007) and use of boundaries subjectively drawn by eye (Agrawal 1999). The reconstruction of ternary variables from any kind of experimentally measured variables imposes a further constant-sum constraint on these diagrams. Note that these ternary diagrams can be easily replaced by natural log-ratio bivariate diagrams (Verma & Agrawal, in preparation) and, if necessary, new bivariate diagrams based on only three variables can be proposed.

(5) Zr-3Y-Ti/1000 Ternary Diagram of Pearce & Cann (1973)

This ternary diagram (Pearce & Cann 1973) has been very popular with thousands of references in the published literature; recent ones include: Ghosh *et al.* (2007); Shekhawat *et al.* (2007); Çelik & Chiaradia (2008); and Kumar & Rathna (2008).

This diagram includes fields for island arc tholeiites (IAT; field A in Figure 5), calc-alkaline basalts (CAB; field C), and within-plate basalts (WPB; field D). An overlap region (field B) of IAT and CAB with MORB or ocean floor basalt (OFB) was also proposed. Because MORB setting was not discriminated without overlap (i.e., it was proposed to overlap with the arc setting), MORB samples were not used in this evaluation. The fields are enclosed in distinct areas (Figure 5). An error in the ternary coordinates of field boundaries summarised by Rollinson (1993) was also corrected.

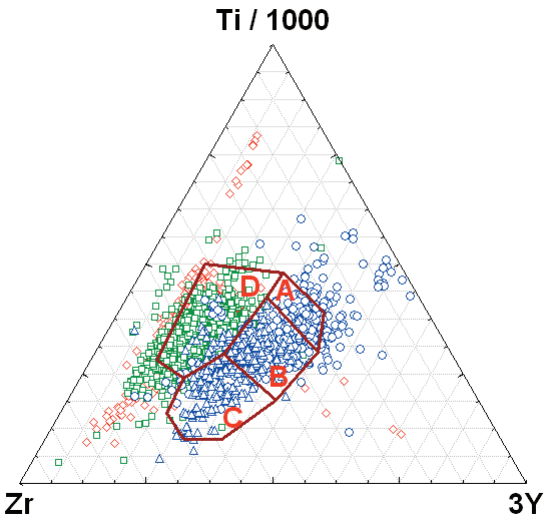

Figure 5. Statistical evaluation of the Zr-3Y-Ti/1000 ternary diagram (Pearce & Cann 1973) for island arc tholeiites (IAT; field A), calc-alkaline basalts (CAB; field C), and within-plate basalts (WPB; field D), using basic and ultrabasic rocks from different tectonic settings. Field B is overlap region of IAT, CAB, and MORB. For symbols see Figure 1. Statistical results are summarised in Table 5.

The statistical results are presented in Table 5. The nomenclature of IAT and CAB used by Pearce &

Table 5. Statistical evaluation information of Zr-3Y-Ti/1000 ternary diagram (Pearce & Cann 1973) for island arc tholeiites (IAT), calc-alkaline basalts (CAB), and within plate basalts (WPB).

Tectonic setting	Total samples	Number of discriminated samples (%)				
		IAT	CAB	WPB	Overlap (IAT+CAB+ OFB)*	Other (outside any field)
Island arc	579 (100)	***129 (22.3)***	***66 (11.4)***	16 (2.8)	**264 (45.6)**	104 (18.0)
Island back arc	259 (100)	***1 (0.4)***	***113 (43.6)***	24 (9.3)	**115 (44.4)**	6 (2.3)
Continental rift	1039 (100)	6 (0.6)	54 (5.2)	**746 (71.8)**	49 (4.7)	184 (17.7)
Ocean-island	1198 (100)	0 (0)	13 (1.1)	**1000 (83.5)**	7 (0.6)	178 (14.8)

* OFB–ocean floor basalt.

Cann (1973) is no longer recommended by the IUGS for the classification of volcanic rocks (see Le Bas *et al.* 1986; Le Bas 2000; Le Maitre *et al.* 2002). Any genetic meaning of the 'calc-alkaline' term has been also questioned (Sheth *et al.* 2002). In spite of these objections, in order to evaluate this diagram we must assume that IAT and CAB, including their overlap region, represent island arc magmas (main arcs as well as back arcs), and WPB includes the CRB and OIB settings. If so, this diagram (Figure 5) may discriminate only two sets of tectonic settings: IAB on one hand (correct discrimination being represented by IAT, CAB and the overlap region) and combined CRB and OIB on the other (WPB region).

With this assumption, only 22.3% and 11.4% of island arc magmas plot in the IAT and CAB fields, respectively, with the bulk of samples (45.6%) falling in the overlap region with MORB (Table 5). Thus, the total success rate of about 33.7% was unacceptably low for arc magmas. Only about 2.8% and 18.0% of the samples plot incorrectly as within-plate or outside of any of these fields, respectively. Back arc magmas were mostly discriminated in the CAB (43.6%) and overlap region (44.4%), with only 11.6% mis-discriminated samples. 71.8% of the CRB and 83.5% of the OIB samples plot in the WPB field, whereas most of the remaining mis-discriminated samples (17.7% and 14.8%, respectively) plot outside any of the specified fields.

Although from the above assumption a fairly good discrimination results for within-plate magmas, the limitation of this ternary diagram is that it discriminates only two groups of tectonic settings (IAB –with IAB+MORB– and CRB+OIB), with no provision for either discriminating MORB, or for the separate identification of CRB and OIB. Holm (1982) noted that continental tholeiites were poorly recognised as IAT on this diagram (Figure 5).

The use of this diagram is not recommended: it should be abandoned in favour of the newer (2004–2008, 2010) diagrams.

(6) MgO-Al_2O_3-FeO^t of Pearce et al. (1977)

This diagram has been used and remains in use (e.g., Yang *et al.* 2007; Appelquist *et al.* 2008; Nardi *et al.* 2008). Because only major elements are required to construct this diagram, it is easy to use it for most applications. The mobility of major elements, however, casts doubt on results from older, altered terrains, which may be one of the reasons not to use this diagram.

All tectonic settings except continental arc are represented in this diagram (Figure 6). For its evaluation, I separated subalkaline rocks in the silica range of 51–56% on an anhydrous basis (using SINCLAS program, Verma *et al.* 2002). The arc and MORB magmas show relatively high success rates (63.9–72.9%; Table 6). However, continental rift and ocean-island are very poorly discriminated (only 17.6% and 14.9%, respectively, plot in the correct fields; Table 6); most of them (52.1% and 70.2%) were wrongly discriminated as MORB. The success rates that characterise this diagram have been totally superseded by new major element based discriminant function diagrams (Agrawal *et al.* 2004; Verma *et al.* 2006).

For all the above reasons, continued use of this diagram is not recommended.

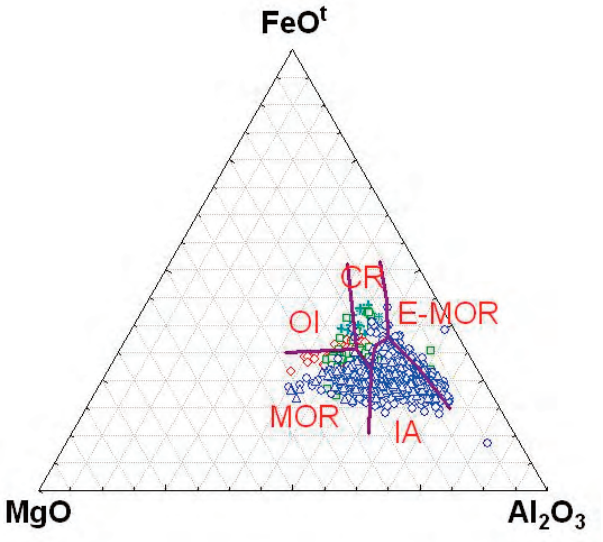

Figure 6. Statistical evaluation of the MgO-Al_2O_3-FeO^t ternary diagram (Pearce *et al.* 1977) for island and continental arc (IA+CA shown as IA), mid-ocean ridge and ocean floor (termed as MOR), continental rift (CR), ocean-island (OI), and spreading centre island (termed in the present work as E-MOR), using basaltic and andesitic rocks (samples with $(SiO_2)_{adj}$ between 51–56%) from different tectonic settings. For symbols see Figure 1. Statistical results are summarised in Table 6.

Table 6. Statistical evaluation information* of MgO-FeO^t-Al_2O_3 ternary diagram (Pearce *et al.* 1977) for island and continental arc (IA+CA), mid-ocean ridge (MOR) and ocean floor, continental rift (CR), ocean-island (OI) and spreading centre island (also termed here as E-MOR).

Tectonic setting	Total samples	Number of discriminated samples (%)					
		(IA+CA)	CR	OI	MOR	E-MOR	Other (outside any field)
Island arc	583 (100)	***425 (72.9)***	12 (2.1)	37 (6.3)	36 (6.2)	72 (12.3)	1 (0.2)
Island back arc	194 (100)	***124 (63.9)***	1 (0.5)	0 (0.0)	67 (34.6)	2 (1.0)	0 (0.0)
Continental rift	142 (100)	36 (25.4)	***25 (17.6)***	4 (2.8)	74 (52.1)	3 (2.1)	0 (0.0)
Ocean-island	94 (100)	1 (1.1)	13 (13.8)	***14 (14.9)***	66 (70.2)	0 (0.0)	0 (0.0)
MORB	200 (100)	16 (8.0)	26 (13.0)	22 (11.0)	***136 (68.0)***	0 (0.0)	0 (0.0)
E-MORB	3	0	2	0	0	***1***	0

* Only subalkaline rocks used with 51–56% $(SiO_2)_{adj}$ (see Verma *et al.* 2002, for the correct meaning of the subscript adj).

(7) Th-Ta-Hf/3 of Wood (1980)

This ternary diagram (Wood 1980; see also Wood *et al.* 1979) remains widely used, e.g., by Rahmani *et al.* (2007); Keskin *et al.* (2008); and Peng *et al.* (2008). The proposed fields are closed and are of complicated shapes (Figure 7).

In addition to N-MORB, an E-MORB setting is also discriminated on this diagram (Figure 7). The arc field is subdivided into island arc tholeiite and calc-alkali basalt, but because this is not the accepted nomenclature by the IUGS (Le Bas *et al.* 1986; Le Maitre *et al.* 2002), I did not make this distinction in the present evaluation. Nevertheless, the within-plate setting is not subdivided into continental rift and ocean-island settings.

Both island arc and back arc magmas are correctly discriminated, with high success rates of about 87.4% and 75.0%, respectively (Table 7). The discrimination of continental rift and ocean-island magmas as within-plate magmas is also acceptable (63.0% and 69.9%). Finally, a fairly large proportion (68.1%) of mid-ocean ridge basalt is also correctly discriminated. However, these success rates are certainly smaller than those obtained for some discriminant function diagrams (see the later section). I did not calculate the percentages of E-MORB discrimination, because the total number of E-MORB samples with the chemical variables for this ternary diagram was very small (only 10). One major drawback, besides of course the closure problem and the combined within-plate field (without distinguishing rift from ocean-island), is that numerous samples (2.4% to 17.3%) plot outside all fields (Figure 7; Table 7).

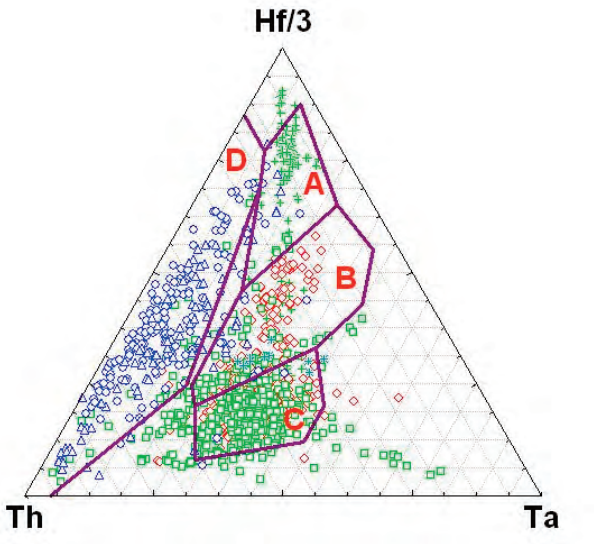

Figure 7. Statistical evaluation of the Th-Ta-Hf/3 ternary diagram (Wood 1980) for island arc basalt (IAB; field D), within-plate basalt (WPB; field C), normal type mid-ocean ridge basalt (N-MORB; field A), and enriched type mid-ocean ridge basalt (E-MORB; field B), using basic and ultrabasic rocks from different tectonic settings. For symbols see Figure 1. Statistical results are summarised in Table 7.

Table 7. Statistical evaluation information of Th-Ta-Hf/3 ternary diagram (Wood 1980) for island arc basalt (IAB), within plate basalt (WPB), normal type mid-ocean ridge basalt (N-MORB), and enriched type mid-ocean ridge basalt (E-MORB).

Tectonic setting	Total samples	Number of discriminated samples (%)				
		IAB	WPB	N-MORB	E-MORB	Other (outside any field)
Island arc	175 (100)	***153 (87.4)***	2 (1.1)	5 (2.9)	8 (4.6)	7 (4.0)
Island back arc	92 (100)	***69 (75.0)***	1 (1.1)	5 (5.4)	7 (7.6)	10 (10.9)
Continental rift	508 (100)	26 (5.1)	**320 (63.0)**	5 (1.0)	69 (13.6)	88 (17.3)
Ocean-island	502 (100)	2 (0.4)	**351 (69.9)**	2 (0.4)	135 (26.9)	12 (2.4)
MORB	138 (100)	2 (1.5)	11 (8.0)	***94 (68.1)***	18 (13.0)	13 (9.4)
E-MORB	10	0	2	0	**7**	1

Although the diagram seems to perform satisfactorily, the closure problem and eye-fitted boundaries related to ternary diagrams still apply, and therefore, the excellent discriminating properties of elements such as Th, Hf and Ta, should be used to advantage in a new set of discriminant function diagrams (see Agrawal *et al.* 2008; Verma & Agrawal, manuscript in preparation).

(8) 10MnO-15P_2O_5-TiO_2 of Mullen (1983)

Pal *et al.* (2007), Çelik (2008), and Bonev & Stampfli (2008) are among the recent references that still used this major element based ternary diagram. Contrary to other ternary diagrams, this diagram has divided the entire ternary field into six tectonic regions, although boninite and calc-alkali basalt fields are not clearly subdivided by a boundary (Figure 8). The setting of IAB can be assumed to be represented collectively by IAT, CAB and Bon (Table 8); similarly, OIB can be supposed to include OIT and OIA.

With these assumptions, island arc and back arc magmas show high collective success rates of about 96.2% and 84.2%, respectively (Table 8). The collective success rates of continental rift and ocean-island were also high (92.1% and 65.6%; Table 8). MORB magmas were not efficiently discriminated on this diagram (only about 54.2% plotted as MORB; Table 8). E-MORB samples were mostly wrongly discriminated as IAT (46.1%). Additionally, the relative mobility of these major elements, particularly Mn, may also be of concern in its use for older terrains. The error distortion and closure problems will persist in all ternary diagrams, including this one (Verma, in preparation).

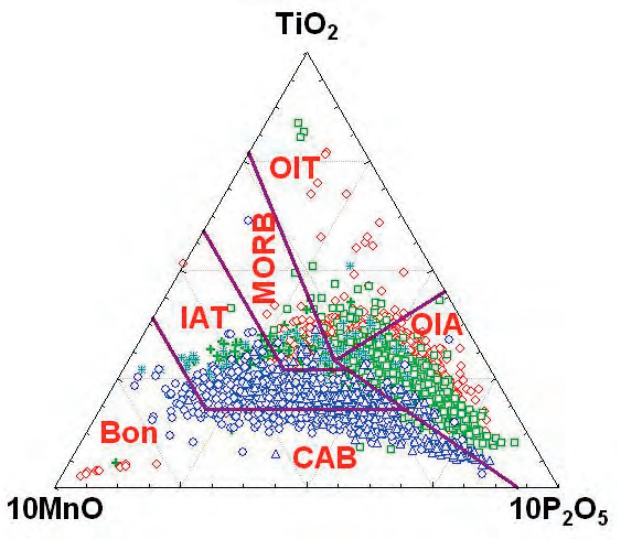

Figure 8. Statistical evaluation of the 10MnO-10P_2O_5-TiO_2 ternary diagram (Mullen 1983) for island arc tholeiite (IAT), calc-alkaline basalt (CAB), boninite (Bon), ocean-island tholeiite (OIT), ocean-island alkali basalt (OIA), and mid-ocean ridge basalt (MORB), using basic and ultrabasic rocks from different tectonic settings. CAB+IAT+Bon could be collectively termed as island arc, whereas OIT+OIA can be named as ocean-island or within-plate (because rift setting was not included here). For symbols see Figure 1. Statistical results are summarised in Table 8.

Better alternatives of discriminant function diagrams should be sought. Nevertheless, for relatively unaltered samples the diagram performs better than most other bivariate and ternary

Table 8. Statistical evaluation information of $10MnO-10P_2O_5-TiO_2$ ternary diagram (Mullen 1983) for island arc calc-alkaline basalt (CAB), island arc tholeiite (IAT) and boninite (Bon), ocean-island tholeiite (OIT), ocean-island alkali basalt (OIA), and mid-ocean ridge basalt (MORB).

Tectonic setting	Total samples	Number of discriminated samples (%)					
		Island arc			Ocean-island		MORB
		CAB	IAT	Bon	OIT	OIA	
Island arc	628 (100)	***209 (33.3)***	***365 (58.1)***	***30 (4.8)***	0 (0.0)	18 (2.9)	6 (0.9)
Island back arc	272 (100)	***111 (40.8)***	***117 (43.0)***	***1 (0.4)***	0 (0.0)	33 (12.1)	10 (3.7)
Continental rift	1274 (100)	15 (1.2)	68 (5.3)	0 (0.0)	**84 (6.6)**	**1077 (85.5)**	30 (2.4)
Ocean-island	1474 (100)	0 (0.0)	0 (0.0)	412 (34.4)	***2 (0.2)***	***784 (65.4)***	66 (0.0)
MORB	963 (100)	3 (0.3)	282 (29.3)	1 (0.1)	76 (7.9)	79 (8.2)	***522 (54.2)***
E-MORB	91 (100)	1 (1.1)	42 (46.1)	4 (4.4)	14 (15.4)	16 (17.6)	***14 (15.4)***

diagrams hitherto discussed, except for MORB samples. I propose that newer major element based discriminant function diagrams (set of five diagrams by Verma *et al.* 2006) with greater discriminating power, be adopted as the best alternative to this major element based ternary diagram.

(9) Zr/4-Y-2Nb of Meschede (1986)

This diagram is still in use, e.g., Raza *et al.* (2007), Rao & Rai (2007), Keskin *et al.* (2008), Ahmad *et al.* (2008); and Çelik & Chiaradia (2008).

No overlap-free region for IAB or MORB was proposed in this diagram (Figure 9). CRB and OIB also can only be collectively discriminated. An advantage seems to be that it supposedly discriminates E-MORB from other tectonic varieties. A large proportion of arc magmas (about 68.6%) plot in the overlap region of IAB+MORB, whereas about 42.4% of back arc magmas occupy the overlap region of IAB+WPT (Table 9; Figure 9). The success rates for continental rift and ocean-island were relatively high, with about 76.1% and 79.7% samples plotting in the within-plate field. MORB magmas mostly plot in the overlap region with IAB (about 73.2%; Table 9). However, E-MORB samples were erroneously discriminated mostly as overlap of IAB+MORB (46.0%) and WPB (31.7%), with only about 12.7% correctly discriminated as E-MORB (Table 9). A considerable number of samples of OIB and CRB also plotted outside of any tectonic field (11.7% and 15.6%, respectively; Figure 9; Table 9).

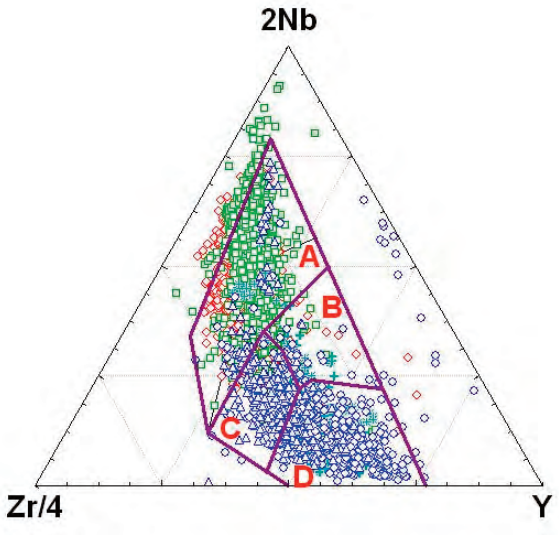

Figure 9. Statistical evaluation of the Zr/4-Y-2Nb ternary diagram (Meschede 1986) for within-plate alkali basalt and tholeiite (WPB; regions A), enriched type mid-ocean ridge basalt (E-MORB; region B), overlap region of island arc basalt and within-plate tholeiite (IAB+WPT; region C), and overlap region of normal type island arc basalt and mid-ocean ridge basalt (IAB+N-MORB; region D), using basic and ultrabasic rocks from different tectonic settings. For symbols see Figure 1. Statistical results are summarised in Table 9.

The major defect of this diagram is that it does not specify an overlap-free region for either IAB, or for MORB. Furthermore, the problems of wrong discrimination of E-MORB and the inability to separate continental rift and ocean-island are sufficient reasons to abandon this diagram as well.

Table 9. Statistical evaluation information of Zr/4-Y-2Nb ternary diagram (Meschede 1986) for within-plate alkali basalt and tholeiite (WPB), enriched type mid-ocean ridge basalt (E-MORB), overlap region of within-plate tholeiite and island arc basalt (WPT+IAB) and overlap region of normal type mid-ocean ridge basalt and island arc basalt (IAB+N-MORB).

Tectonic setting	Total samples	Number of discriminated samples (%)				
		WPB	E-MORB	Overlap region		Other (outside any field)
				(IAB+WPT)	(IAB+MORB)	
Island arc	437 (100)	14 (3.2)	23 (5.3)	**76 (17.4)**	**300 (68.6)**	24 (5.5)
Island back arc	250(100)	42 (16.8)	10 (4.0)	**106 (42.4)**	**91 (36.4)**	1 (0.4)
Continental rift	1020 (100)	**3776(76.1)**	25 (2.4)	40 (3.9)	20 (2.0)	159 (15.6)
Ocean-island	1197 (100)	**954 (79.7)**	100 (8.4)	3 (0.2)	0 (0.0)	140 (11.7)
MORB	617 (100)	27 (4.4)	66 (10.7)	72 (11.7)	**452 (73.2)**	0 (0.0)
E-MORB	63 (100)	20 (31.7)	**8 (12.7)**	5 (7.9)	29 (46.0)	1 (1)

All of these problems have been overcome in newer diagrams (Agrawal *et al.* 2008; Verma & Agrawal, in preparation).

(10) La/10-Nb/8-Y/15 of Cabanis & Lecolle (1989)

Raveggi *et al.* (2007), Koçak (2008) and Kurt *et al.* (2008) are among the recent authors that used this ternary diagram. The diagram basically includes fields for volcanic arc basalt (field A), continental basalt (field B), and oceanic basalt (field C). Futher subdivisions of fields were also proposed, which are not evaluated in the present work. For example, field A includes IAT and CAB and an overlap region of IAT and CAB. Field B includes (perhaps less conventionally) continental basalt and back-arc basin basalt. Field C of oceanic basalt is subdivided into alkali basalt from intercontinental rift (again, not a valid nomenclature), E-type MORB and normal MORB. In the present evaluation, however, and for simplicity, field A was assumed to correspond to IAB, field B to CRB, and field C to OIB+MORB. This simple approach is the only one that can be practiced in the light of the confused nomenclature used by these authors.

Figure 10 presents a plot of all data on this ternary diagram. The results are summarized in Table 10. About 78.1% and 74.3% of island arc and back arc magmas, respectively, correctly plot in the IAB field, with most of the remaining samples being mis-discriminated as field B (CRB in Table 10). Only

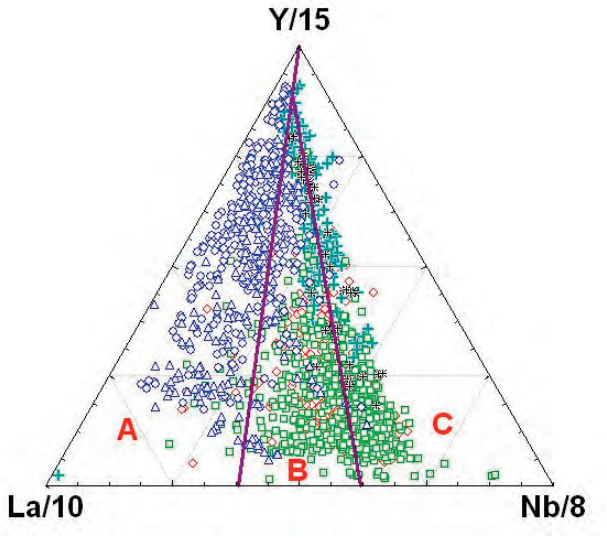

Figure 10. Statistical evaluation of the La/10-Nb/8-Y/15 ternary diagram (Cabanis & Lecolle 1989) assumed to discriminate arc basalt (IAB), continental basalt (CRB), and ocean floor basalt (OIB+N-MORB+E-MORB), using basic and ultrabasic rocks from different tectonic settings. For symbols see Figure 1. Statistical results are summarised in Table 10.

about 41.6% of the CRB samples were correctly discriminated in field B, with the greater number of the samples (55.4%) being mis-discriminated as OIB+MORB (field C in Figure 10). Similarly, numerous OIB samples (54.6%) were wrongly discriminated as CRB (field B) as compared to 44.6% correctly discriminated in the overlap region of OIB+MORB (field C, OIB+MORB). For MORB too,

Table 10. Statistical evaluation information of La/10-Nb/8-Y/15 ternary diagram (Cabanis & Lecolle 1989), assumed to discriminate arc basalt (IAB), continental basalt (CRB), and ocean floor basalt (OIB+N-MORB+E-MORB).

Tectonic setting	Total samples	Number of discriminated samples (%)		
		IAB	CRB	OIB+MORB
Island arc	347 (100)	***271 (78.1)***	72 (20.7)	4 (1.2)
Island back arc	167 (100)	***124 (74.3)***	42 (25.1)	1 (0.6)
Continental rift	796 (100)	24 (3.0)	***331 (41.6)***	441 (55.4)
Ocean-island	793 (100)	6 (0.8)	433 (54.6)	**354 (44.6)**
MORB	489 (100)	46 (0.8)	299 (61.1)	**144 (29.4)**
E-MORB	55 (100)	0 (0.0)	21 (38.2)	**34 (61.8)**

the correct discrimination was very poor (only about 29.4% samples plotting in field C, with most of them erroneously plotting in field B). The number of E-MORB samples having data for these ternary elements (La, Nb, and Y) was limited in our database (only 55 samples), although most of them (about 61.8%) plotted in field C (OIB+MORB).

The limitations of this ternary diagram are that it does not discriminate an ocean-island setting from MORB or continental rift, and that the CRB, OIB and MORB magmas compiled in the present work were poorly discriminated. Additionally, the main drawback of this diagram is that the nomenclature used (such as intercontinental rift) does not strictly correspond to plate tectonic theory.

Due to the above complications and relatively poor performance of the diagram, I propose that it should also be abandoned in favour of the newer set of diagrams, e.g., the set of five new diagrams by Agrawal *et al.* (2008) discussed in the next section, '*discriminant function diagrams*', and still newer (2010) diagrams (Verma & Agrawal, in preparation).

Old and New Sets of Discriminant Function Diagrams

The old diagrams in this category have been very few ($Score_1$-$Score_2$ diagram of Butler & Woronow 1986; and two bivariate diagrams based on F_1-F_2-F_3 of Pearce 1976). Newer diagrams were proposed during 2004–2008, and yet another set (2010) is currently under preparation. The constant sum or closure problem of compositional data can be overcome by discriminant function diagrams (Aitchison 1982, 1986; Rollinson 1993; Agrawal & Verma 2007). Use of probability-based objective boundaries can be another asset of new discrimination diagrams (Agrawal 1999; Agrawal *et al.* 2004, 2008; Verma *et al.* 2006). These reasons, combined with significantly high success rates documented for the newer diagrams (2004–2008; see the later part of this section), are sufficient to justify adopting them for all future applications of this geochemical tool.

(11) $Score_1$-$Score_2$ Diagram of Butler & Woronow (1986)

Besides Verma *et al.* (2006), Verma (2006), and Agrawal *et al.* (2008), there has been no other reference during 2006–2008 to the paper by Butler & Woronow (1986). The $Score_1$-$Score_2$ diagram is much less used probably because of the complicated calculations involved, which are more difficult than those for the simpler bivariate and ternary diagrams. Furthermore, Rollinson (1993; p. 179) committed a serious reproduction error in the $score_1$ equation and failed to explain correctly the meaning of Ti (=100 times TiO_2) and Y (=3 times Y) in the $score_1$ and $score_2$ equations. However, Verma (2006, 2009a), basing the application on the original paper by Butler & Woronow (1986), successfully used this diagram for the complex and controversial tectonic setting of Mexican Volcanic Belt and Los Tuxtlas volcanic field of southern Mexico.

The correct equations are as follows:

$$Score_1 = -(37.07 \times TiO_2) - (0.0668 \times Zr) - (1.1961 \times Y) + (0.8362 \times Sr) \quad (1)$$

$$Score_2 = -(33.76 \times TiO_2) - (0.5602 \times Zr) + (2.2191 \times Y) + (0.1582 \times Sr) \quad (2)$$

where TiO_2 is in %m/m, Zr, Y and Sr are in µg/g.

Butler & Woronow (1986) elaborated on the closure problem encountered in the conventional Zr–3Y–Ti/1000 ternary diagram (Figure 5) of Pearce & Cann (1973) and, using the combination of Aitchison's proposal (Aitchison 1982, 1984, 1986) and principal component analysis, proposed a new diagram to discriminate the tectonic settings of IAB, WPB and MORB.

The results of statistical evaluation are presented graphically in Figure 11 and numerically in Table 11. All IAB, continental rift and ocean-island settings showed very high success rates from 80.5% to 98.7%. About 69.8% of the back arc magmas plotted in the IAB field, whereas only about 55.5% of the E-MORB occupied the MORB field. Although Butler & Woronow (1986) based their proposal on average values from a total of 35 locations, I have used, for simplicity, individual analyses to evaluate this diagram. Given the very high success rates for individual magmas, the results will not significantly change even if average values were used.

One drawback of this diagram is that continental rift and ocean-island magmas cannot be discriminated from one another. Another problem is that many samples plot outside the eye-drawn boundaries (Figure 11), for which an approximate continuation of these boundaries was assumed for discrimination.

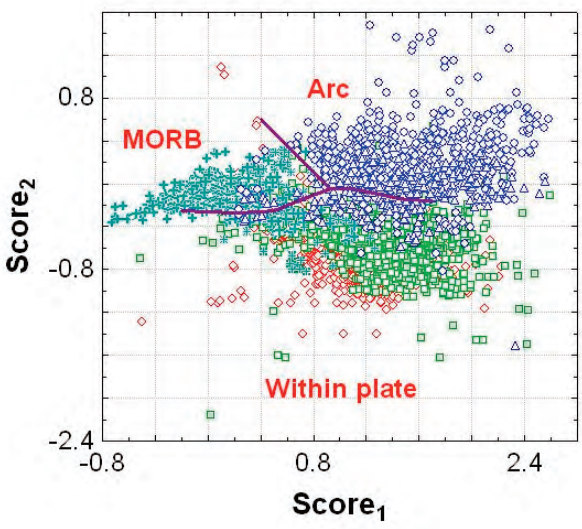

Figure 11. Statistical evaluation of the $Score_1$–$Score_2$ diagram (Butler & Woronow 1986) for arc (IAB), within-plate (WPB), and mid-ocean ridge (MORB), using basic and ultrabasic rocks from different tectonic settings. For symbols see Figure 1. Statistical results are summarised in Table 11.

I suggest that this diagram can be successfully used for discriminating these tectonic settings. Nevertheless, it is unfortunate that during the past 30 years this diagram has not found much application outside the work of Verma and collaborators. From the above considerations and in view of the newer diagrams that, in addition, successfully discriminate the continental rift and ocean-island settings, the present $Score_1$–$Score_2$ diagram can be replaced in favour of these new ones capable of discriminating four tectonic settings, instead of three (Figure 11).

Table 11. Statistical evaluation information of $Score_1$-$Score_2$ discriminant function diagram (Butler & Woronow 1986) for arc (IAB), within-plate (WPB), and mid-ocean ridge (MORB).

Tectonic setting	Total samples	Number of discriminated samples (%)		
		IAB	WPB	MORB
Island arc	516 (100)	***467 (90.5)***	41 (7.9)	8 (1.6)
Island back arc	258 (100)	***180 (69.8)***	67 (26.0)	11 (4.2)
Continental rift	1065 (100)	25 (2.3)	**1021 (95.9)**	19 (1.8)
Ocean-island	1198 (100)	2 (0.2)	**1183 (98.7)**	13 (1.1)
MORB	678 (100)	1 (0.2)	131 (19.3)	***546 (80.5)***
E-MORB	72 (100)	1 (1.4)	31 (43.1)	**40 (55.5)**

(12) F_1-F_2 of Pearce (1976)

Surprisingly similar to the $Score_1$-$Score_2$ diagram, the F_1-F_2 diagram has also been much less used even though this latter was proposed by the same pioneering author (J.A. Pearce) of several widely used bivariate and ternary diagrams.

Pearce (1976) advocated in favour of discriminant analysis of major elements as a superior technique for basalt discrimination from different tectonic settings. That compositions had to be treated differently in such statistical analysis (see Aitchison 1982, 1986) was not recognised at that time (1977). Further, the boundaries were fitted by eye. Nevertheless, Pearce (1976) set stringent control on data quality, such as requiring that the sum of all initially measured major oxides including volatiles must be between 99 and 101, that only fresh samples with $FeO/Fe_2O_3 > 0.5$ were to be used, and that CaO+MgO must be between 12 and 20%. With these conditions, the proposed functions F_1 and F_2 were as follows:

$$\begin{aligned} F_1 = &+(0.0088\times SiO_2)-(0.0774\times TiO_2)+\\ &(0.0102\times Al_2O_3)+(0.0066\times FeO^t)-\\ &(0.0017\times MgO)-(0.0143\times CaO)-\\ &(0.0155\times Na_2O)-(0.0007\times K_2O) \end{aligned} \quad (3)$$

$$\begin{aligned} F_2 = &-(0.0130\times SiO_2)-(0.0185\times TiO_2)-\\ &(0.0129\times Al_2O_3)-(0.0134\times FeO^t)-\\ &(0.0300\times MgO)-(0.0204\times CaO)-\\ &(0.0481\times Na_2O)+(0.0715\times K_2O) \end{aligned} \quad (4)$$

where FeO^t is total Fe expressed as FeO.

The F_1-F_2 diagram was designed to discriminate the combination of low-potassium tholeiite (LKT) and calc-alkali basalt (CAB), assumed collectively as island arc basalts (IAB=LKT+CAB) in this evaluation, shoshonite (SHO, not assumed to belong to any specific tectonic setting), ocean floor basalt assumed to be MORB (OFB=MORB), and CRB and OIB assumed collectively to be within-plate basalt (WPB).

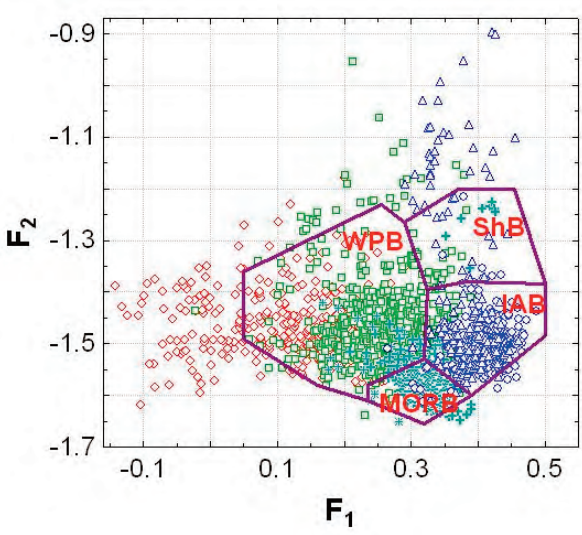

Figure 12. Statistical evaluation of the F_1-F_2 discriminant function diagram (Pearce 1976) for low-potassium tholeiite and calc-alkali basalt (LKT+CAB; assumed as arc –IAB– setting), within-plate (WPB), shoshonite (SHO; not assumed to belong to any of the four settings evaluated in the present work), ocean floor basalt (OFB; assumed as mid-ocean ridge basalt –MORB– setting), using selected basic rocks from different tectonic settings. See the text for restrictions imposed by the original author on the use of this diagram. For symbols see Figure 1. Statistical results are summarised in Table 12.

Figure 12 and Table 12 present the results of my evaluation. Fairly high success rates were obtained for arc and back arc (93.7% and 70.2%, respectively, in Table 12). MORB samples are also well discriminated as OFB (80.5%), whereas continental rift and ocean-island do so with 65.8% and 78.7% success rates as WPB. Significant percentages of the samples (2.1% to 18.7%), however, plot outside any given field (Table 12).

The major drawbacks of this diagram are the eye-drawn boundaries and the inability to discriminate between continental rift and ocean-island settings. It is not clear to which tectonic setting the shosonite (SHO) should belong. Although such rocks are more common in within-plate settings, they are also encountered in an arc environment. The strict controls (see above) will be other factors that would, in practice, make the routine application of this diagram difficult. In any case, this diagram has not been much used during the last 30 years.

Table 12. Statistical evaluation information of F_1-F_2 discriminant function diagram (Pearce 1976) for low-potassium tholeiite and calc-alkali basalt (LKT+CAB; assumed as arc –IAB– setting), shoshonite (SHO; not assumed to belong to any tectonic setting), within-plate (WPB), ocean floor basalt (OFB; assumed as mid-ocean ridge basalt –MORB– setting.

Tectonic setting	Total samples	Number of discriminated samples (%)				
		Overlap region (LKT+CAB; assumed IAB)	WPB	SHO	(OFB; assumed MORB)	Other (outside any field)
Island arc	381 (100)	***357 (93.7)***	1 (0.3)	7 (1.8)	8 (2.1)	8 (2.1)
Island back arc	171 (100)	***120 (70.2)***	1 (0.6)	16 (9.3)	2 (1.2)	32 (18.7)
Continental rift	661 (100)	128 (19.4)	**435 (65.8)**	22 (3.3)	45 (6.8)	31 (4.7)
Ocean-island	550 (100)	1 (0.2)	**433 (78.7)**	0 (0.0)	33 (6.0)	83 (15.1)
MORB	558 (100)	52 (9.3)	36 (6.5)	9 (1.6)	***449 (80.5)***	12 (2.1)
E-MORB	30 (100)	10 (30)	18 (55)	0 (0)	**4 (12)**	1 (3)

(13) F_2-F_3 of Pearce (1976)

As a complement to the F_1-F_2 diagram, Pearce (1976) proposed a companion diagram (F_2-F_3) to better separate the volcanic arc subdivisions, namely, LKT and CAB. The function F_2 is the same as above (equation 4) whereas F_3 is as follows:

$$F_3 = -(0.0221\times SiO_2) - (0.0532\times TiO_2) - (0.0361\times Al_2O_3) - (0.0016\times FeO^t) - (0.0310\times MgO) - (0.0237\times CaO) - (0.0614\times Na_2O) - (0.0289\times K_2O) \quad (5)$$

Note the correct value of the coefficient for SiO_2 (–0.0221, instead of –0.221 wrongly printed in the journal) as modified by Pearce (1976) in a reprint that I obtained from J.A. Pearce during the late seventies.

The discriminating power of this diagram (Figure 13; Table 13) is somewhat less than the earlier (F_1-F_2) diagram. Here, the success rates for arc, back arc and MORB were respectively, about 80.9%, 82.3% and 78.0%, for assumed settings of island arc and MORB (Table 13). The diagram will not work for within-plate magmas, because this setting is actually missing from this diagram. It should be used to distinguish between LKT and CAB for arc magmas, because LKT and CAB are effectively separated from one another (Figure 13). However, in view of the nomenclature of basaltic rocks (Le Bas *et al.* 1986), this so-called advantage does not really matter, because these terms are not recommended by the IUGS any more (Le Bas 2000; Le Maitre *et al.* 2002).

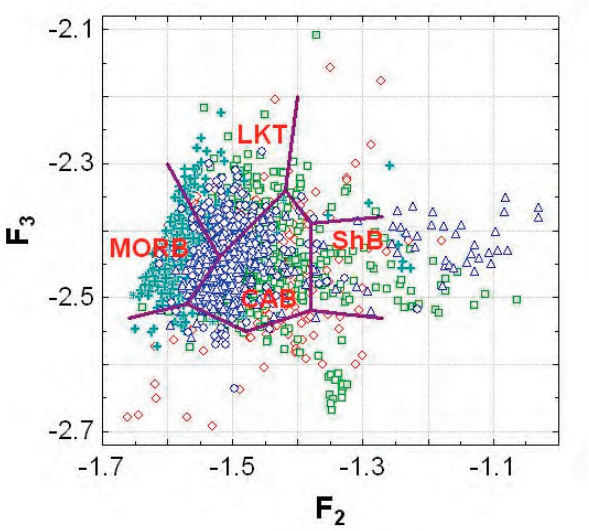

Figure 13. Statistical evaluation of the F_2-F_3 discriminant function diagram (Pearce 1976) for low-potassium tholeiite (LKT), calc-alkali basalt (CAB), shoshonite (SHO), ocean floor basalt (OFB; assumed as mid-ocean ridge basalt MORB), using selected basic rocks from different tectonic settings. LKT+CAB were assumed as arc –IAB– setting. Same restrictions apply for this diagram as for Figure 12. For symbols see Figure 1. Statistical results are summarised in Table 13.

Both sets of F diagrams of Pearce (1976) are not capable of discriminating continental rift and ocean-island settings. Their discriminating power for IAB and MORB is also superseded by the newer diagrams (2004–2010). The statistical handling also is not up to the present expectations (Aitchison 1986; Agrawal *et al.* 2008). Therefore, I recommend replacing these F_1-F_2-F_3 diagrams in future with the newer alternatives (see below).

Table 13. Statistical evaluation information of F_2-F_3 plot (Pearce 1976) for low-potassium tholeiite (LKT), calc-alkali basalt (CAB), shoshonites (SHO), ocean floor basalt (OFB; assumed as mid-ocean ridge basalt MORB).

Tectonic setting	Total samples	Number of discriminated samples (%)				
		Assumed IAB setting		SHO	(OFB; assumed MORB setting)	Other (outside any field)
		LKT	CAB			
Island arc	381 (100)	***131 (34.4)***	***177 (46.5)***	5 (1.3)	46 (12.1)	22 (5.8)
Island back arc	171 (100)	**6 (16.8)**	**112 (65.5)**	8 (4.7)	29 (17.0)	16 (9.3)
Continental rift	661 (100)	116 (17.6)	347 (52.5)	36 (5.4)	105 (15.9)	57 (8.6)
Ocean-island	550 (100)	152 (27.6)	227 (41.3)	14 (2.5)	90 (16.4)	67 (12.2)
MORB	558 (100)	73 (13.1)	27 (4.8)	0 (0.0)	***435 (78.0)***	23 (4.1)
E-MORB	30 (100)	9 (27)	13 (40)	1 (3)	**9 (27)**	1 (3)

(14) Set of Five Diagrams Based on Major-elements (Agrawal *et al.* 2004)

These relatively new discriminant function discrimination diagrams have been cited by several workers. Recent references include: Srivastava & Sinha (2007); Wiszniewska *et al.* (2007); Jafarzadeh & Hosseini-Barzi (2008); Sheth (2008); Díaz-González *et al.* (2008); and Pandarinath (2009).

This was, in fact, the first set of diagrams that actually allowed discriminating of two very similar tectonic settings of continental rift and ocean-island. For the modern plate tectonics theory, I consider that the discrimination of these two tectonic settings for older terrains is important because continental rifting should have occurred, as its name suggests, from extensional features on a continental crust whereas the ocean-island setting would correspond to an oceanic crust. The search for old oceanic crust, being of interest to the scientific community (Pearce 2008), should be facilitated by such a distinction of continental rift and ocean-island settings if one is capable of discriminating them with high success rates.

The first of the five diagrams in this set consists of a four-field DF1-DF2 plot to discriminate the four tectonic settings: IAB, CRB, OIB, and MORB. The two functions that account for about 97.2% of the between-groups variances are as follows (Agrawal *et al.* 2004):

$$\begin{aligned}(DF1)_{(IAB\text{-}CRB\text{-}OIB\text{-}MORB)} = {} & 0.258\times(SiO_2)_{adj} + \\ & 2.395\times(TiO_2)_{adj} + 0.106\times(Al_2O_3)_{adj} + \\ & 1.019\times(Fe_2O_3)_{adj} - 6.778\times(MnO)_{adj} + \\ & 0.405\times(MgO)_{adj} + 0.119\times(CaO)_{adj} + \\ & 0.071\times(Na_2O)_{adj} - 0.198\times(K_2O)_{adj} + \\ & 0.613\times(P_2O_5)_{adj} - 24.065\end{aligned} \quad (6)$$

$$\begin{aligned}DF2_{(IAB\text{-}CRB\text{-}OIB\text{-}MORB)} = {} & 0.730\times(SiO_2)_{adj} + \\ & 1.119\times(TiO_2)_{adj} + 0.156\times(Al_2O_3)_{adj} + \\ & 1.332\times(Fe_2O_3)_{adj} + 4.376\times(MnO)_{adj} + \\ & 0.493\times(MgO)_{adj} + 0.936\times(CaO)_{adj} + \\ & 0.882\times(Na_2O)_{adj} - 0.291\times(K_2O)_{adj} - \\ & 1.572\times(P_2O_5)_{adj} - 59.472\end{aligned} \quad (7)$$

where the subscript $_{adj}$ refers to the adjusted data from SINCLAS (Verma *et al.* 2002).

The discriminant function for the other four diagrams corresponding to three groups at a time, are calculated similarly (equations 8–15).

For IAB-CRB-OIB discrimination, the equations are (note P_2O_5 is absent from equations 8 and 9):

$$(DF1)_{(IAB\text{-}CRB\text{-}OIB)} = 0.251 \times (SiO_2)_{adj} + 2.034 \times (TiO_2)_{adj} - 0.100 \times (Al_2O_3)_{adj} + 0.573 \times (Fe_2O_3)_{adj} + 0.032 \times (FeO)_{adj} - 2.877 \times (MnO)_{adj} + 0.260 \times (MgO)_{adj} + 0.052 \times (CaO)_{adj} + 0.322 \times (Na_2O)_{adj} - 0.229 \times (K_2O)_{adj} - 18.974 \quad (8)$$

$$(DF2)_{(IAB\text{-}CRB\text{-}OIB)} = 2.150 \times (SiO_2)_{adj} + 2.711 \times (TiO_2)_{adj} + 1.792 \times (Al_2O_3)_{adj} + 2.295 \times (Fe_2O_3)_{adj} + 1.484 \times (FeO)_{adj} + 8.594 \times (MnO)_{adj} + 1.896 \times (MgO)_{adj} + 2.158 \times (CaO)_{adj} + 1.201 \times (Na_2O)_{adj} + 1.763 \times (K_2O)_{adj} - 200.276 \quad (9)$$

For IAB-CRB-MORB discrimination (equations 10-11):

$$(DF1)_{(IAB\text{-}CRB\text{-}MORB)} = 0.435 \times (SiO_2)_{adj} - 1.392 \times (TiO_2)_{adj} + 0.183 \times (Al_2O_3)_{adj} + 0.148 \times (FeO)_{adj} + 7.690 \times (MnO)_{adj} + 0.021 \times (MgO)_{adj} + 0.380 \times (CaO)_{adj} + 0.036 \times (Na_2O)_{adj} + 0.462 \times (K_2O)_{adj} - 1.192 \times (P_2O_5)_{adj} - 29.435 \quad (10)$$

$$(DF2)_{(IAB\text{-}CRB\text{-}MORB)} = 0.601 \times (SiO_2)_{adj} - 0.335 \times (TiO_2)_{adj} + 1.332 \times (Al_2O_3)_{adj} + 1.449 \times (FeO)_{adj} + 0.756 \times (MnO)_{adj} + 0.893 \times (MgO)_{adj} + 0.448 \times (CaO)_{adj} + 0.525 \times (Na_2O)_{adj} + 1.734 \times (K_2O)_{adj} + 2.494 \times (P_2O_5)_{adj} - 78.236 \quad (11)$$

For IAB-OIB-MORB discrimination (equations 12–13; note P_2O_5 is absent from these equations):

$$(DF1)_{(IAB\text{-}OIB\text{-}MORB)} = 1.232 \times (SiO_2)_{adj} + 4.166 \times (TiO_2)_{adj} + 1.085 \times (Al_2O_3)_{adj} + 3.522 \times (Fe_2O_3)_{adj} + 0.500 \times (FeO)_{adj} - 3.930 \times (MnO)_{adj} + 1.334 \times (MgO)_{adj} + 1.085 \times (CaO)_{adj} + 0.416 \times (Na_2O)_{adj} + 0.827 \times (K_2O)_{adj} - 119.050 \quad (12)$$

$$(DF2)_{(IAB\text{-}OIB\text{-}MORB)} = 1.384 \times (SiO_2)_{adj} + 1.091 \times (TiO_2)_{adj} + 0.908 \times (Al_2O_3)_{adj} + 2.419 \times (Fe_2O_3)_{adj} + 0.886 \times (FeO)_{adj} + 5.281 \times (MnO)_{adj} + 1.269 \times (MgO)_{adj} + 1.790 \times (CaO)_{adj} + 2.572 \times (Na_2O)_{adj} + 0.138 \times (K_2O)_{adj} - 134.295 \quad (13)$$

For CRB-OIB-MORB discrimination (equations 14–15):

$$(DF1)_{(CRB\text{-}OIB\text{-}MORB)} = 0.310 \times (SiO_2)_{adj} + 1.936 \times (TiO_2)_{adj} + 0.341 \times (Al_2O_3)_{adj} + 0.760 \times (Fe_2O_3)_{adj} + 0.351 \times (FeO)_{adj} - 11.315 \times (MnO)_{adj} + 0.526 \times (MgO)_{adj} + 0.084 \times (CaO)_{adj} + 0.312 \times (K_2O)_{adj} + 1.892 \times (P_2O_5)_{adj} - 32.909 \quad (14)$$

$$(DF2)_{(CRB\text{-}OIB\text{-}MORB)} = 0.703 \times (SiO_2)_{adj} + 2.454 \times (TiO_2)_{adj} + 0.233 \times (Al_2O_3)_{adj} + 1.943 \times (Fe_2O_3)_{adj} - 0.182 \times (FeO)_{adj} - 2.421 \times (MnO)_{adj} + 0.618 \times (MgO)_{adj} + 0.712 \times (CaO)_{adj} - 0.866 \times (K_2O)_{adj} - 1.180 \times (P_2O_5)_{adj} - 56.455 \quad (15)$$

These discriminant functions were calculated for each data set and the corresponding discrimination diagrams were constructed (Figure 14a–e), from which the statistical synthesis was prepared (Table 14). For the corresponding discriminant function

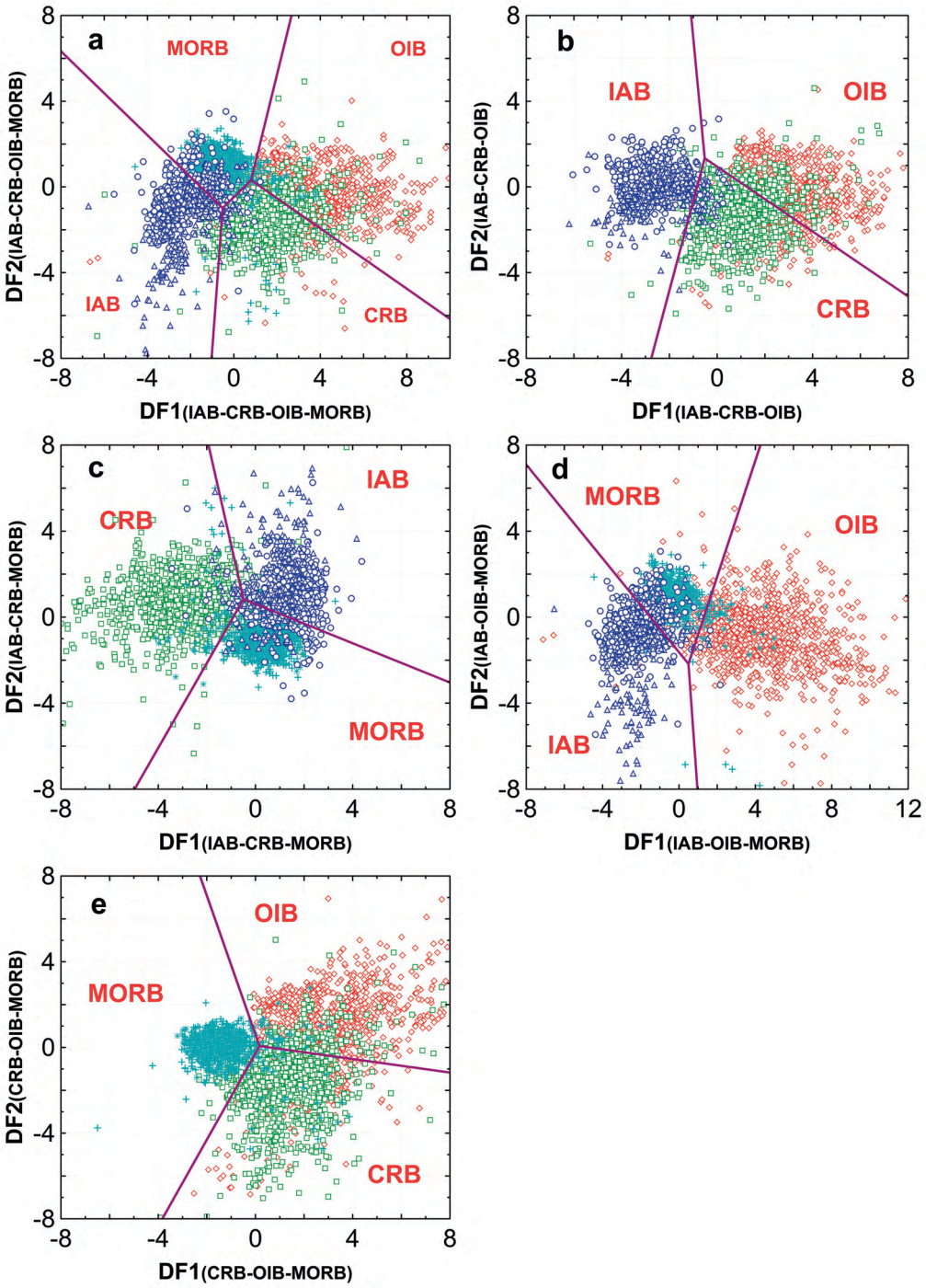

Figure 14. Statistical evaluation of the set of five major-element based discriminant function DF1–DF2 discrimination diagrams (Agrawal *et al.* 2004) for island arc basalt (IAB), continental rift basalt (CRB), ocean-island basalt (OIB) and mid-ocean ridge basalt (MORB), using basic and ultrabasic rocks from different tectonic settings. For probability-based discrimination boundaries see the original paper by Agrawal *et al.* (2004). For symbols see Figure 1. Statistical results are summarised in Table 14. **(a)** four-groups IAB-CRB-OIB-MORB diagram; **(b)** three-groups IAB-CRB-OIB diagram; **(c)** three-groups IAB-CRB-MORB diagram; **(d)** three-groups IAB-OIB-MORB diagram; and **(e)** three-groups CRB-OIB-MORB diagram.

Table 14. Statistical evaluation information of the set of five major-element based discriminant function DF1-DF2 discrimination diagrams (Agrawal *et al.* 2004) for island arc basalt (IAB), continental rift basalt (CRB), ocean-island basalt (OIB) and mid-ocean ridge basalt (MORB).

Tectonic setting	Total samples	Number of discriminated samples (%)			
		IAB	CRB	OIB	MORB
IAB-CRB-OIB-MORB					
Island arc	639 (100)	***516 (80.7)***	16 (2.5)	1 (0.2)	106 (16.6)
Island back arc	285 (100)	**212 (74.4)**	23 (8.1)	0 (0.0)	50 (17.5)
Continental rift	1271 (100)	76 (6.0)	***864 (68.0)***	232 (18.2)	99 (7.8)
Ocean-island	1479 (100)	15 (1.0)	386 (26.1)	***1069 (72.3)***	9 (0.6)
MORB	963 (100)	26 (2.7)	21 (2.2)	27 (2.8)	***889 (92.3)***
E-MORB	91 (100)	6 (6.6)	9 (9.9)	14 (15.4)	**62 (68.1)**
IAB-CRB-OIB					
Island arc	639 (100)	***612 (95.8)***	25 (3.9)	2 (0.3)	–
Island back arc	285 (100)	**250 (87.7)**	35 (12.3)	0 (0.0)	–
Continental rift	1271 (100)	79 (6.2)	***1006 (79.2)***	186 (14.6)	–
Ocean-island	1479 (100)	6 (0.4)	520 (35.2)	***943 (64.4)***	–
IAB-CRB-MORB					
Island arc	639 (100)	***521 (81.5)***	19 (3.0)	–	99 (15.5)
Island back arc	285 (100)	**208 (73.0)**	21 (7.4)	–	56 (19.6)
Continental rift	1271 (100)	55 (4.3)	***1099 (86.5)***	–	117 (9.2)
MORB	963 (100)	30 (3.1)	30 (3.1)	–	***903 (93.8)***
E-MORB	91 (100)	5 (5.5)	25 (27.5)	–	**61 (67.0)**
IAB-OIB-MORB					
Island arc	639 (100)	***536 (83.9)***	–	3 (0.5)	100 (15.6)
Island back arc	285 (100)	**227 (79.7)**	–	2 (0.7)	56 (19.6)
Ocean-island	1479 (100)	6 (0.4)	–	***1372 (92.8)***	101 (6.8)
MORB	963 (100)	19 (2.0)	–	39 (4.0)	***905 (94.0)***
E-MORB	91 (100)	5 (5.5)	–	20 (22.0)	**66 (72.5)**
CRB-OIB-MORB					
Continental rift	1271 (100)	–	***960 (75.5)***	204 (16.1)	106 (8.3)
Ocean-island	1479 (100)	–	428 (28.9)	***1036 (70.5)***	9 (0.6)
MORB	963 (100)	–	25 (2.6)	23 (2.4)	***915 (95.0)***
E-MORB	91 (100)	–	8 (8.8)	12 (13.2)	**71 (78.0)**

boundaries in Figure 14a–e as objectively inferred from LDA of the data, the reader is referred to Agrawal *et al.* (2004).

In the first four-field diagram (Figure 14a), both arc and back arc magmas were discriminated with success rates of about 80.7% and 74.4%, respectively (Table 14). MORB samples were also successfully discriminated with still greater success rate of about 92.3%, whereas the enriched MORB variety showed 68.1%. Samples from continental rift and ocean-island settings could be discriminated, for the first time, although with relatively small success rates of about 68.0 and 72.3% in this particular diagram (Figure 14a; Table 14). This discrimination was in fact improved in the other diagrams (Figure 14b–e; Table 14) of this set (see the next paragraph). Nevertheless, these percentages (68.1% to 92.3%; Figure 14a; Table 14) are similar to 70.3% to 93.0% values for IAB, CRB, OIB, and MORB settings obtained by Agrawal *et al.* (2004) using their training and testing sets.

The other four diagrams for three tectonic settings at a time (IAB-CRB-OIB, IAB-CRB-MORB, IAB-OIB-MORB, and CRB-OIB-MORB; Figure

14b–e) performed better, as expected, than the above four-field diagram (Figure 14a). The success rates for the main tectonic varieties of magmas as discriminated in these four diagrams (Figure 14b–e) were 64.4–95.8%, 81.5–93.8%, 83.9–94.0%, and 70.5–95.0%, respectively. In comparison, Agrawal *et al.* (2004) reported success rates of 79.4–92.0%, 80.8–96.0%, 84.8–96.0%, and 71.8–96.0%, respectively, for these four diagrams.

Back arc and E-MORB magmas (Figure 14b–e) were also successfully discriminated as, respectively, arc and MORB, with high success rates of 73.0–87.7% and 67.0–78.0% (Table 14), this being a great advantage of these diagrams as compared to all earlier bivariate, ternary, and discriminant function diagrams. From the tectonics point of view and irrespective of petrological arguments of magma sources, it should be beyond doubt that if a tectonomagmatic diagram is capable of discriminating arc and MORB settings, back arc magmas should be discriminated as arc and E-MORB from mid-ocean ridges as MORB. This would then justify their names as back arc and E-MORB, respectively. Otherwise, does it make any sense to use a discrimination diagram? Petrological modelling, if correctly done, would suffice. I suggest that correct discrimination with high success rates (back arc as arc and E-MORB from mid-ocean ridges as MORB) would render this methodology to be truly complementary to petrological modelling.

Thus, in terms of the success rates for discriminating all four major tectonic settings, this set of five new diagrams performed better than all other discrimination diagrams available prior to 2004. The proposal of these discriminant function major element diagrams was a major step forward, because it used an extensive database in the LDA and the discrimination boundaries were objectively drawn from probabilities. The drawback of statistical methodology still persisted because the compositional data were not correctly handled (Aitchison 1982, 1986). Therefore, these diagrams can also be replaced by the newer (2006–2010) major element (or trace element) based diagrams that in addition, incorporate log-ratio transformation of compositional variables.

(15) Set of Five Discriminant Function Diagrams Based on Log-transformed Ratios of Major-elements (Verma *et al.* 2006)

Besides many of the papers cited for the discriminant function diagrams of Agrawal *et al.* (2004), the following references also cite the paper by Verma *et al.* (2006): Rajesh (2007); Shekhawat *et al.* (2007); Vermeesch (2007); and Torres-Alvarado *et al.* (2010). Sheth (2008) positively evaluated these (Verma *et al.* 2006) and earlier (Agrawal *et al.* 2004) diagrams using mafic volcanics and ophiolites and inferred that most rocks were discriminated with relatively high success rates.

A major advance in the application of discrimination diagrams was probably achieved by Verma *et al.* (2006), who solved the final problem related to the older discrimination diagrams. Other problems common to all simple bivariate and ternary diagrams as well as old discriminant function diagrams were already overcome by Agrawal *et al.* (2004). The final step forward was the statistically correct handling of compositional data (Chayes 1960, 1965, 1978; Aitchison 1981, 1982, 1984, 1986, 1989; Aitchison *et al.* 2000, 2003; Egozcue *et al.* 2003; Aitchison & Egozcue 2005). These authors (Verma *et al.* 2006) calculated the natural logarithm of element ratios using a common divisor, in this case $(SiO_2)_{adj}$ before carrying out LDA. Thus, ratios of all other major elements in the natural logarithm space, viz., $\ln(TiO_2/SiO_2)_{adj}$, $\ln(Al_2O_3/SiO_2)_{adj}$, $\ln(Fe_2O_3/SiO_2)_{adj}$, $\ln(FeO/SiO_2)_{adj}$, $\ln(MnO/SiO_2)_{adj}$, $\ln(MgO/SiO_2)_{adj}$, $\ln(CaO/SiO_2)_{adj}$, $\ln(Na_2O/SiO_2)_{adj}$, $\ln(K_2O/SiO_2)_{adj}$, and $\ln(P_2O_5/SiO_2)_{adj}$ were used in LDA. Note ratios eliminate the chemical measurement units (converts compositional data theoretically restricted to 0–1 or 0–100% space, to non-compositional space), and the natural logarithms of the ratio variables open up the restriction of the space to practically from $-\infty$ to $+\infty$. The common divisor ascertains that we are dealing with the compositions as a multivariate problem (instead of a series of univariate data; see Verma *et al.* (2006) and Agrawal & Verma (2007) for more discussion on this innovation in compositional data handling, and Vermeesch (2006, 2007) for probably erroneous treatment of them).

The discriminant functions for the four groups diagram (representing about 94.2% of the between groups variance) were as follows:

$$DF1_{(IAB\text{-}CRB\text{-}OIB\text{-}MORB)_m} = -4.6761 \times \ln(TiO_2/SiO_2)_{adj} + 2.5330 \times \ln(Al_2O_3/SiO_2)_{adj} - 0.3884 \times \ln(Fe_2O_3/SiO_2)_{adj} + 3.9688 \times \ln(FeO/SiO_2)_{adj} + 0.8980 \times \ln(MnO/SiO_2)_{adj} - 0.5832 \times \ln(MgO/SiO_2)_{adj} - 0.2896 \times \ln(CaO/SiO_2)_{adj} - 0.2704 \times \ln(Na_2O/SiO_2)_{adj} + 1.0810 \times \ln(K_2O/SiO_2)_{adj} + 0.1845 \times \ln(P_2O_5/SiO_2)_{adj} + 1.5445 \quad (16)$$

$$DF2_{(IAB\text{-}CRB\text{-}OIB\text{-}MORB)_m} = 0.6751 \times \ln(TiO_2/SiO_2)_{adj} + 4.5895 \times \ln(Al_2O_3/SiO_2)_{adj} + 2.0897 \times \ln(Fe_2O_3/SiO_2)_{adj} + 0.8514 \times \ln(FeO/SiO_2)_{adj} - 0.4334 \times \ln(MnO/SiO_2)_{adj} + 1.4832 \times \ln(MgO/SiO_2)_{adj} - 2.3627 \times \ln(CaO/SiO_2)_{adj} - 1.6558 \times \ln(Na_2O/SiO_2)_{adj} + 0.6757 \times \ln(K_2O/SiO_2)_{adj} + 0.4130 \times \ln(P_2O_5/SiO_2)_{adj} + 13.1639 \quad (17)$$

where the subscript after DF1 or DF2 refers to the fields or tectonic settings that are being discriminated, in this case IAB, CRB, OIB, and MORB. The subscript $_m$ indicates that major elements are being used for this purpose (see the chemical symbols on the right side of these equations).

The discriminant function for the other four diagrams corresponding to three groups at a time, were calculated similarly (equations 18–25).

For IAB-CRB-OIB discrimination, the equations are:

$$DF1_{(IAB\text{-}CRB\text{-}OIB)_m} = +3.9998 \times \ln(TiO_2/SiO_2)_{adj} - 2.2385 \times \ln(Al_2O_3/SiO_2)_{adj} + 0.8110 \times \ln(Fe_2O_3/SiO_2)_{adj} - 2.5865 \times \ln(FeO/SiO_2)_{adj} - 1.2433 \times \ln(MnO/SiO_2)_{adj} + 0.4872 \times \ln(MgO/SiO_2)_{adj} - 0.3153 \times \ln(CaO/SiO_2)_{adj} + 0.4325 \times \ln(Na_2O/SiO_2)_{adj} - 1.0262 \times \ln(K_2O/SiO_2)_{adj} + 0.0514 \times \ln(P_2O_5/SiO_2)_{adj} - 0.5718 \quad (18)$$

$$DF2_{(IAB\text{-}CRB\text{-}OIB)_m} = -1.3705 \times \ln(TiO_2/SiO_2)_{adj} + 3.0104 \times \ln(Al_2O_3/SiO_2)_{adj} + 0.3239 \times \ln(Fe_2O_3/SiO_2)_{adj} + 1.8998 \times \ln(FeO/SiO_2)_{adj} - 1.9746 \times \ln(MnO/SiO_2)_{adj} + 1.4411 \times \ln(MgO/SiO_2)_{adj} - 2.2656 \times \ln(CaO/SiO_2)_{adj} + 1.8665 \times \ln(Na_2O/SiO_2)_{adj} + 0.2872 \times \ln(K_2O/SiO_2)_{adj} + 0.8138 \times \ln(P_2O_5/SiO_2)_{adj} + 1.8202 \quad (19)$$

For IAB-CRB-MORB discrimination:

$$DF1_{(IAB\text{-}CRB\text{-}MORB)_m} = -1.5736 \times \ln(TiO_2/SiO_2)_{adj} + 6.1498 \times \ln(Al_2O_3/SiO_2)_{adj} + 1.5544 \times \ln(Fe_2O_3/SiO_2)_{adj} + 3.4134 \times \ln(FeO/SiO_2)_{adj} - 0.0087 \times \ln(MnO/SiO_2)_{adj} + 1.2480 \times \ln(MgO/SiO_2)_{adj} - 2.1103 \times \ln(CaO/SiO_2)_{adj} - 0.7576 \times \ln(Na_2O/SiO_2)_{adj} + 1.1431 \times \ln(K_2O/SiO_2)_{adj} + 0.3524 \times \ln(P_2O_5/SiO_2)_{adj} + 16.8712 \quad (20)$$

$$DF2_{(IAB\text{-}CRB\text{-}MORB)_m} = +3.9844 \times \ln(TiO_2/SiO_2)_{adj} + 0.2200 \times \ln(Al_2O_3/SiO_2)_{adj} + 1.1516 \times \ln(Fe_2O_3/SiO_2)_{adj} - 2.2036 \times \ln(FeO/SiO_2)_{adj} - 1.6228 \times \ln(MnO/SiO_2)_{adj} + 1.4291 \times \ln(MgO/SiO_2)_{adj} - 1.2524 \times \ln(CaO/SiO_2)_{adj} + 0.3581 \times \ln(Na_2O/SiO_2)_{adj} - 0.6414 \times \ln(K_2O/SiO_2)_{adj} + 0.2646 \times \ln(P_2O_5/SiO_2)_{adj} + 5.0546 \quad (21)$$

For IAB-OIB-MORB discrimination:

$$DF1_{(IAB\text{-}OIB\text{-}MORB)_m} = +5.3396 \times \ln(TiO_2/SiO_2)_{adj} - 1.6279 \times \ln(Al_2O_3/SiO_2)_{adj} + 0.8338 \times \ln(Fe_2O_3/SiO_2)_{adj} - 4.7362 \times \ln(FeO/SiO_2)_{adj} - 0.1254 \times \ln(MnO/SiO_2)_{adj} + 0.6452 \times \ln(MgO/SiO_2)_{adj} + 1.5153 \times \ln(CaO/SiO_2)_{adj} - 0.8154 \times \ln(Na_2O/SiO_2)_{adj} - 0.8888 \times \ln(K_2O/SiO_2)_{adj} - 0.2255 \times \ln(P_2O_5/SiO_2)_{adj} + 5.7755 \quad (22)$$

$$DF2_{(IAB\text{-}OIB\text{-}MORB)_m} = +1.1799 \times \ln(TiO_2/SiO_2)_{adj} + 5.5114 \times \ln(Al_2O_3/SiO_2)_{adj} + 2.7737 \times \ln(Fe_2O_3/SiO_2)_{adj} - 0.1341 \times \ln(FeO/SiO_2)_{adj} + 0.6672 \times \ln(MnO/SiO_2)_{adj} + 1.1045 \times \ln(MgO/SiO_2)_{adj} - 1.7231 \times \ln(CaO/SiO_2)_{adj} - 3.8948 \times \ln(Na_2O/SiO_2)_{adj} + 0.9471 \times \ln(K_2O/SiO_2)_{adj} - 0.1082 \times \ln(P_2O_5/SiO_2)_{adj} + 15.4984 \quad (23)$$

Finally, for CRB-OIB-MORB discrimination:

$$DF1_{(CRB\text{-}OIB\text{-}MORB)_m} = -0.5183 \times \ln(TiO_2/SiO_2)_{adj} + 4.9886 \times \ln(Al_2O_3/SiO_2)_{adj} + 2.2204 \times \ln(Fe_2O_3/SiO_2)_{adj} + 1.1801 \times \ln(FeO/SiO_2)_{adj} - 0.3008 \times \ln(MnO/SiO_2)_{adj} + 1.3297 \times \ln(MgO/SiO_2)_{adj} - 2.1834 \times \ln(CaO/SiO_2)_{adj} - 1.9319 \times \ln(Na_2O/SiO_2)_{adj} + 0.6976 \times \ln(K_2O/SiO_2)_{adj} + 0.8998 \times \ln(P_2O_5/SiO_2)_{adj} + 13.2625 \quad (24)$$

$$DF2_{(CRB\text{-}OIB\text{-}MORB)_m} = +5.0509 \times \ln(TiO_2/SiO_2)_{adj} - 0.4972 \times \ln(Al_2O_3/SiO_2)_{adj} + 1.0046 \times \ln(Fe_2O_3/SiO_2)_{adj} - 3.3848 \times \ln(FeO/SiO_2)_{adj} + 0.5528 \times \ln(MnO/SiO_2)_{adj} + 0.2925 \times \ln(MgO/SiO_2)_{adj} + 0.4007 \times \ln(CaO/SiO_2)_{adj} - 2.8637 \times \ln(Na_2O/SiO_2)_{adj} - 0.2189 \times \ln(K_2O/SiO_2)_{adj} - 1.0558 \times \ln(P_2O_5/SiO_2)_{adj} + 2.8877 \quad (25)$$

The results of evaluations for this set of five diagrams are given in Figure 15 and Table 15. The success rates for the IAB-CRB-OIB-MORB diagram (Figure 15a) for arc, rift, ocean-island and mid-ocean ridge were respectively, 94.7%, 76.8%, 72.3% and 94.3% (Table 15). For back arc and E-MORB, these were somewhat smaller (84.2% and 69.2%), but still acceptably high. For three groups at a time diagrams (Figure 15b–e), the success rates for IAB and MORB were extremely high (94.3% to 97.2%; Table 15), as also for CRB and OIB (93.0% and 95.4%) whenever these groups are separately evaluated (Figure 15c, d). When the latter were simultaneously evaluated in a diagram (Figure 15b, e) the success rates were somewhat smaller (74.9% to 77.7%) but still statistically meaningful (Table 15). These success rates are comparable to those obtained by the original authors (83% to 97%; see Table 5 in Verma *et al.* 2006). Thus, the discriminating power of this set of five diagrams for IAB, CRB, OIB, and MORB is reasonably high for back arc and E-MORB settings, although these diagrams do not explicitly contain them.

The back arc and E-MORB magmas were also successfully discriminated as IAB and MORB, respectively, with 83.4–90.5% and 63.7–75.8%. These two types of magmas were not evaluated by the original authors of these diagrams.

The above analysis clearly indicates that this set of five diagrams can be successfully applied to decipher tectonic settings of rocks from areas of a complex tectonic history or even altered rocks from older terranes (see the evaluations by Verma *et al.* 2006; Sheth 2008; see also the Application section below). Nevertheless, the value of these major element based diagrams resides in their application to fresh rocks from a complex tectonic setting such as the Mexican Volcanic Belt (MVB) illustrated by Verma *et al.* (2006). This volcanic province corresponds to the subduction of the Cocos plate, but is also characterized by extensive continuing extensional processes (Verma 2002, 2009a). The application of these diagrams showed that the MVB belongs to a continental rift setting rather than an arc. Similarly, the complex tectonic history of Turkey should find useful applications of such diagrams for the study of relatively fresh rocks.

For older terrains, however, the alteration effects might cause some discrepancies, because these diagrams are based on major elements, which may behave differently during alteration or metamorphism (Rollinson 1993). Therefore, alternative proposals of discriminant function diagrams are required (see below).

(16) Set of Five Discriminant Function Diagrams Based on Log-transformed Ratios of Five Immobile Trace-elements (Agrawal et al. 2008)

These brand new diagrams, whose innovative statistical methodology has already been cited by Díaz-González *et al.* (2008), Pandarinath (2009), and Verma (2009b), are based on natural log-transformation of La/Th, Sm/Th, Yb/Th, and Nb/Th ratios.

Because most authors, including Agrawal *et al.* (2004) and Verma *et al.* (2006), had already noted the difficulty of discriminating continental rift and ocean-island settings and that, in a four-field diagram, the totality (100%) of between-groups variance cannot be represented by two discriminant functions only (three functions are required), Agrawal *et al.* (2008) devised yet another method to improve this discrimination. They combined these two settings (CRB+OIB, called within-plate WPB by some earlier workers) in the four-group diagram and treated it as a three-group type, namely, IAB-CRB+OIB-MORB. Thus, both rift and ocean-island settings were first discriminated as a single overlap region of CRB+OIB (termed within-plate in older diagrams), but contrary to the older diagrams (pre-2004), these two settings were later individually discriminated from one another. From LDA of three groups, only two discriminant functions and one bivariate diagram were obtained explaining the entire 100% between groups variance. The separation of CRB and OIB was achieved in the other four remaining diagrams if the first diagram

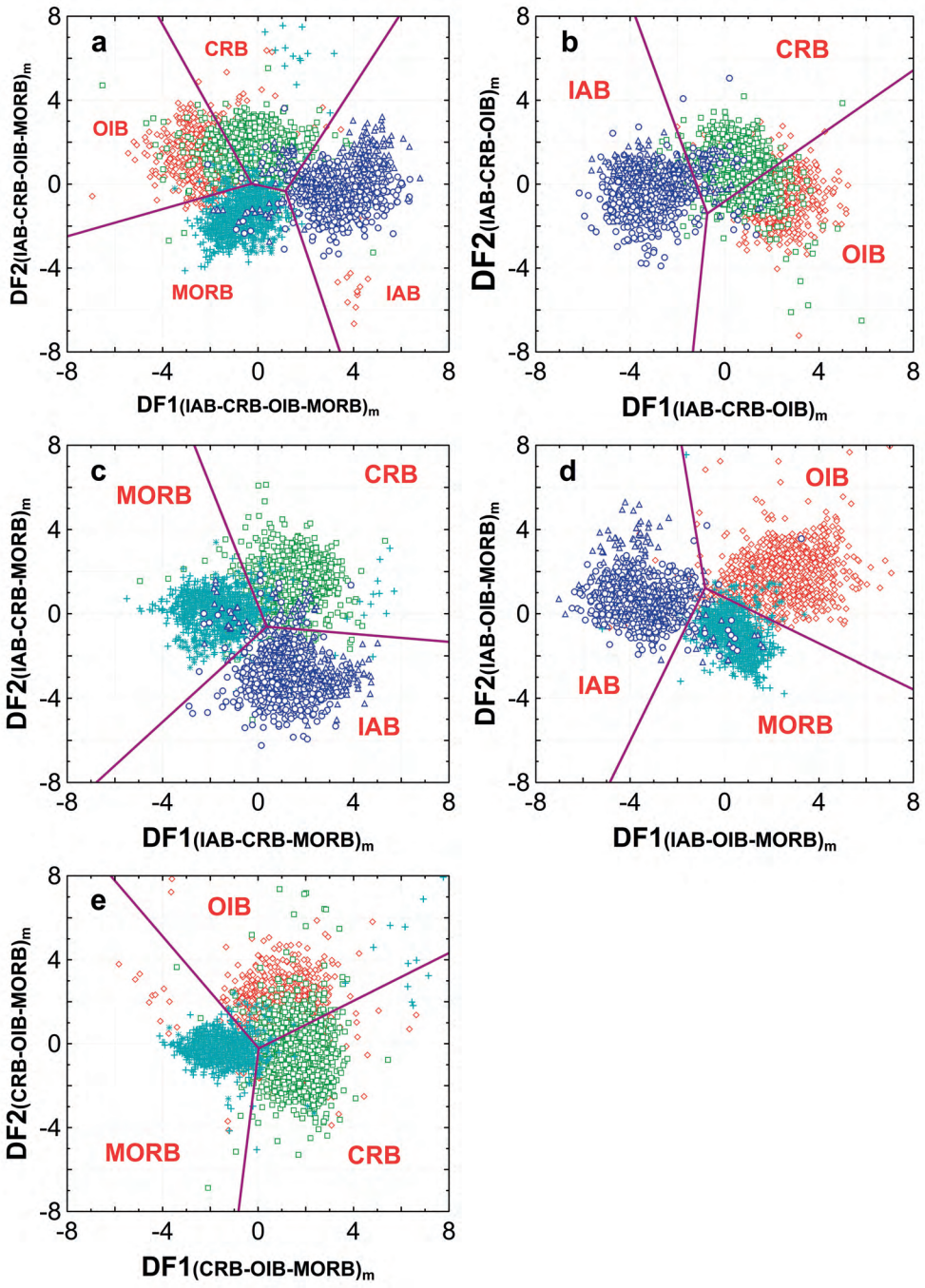

Figure 15. Statistical evaluation information of the set of five discrimination diagrams based on natural logarithm transformation of major-element ratios discriminant function DF1-DF2 (Verma *et al.* 2006) for island arc basalt (IAB), continental rift basalt (CRB), ocean-island basalt (OIB) and mid-ocean ridge basalt (MORB), using basic and ultrabasic rocks from different tectonic settings. For probability-based discrimination boundaries see the original paper by Verma *et al.* (2006). For symbols see Figure 1. Statistical results are summarised in Table 15. The subscript $_m$ refers to log-ratio transformation of major-elements. **(a)** four-groups (IAB-CRB-OIB-MORB)$_m$ diagram; **(b)** three-groups (IAB-CRB-OIB)$_m$ diagram; **(c)** three-groups (IAB-CRB-MORB)$_m$ diagram; **(d)** three-groups (IAB-OIB-MORB)$_m$ diagram; and **(e)** three-groups (CRB-OIB-MORB)$_m$ diagram.

Table 15. Statistical evaluation information of the set of five discrimination diagrams based on natural logarithm transformation of major-element ratios discriminant function DF1-DF2 (Verma *et al.* 2006) for island arc basalt (IAB), continental rift basalt (CRB), ocean-island basalt (OIB) and mid-ocean ridge basalt (MORB).

Tectonic setting	Total samples	Number of discriminated samples (%)			
		IAB	CRB	OIB	MORB
IAB-CRB-OIB-MORB					
Island arc	628 (100)	***595 (94.7)***	20 (3.2)	2 (0.3)	11 (1.8)
Island back arc	272 (100)	**229 (84.2)**	24 (8.8)	0 (0.0)	19 (7.0)
Continental rift	1270 (100)	54 (4.3)	***976 (76.8)***	204 (16.1)	36 (2.8)
Ocean-island	1473 (100)	13 (0.9)	370 (25.1)	***1065 (72.3)***	25 (1.7)
MORB	963 (100)	9 (0.9)	30 (3.1)	16 (1.7)	***908 (94.3)***
E-MORB	91 (100)	4 (4.4)	8 (8.8)	16 (17.6)	**63 (69.2)**
IAB-CRB-OIB					
Island arc	628 (100)	***595 (94.7)***	27 (4.3)	6 (1.0)	–
Island back arc	272 (100)	**228 (83.8)**	37 (13.6)	7 (2.6)	–
Continental rift	1270 (100)	38 (3.0)	***975 (76.8)***	257 (20.2)	–
Ocean-island	1473 (100)	2 (0.1)	343 (23.3)	***1128 (76.6)***	–
IAB-CRB-MORB					
Island arc	628 (100)	***592 (94.3)***	24 (3.8)	–	12 (1.9)
Island back arc	272 (100)	**227 (83.4)**	23 (8.5)	–	22 (8.1)
Continental rift	1270 (100)	36 (2.8)	***1181 (93.0)***	–	53 (4.2)
MORB	963 (100)	11 (1.2)	32 (3.3)	–	***920 (95.5)***
E-MORB	91 (100)	4 (4.4)	18 (19.8)	–	**69 (75.8)**
IAB-OIB-MORB					
Island arc	628 (100)	***610 (97.1)***	–	3 (0.5)	15 (2.4)
Island back arc	272 (100)	**246 (90.5)**	–	2 (0.7)	24 (8.8)
Ocean-island	1473 (100)	15 (1.0)	–	***1405 (95.4)***	53 (3.6)
MORB	963 (100)	8 (0.8)	–	19 (2.0)	***936 (97.2)***
E-MORB	91 (100)	4 (4.4)	–	29 (31.9)	**58 (63.7)**
CRB-OIB-MORB					
Continental rift	1270 (100)	–	***987 (77.7)***	242 (19.1)	41 (3.2)
Ocean-island	1473 (100)	–	339 (23.0)	***1103 (74.9)***	31 (2.1)
MORB	963 (100)	–	24 (2.5)	28 (2.9)	***911 (94.6)***
E-MORB	91 (100)	–	8 (8.8)	23 (25.3)	**60 (65.9)**

indicated that the unknown samples probably came from one of these settings.

The discriminant functions for the four group (IAB-CRB+OIB-MORB, considered as three groups if CRB and OIB are combined in one group) diagram (representing 100% of the between-groups variance) were as follows:

$$\begin{aligned} DF1_{(IAB\text{-}CRB+OIB\text{-}MORB)_{t1}} = {} & +0.3518\times\ln(La/Th)+ \\ & 0.6013\times\ln(Sm/Th)-1.3450\times\ln(Yb/Th)+ \\ & 2.1056\times\ln(Nb/Th)-5.4763 \end{aligned} \quad (26)$$

$$\begin{aligned} DF2_{(IAB\text{-}CRB+OIB\text{-}MORB)_{t1}} = {} & -0.3050\times\ln(La/Th)- \\ & 1.1801\times\ln(Sm/Th)+1.6189\times\ln(Yb/Th) \\ & +1.2260\times\ln(Nb/Th)-0.9944 \end{aligned} \quad (27)$$

The subscript $_{t1}$ refers to the first set of five trace-element based diagrams incorporating natural logarithm-transformed ratios.

Similarly, the equations (28–35) for other four diagrams are listed below. These are:

For IAB-CRB-OIB discrimination,

$$DF1_{(IAB\text{-}CRB\text{-}OIB)_{t1}} = +0.5533 \times \ln(La/Th) + 0.2173 \times \ln(Sm/Th) - 0.0969 \times \ln(Yb/Th) + 2.0454 \times \ln(Nb/Th) - 5.6305 \quad (28)$$

$$DF2_{(IAB\text{-}CRB\text{-}OIB)_{t1}} = -2.4498 \times \ln(La/Th) + 4.8562 \times \ln(Sm/Th) - 2.1240 \times \ln(Yb/Th) - 0.1567 \times \ln(Nb/Th) + 0.9400 \quad (29)$$

For IAB-CRB-MORB discrimination,

$$DF1_{(IAB\text{-}CRB\text{-}MORB)_{t1}} = +0.3305 \times \ln(La/Th) + 0.3484 \times \ln(Sm/Th) - 0.9562 \times \ln(Yb/Th) + 2.0777 \times \ln(Nb/Th) - 4.5628 \quad (30)$$

$$DF2_{(IAB\text{-}CRB\text{-}MORB)_{t1}} = -0.1928 \times \ln(La/Th) - 1.1989 \times \ln(Sm/Th) + 1.7531 \times \ln(Yb/Th) + 0.6607 \times \ln(Nb/Th) - 0.4384 \quad (31)$$

For IAB-OIB-MORB discrimination (note here discriminant function La/Th was not found to be significant in LDA),

$$DF1_{(IAB\text{-}OIB\text{-}MORB)_{t1}} = +1.7517 \times \ln(Sm/Th) - 1.9508 \times \ln(Yb/Th) + 1.9573 \times \ln(Nb/Th) - 5.0928 \quad (32)$$

$$DF2_{(IAB\text{-}OIB\text{-}MORB)_{t1}} = -2.2412 \times \ln(Sm/Th) + 2.2060 \times \ln(Yb/Th) + 1.2481 \times \ln(Nb/Th) - 0.8243 \quad (33)$$

Finally, for CRB-OIB-MORB discrimination,

$$DF1_{(CRB\text{-}OIB\text{-}MORB)_{t1}} = -0.5558 \times \ln(La/Th) - 1.4260 \times \ln(Sm/Th) + 2.2935 \times \ln(Yb/Th) - 0.6890 \times \ln(Nb/Th) + 4.1422 \quad (34)$$

$$DF2_{(CRB\text{-}OIB\text{-}MORB)_{t1}} = -0.9207 \times \ln(La/Th) + 3.6520 \times \ln(Sm/Th) - 1.9866 \times \ln(Yb/Th) + 1.0574 \times \ln(Nb/Th) - 4.4283 \quad (35)$$

The above equations were used to evaluate this final set of five diagrams (Figure 16 and Table 16). Whether CRB and OIB are presented as combined (Figure 16a) or individually (Figure 16c, d), the success rates for all four settings (IAB, CRB, OIB, and MORB) were extremely high (90.7% to 99.2%; Table 16). These rates are similar to those estimated by Agrawal *et al.* (2008) for their training and testing sets (90.9% to 98.7%).

It is also interesting to point out that Verma *et al.* (2006), using major elements, and Agrawal *et al.* (2008), using trace elements, also compared the performance (success rates) of identical datasets for LDA when crude data and log ratio-transformed data were used, and demonstrated that the success rates significantly increased when the log ratio-transformation process was combined with LDA, i.e., when correct statistical treatment for compositional data was employed (see Agrawal & Verma 2007).

When CRB and OIB were both present in a given diagram (Figure 16b, e), the success rates for these two settings were considerably smaller (55.0% to 74.7%, compared to 93.4% to 99.2% in Figure 16a, c, e; Table 16) and slightly less than those (56.2% to 85.0%) estimated by Agrawal *et al.* (2008) for their training and testing sets.

In this work, I also evaluated the performance of back arc data in these five diagrams (Figure 16a–e). About 79.0% to 84.0% of samples were correctly discriminated as IAB (Table 16). The performance of these diagrams for E-MORB could not be evaluated because very small number of samples had the required chemical elements compiled in the present work (only 11 samples with all five trace-elements; Table 16).

The above analysis clearly indicates that this set of five diagrams, based on relatively immobile elements, can be successfully applied to decipher tectonic settings of tectonically complex areas as well as older terranes with unknown or undetermined

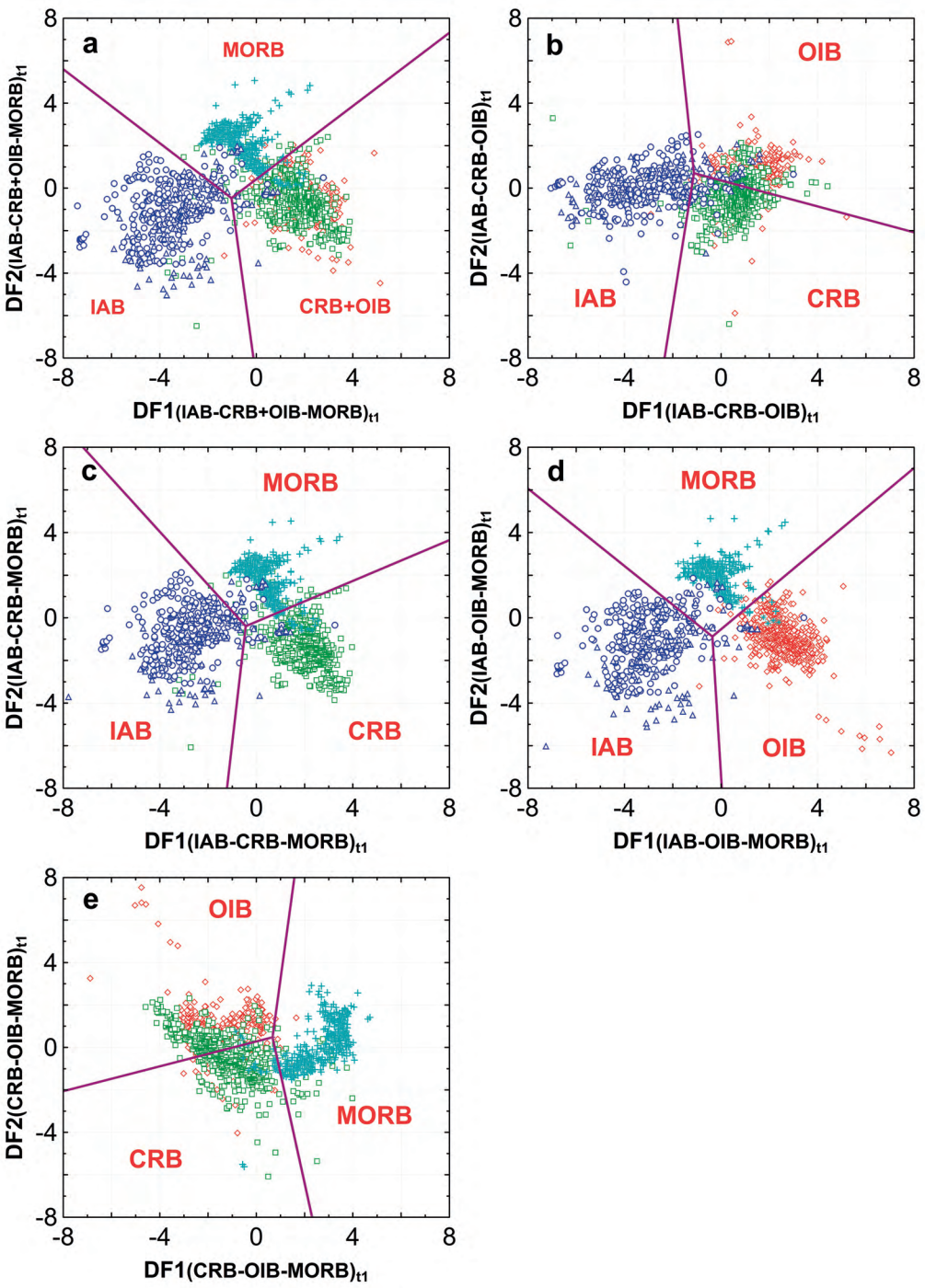

Figure 16. Statistical evaluation of the set of five discrimination diagrams based on natural logarithm transformation of trace-element ratios discriminant function DF1-DF2 (Agrawal *et al.* 2008) for island arc basalt (IAB), continental rift basalt (CRB), ocean-island basalt (OIB) and mid-ocean ridge basalt (MORB), using basic and ultrabasic rocks from different tectonic settings. For probability-based discrimination boundaries see the original paper by Agrawal *et al.* (2008). For symbols see Figure 1. Statistical results are summarised in Table 16. The subscript $_{t1}$ refers to log-ratio transformation of trace-elements (subscript $_{t1}$ instead of simply $_{t}$ was used, so this set of diagrams could be distinguished from the other set currently under preparation by Verma & Agrawal). **(a)** four-groups $(IAB\text{-}CRB+OIB\text{-}MORB)_{t1}$ diagram; **(b)** three-groups $(IAB\text{-}CRB\text{-}OIB)_{t1}$ diagram; **(c)** three-groups $(IAB\text{-}CRB\text{-}MORB)_{t1}$ diagram; **(d)** three-groups $(IAB\text{-}OIB\text{-}MORB)_{t1}$ diagram; and **(e)** three-groups $(CRB\text{-}OIB\text{-}MORB)_{t1}$ diagram.

Table 16. Statistical evaluation of the set of five discrimination diagrams based on natural logarithm transformation of trace-element ratios discriminant function DF1–DF2 (Agrawal *et al.* 2008) for island arc basalt (IAB), continental rift basalt (CRB), ocean-island basalt (OIB) and mid-ocean ridge basalt (MORB).

Tectonic setting	Total samples	Number of discriminated samples (%)				
		IAB	Within-plate			MORB
			CRB+OIB	CRB	OIB	
IAB-CRB-OIB-MORB						
Island arc	280 (100)	***255 (91.1)***	8 (2.8)	–	–	17 (6.1)
Island back arc	119 (100)	**99 (83.2)**	11 (9.2)	–	–	9 (7.6)
Continental rift	604 (100)	10 (1.6)	**564 (93.4)**	–	–	30 (5.0)
Ocean-island	726 (100)	1 (0.1)	**720 (99.2)**	–	–	5 (0.7)
MORB	404 (100)	0 (0.0)	14 (3.5)	–	–	***390 (96.5)***
E-MORB	11	–	–	–	–	–
IAB-CRB-OIB						
Island arc	280 (100)	***250 (89.3)***	–	19 (6.8)	11 (3.9)	–
Island back arc	119 (100)	**94 (79.0)**	–	5 (4.2)	20 (16.8)	–
Continental rift	604 (100)	16 (2.6)	–	***389 (64.4)***	199 (32.9)	–
Ocean-island	726 (100)	3 (0.4)	–	214 (29.5)	***509 (70.1)***	–
IAB-CRB-MORB						
Island arc	280 (100)	***259 (92.5)***	–	8 (2.9)	–	13 (4.6)
Island back arc	119 (100)	**100 (84.0)**	–	10 (8.4)	–	9 (7.6)
Continental rift	604 (100)	9 (1.5)	–	***564 (93.4)***	–	31 (5.1)
MORB	404 (100)	0 (0.0)	–	19 (4.7)	–	***385 (95.3)***
IAB-OIB-MORB						
Island arc	280 (100)	***254 (90.7)***	–	–	5 (1.8)	21 (7.5)
Island back arc	119 (100)	**97 (81.5)**	–	–	10 (8.4)	12 (10.1)
Ocean-island	726 (100)	1 (0.1)	–	–	***715 (98.5)***	10 (1.4)
MORB	404 (100)	0 (0.0)	–	–	7 (1.7)	***397 (98.3)***
CRB-OIB-MORB						
Continental rift	604 (100)	–	–	***332 (55.0)***	242 (40.1)	30 (5.0)
Ocean-island	726 (100)	–	–	178 (24.5)	***542 (74.7)***	6 (0.8)
MORB	404 (100)	–	–	1 (0.3)	19 (4.7)	***384 (95.0)***

tectonic setting. These two most recent sets of diagrams (Verma *et al.* 2006; Agrawal *et al.* 2008) are therefore the best choice for most applications until newer (2010) diagrams (work in progress; see the Discussion section) are published for this purpose.

Application of New Discriminant Function Diagrams

From the statistical evaluation presented in this paper, only the new discriminant function diagrams seem to provide reliable results for discriminating all four tectonic settings of IAB, CRB, OIB, and MORB. In order to illustrate the use of the most recent sets of diagrams (Verma *et al.* 2006; Agrawal *et al.* 2008) to geochemical data from Turkey, many papers were found to present interesting data (e.g., Floyd 1993; Boztuğ *et al.* 1998; Floyd *et al.* 1998; Parlak *et al.* 1998; Şen *et al.* 1998; Tankut *et al.* 1998; Yılmaz & Boztuğ 1998; Parlak 2000; Akal 2003; Tokcaer *et al.* 2005; Aldanmaz 2006; Ersoy & Helvacı 2007; Şen 2007; Tatar *et al.* 2007; Bağcı *et al.* 2008; Çelik 2008; Çelik & Chiaradia 2008; Önal 2008; Varol *et al.* 2008), to any of which this discrimination technique can be applied.

Three case studies were selected to illustrate the use of these two sets of diagrams: (i) Quaternary Kula volcanic rocks from western Anatolia (Tokcaer *et al.* 2005; complemented from other papers); (ii) Jurassic volcanism in the eastern Pontides (Şen 2007); and (iii) dykes from Tauride belt ophiolites, SW Turkey (Çelik & Chiaradia 2008). The results are presented in Figure 17 and Table 17 for major element based diagrams (Verma *et al.* 2006) and in Figure 18 and Table 18 for trace element based diagrams (Agrawal *et al.* 2008).

Quaternary Kula Plateau Basalt, Western Anatolia (Tokcaer et al. 2005)

The complex tectonic history of western Anatolia was summarised by Tokcaer *et al.* (2005). These authors presented major element geochemical data for ten samples of Kula plateau basaltic volcanism and also reported complete trace element data for five of these samples. They concluded that the Kula basaltic magmas record rapid uplifting of asthenospheric material in western Anatolia and related their origin to the slab window formation. In the light of the complex tectonic and petrogenetic models, I ask the question: What tectonic setting do the major-element compositions of these magmas reflect? And is it the same as inferred from their trace-element data?

In answer, I applied the new discriminant function diagrams to the geochemical data of Tokcaer *et al.* (2005). Additionally, data from other researchers (Borsi *et al.* 1972; Ercan 1981; Ercan *et al.* 1985, 1996; Güleç 1991; Richardson-Bunbury 1996; Alıcı *et al.* 2002; Agostini 2003; Innocenti *et al.* 2005; also F. Innocenti, unpublished data–compiled by S. Agostini) were considered in this interpretation.

The results of this application (Figures 17 & 18; Tables 17 & 18) clearly indicate a continental rift setting for the Kula volcanic rocks.

The procedure to use the correct four of the five major- or trace-element based diagrams is as follows (see Table 17 or 18 in combination with Figure 17 or 18, respectively):

The first four-groups diagram (IAB-CRB-OIB-MORB in Figure 17a or IAB-CRB+OIB-MORB in Figure 18a) is used to check whether the indicated setting is either CRB or OIB (Table 17), or CRB+OIB (Table 18). For Kula, Figure 17a (major-elements; Table 17) indicates that CRB is likely and Figure 18a (trace-elements; Table 18) indicates that CRB+OIB is likely.

In the next step, use the first three-groups IAB-CRB-OIB diagram (Figure 17b or 18b) to confirm the conclusion of step (i) for major-elements (whether CRB or OIB) (Figure 17b; Table 17) and to decide which of the two (CRB or OIB) is more likely for trace-elements (Figure 18b; Table 18). For Kula, Figure 17b (Table 17) confirms its CRB setting, whereas on Figure 18b (Table 18), a CRB setting is to be preferred to OIB. The choice is therefore confirmed in this case in favour of the CRB setting from both sets of diagrams.

In the final step, we should omit the diagram that does not contain the indicated setting in steps (i) and (ii). For Kula, because CRB setting is indicated, we should discard the diagram IAB-OIB-MORB (Figure 17d for major-elements and Figure 18b for trace-elements) from further considerations.

The conclusion for Kula is a CRB setting, as consistently inferred from both the major- and trace-element data interpreted in these discriminant function diagrams. Because alteration effects probably are of no concern in these Quaternary rocks, the indications from both sets of diagrams (Figures 17 & 18) are fully consistent. It is important to note that the limited data of Tokcaer *et al.* (2005) are fully consistent with the more complete dataset from Kula (see Figures 17 & 18 and Tables 17 & 18). The results clearly indicate a continental rift setting for Kula.

Jurassic Volcanism in the Eastern Pontides (Şen 2007)

Şen asked the question in the very title of this paper (Şen 2007): 'Is this volcanism rift related or subduction related?'. It was suggested from various lines of evidence that these Jurassic rocks from the eastern Pontides are subduction-related. Other authors (cited in Şen 2007) had also argued that this volcanism was, in fact, rift-related. I chose this

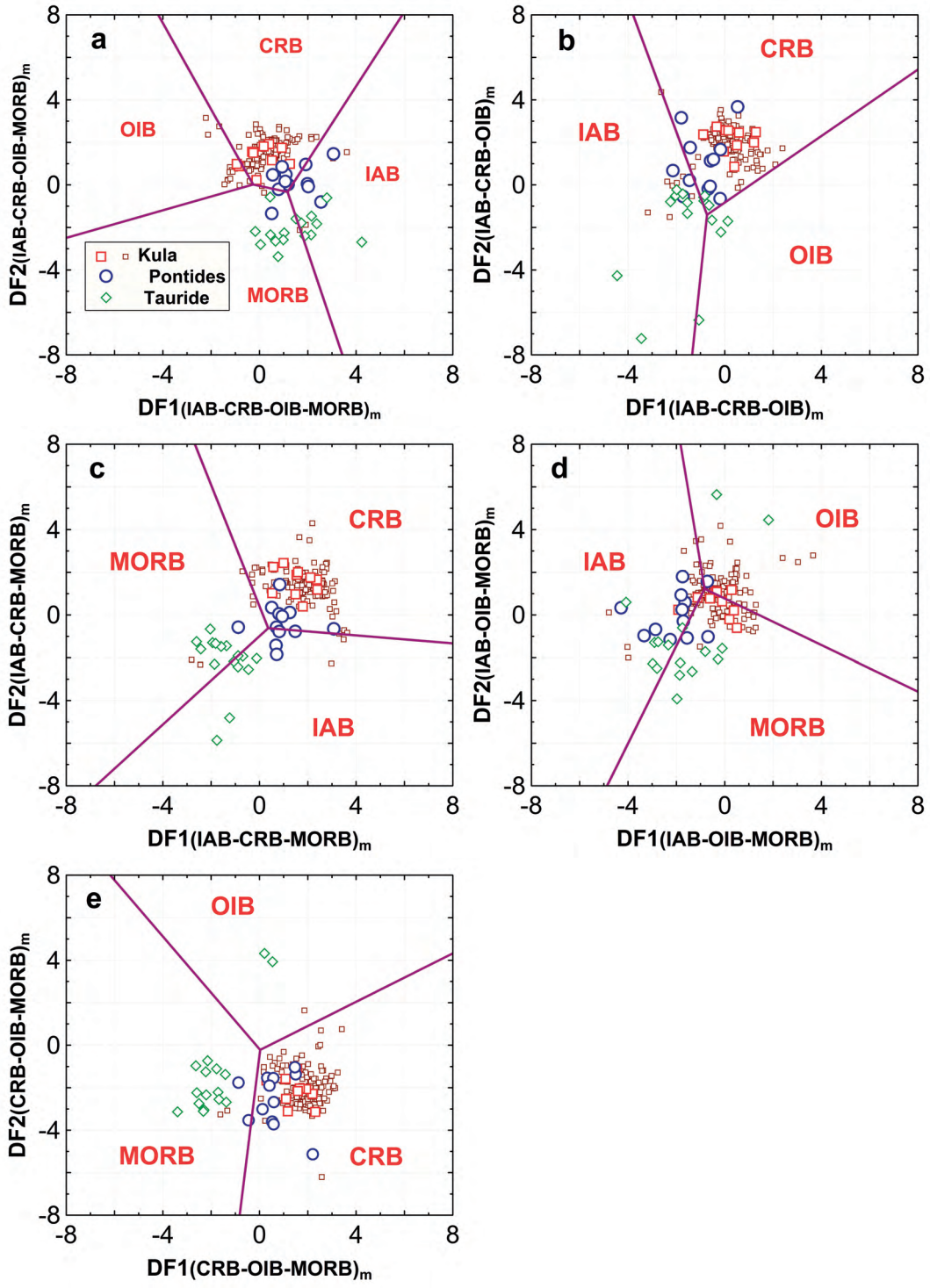

Figure 17. Statistical evaluation of the application of the set of five discrimination diagrams based on natural logarithm transformation of major-element ratios discriminant function DF1–DF2 (Verma *et al.* 2006) for island arc basalt (IAB), continental rift basalt (CRB), ocean-island basalt (OIB) and mid-ocean ridge basalt (MORB), to three areas of Turkey (Kula volcanics: Tokcaer *et al.* 2005 and other sources – see text for more details; Eastern Pontides: Şen 2007; and dikes in Lycian ophiolites: Çelik & Chiaradia 2008). Symbols are explained as inset in Figure 17a, except that large red squares are for data from Tokcaer *et al.* (2005) and smaller squares are for other sources. Statistical results are summarised in Table 17.

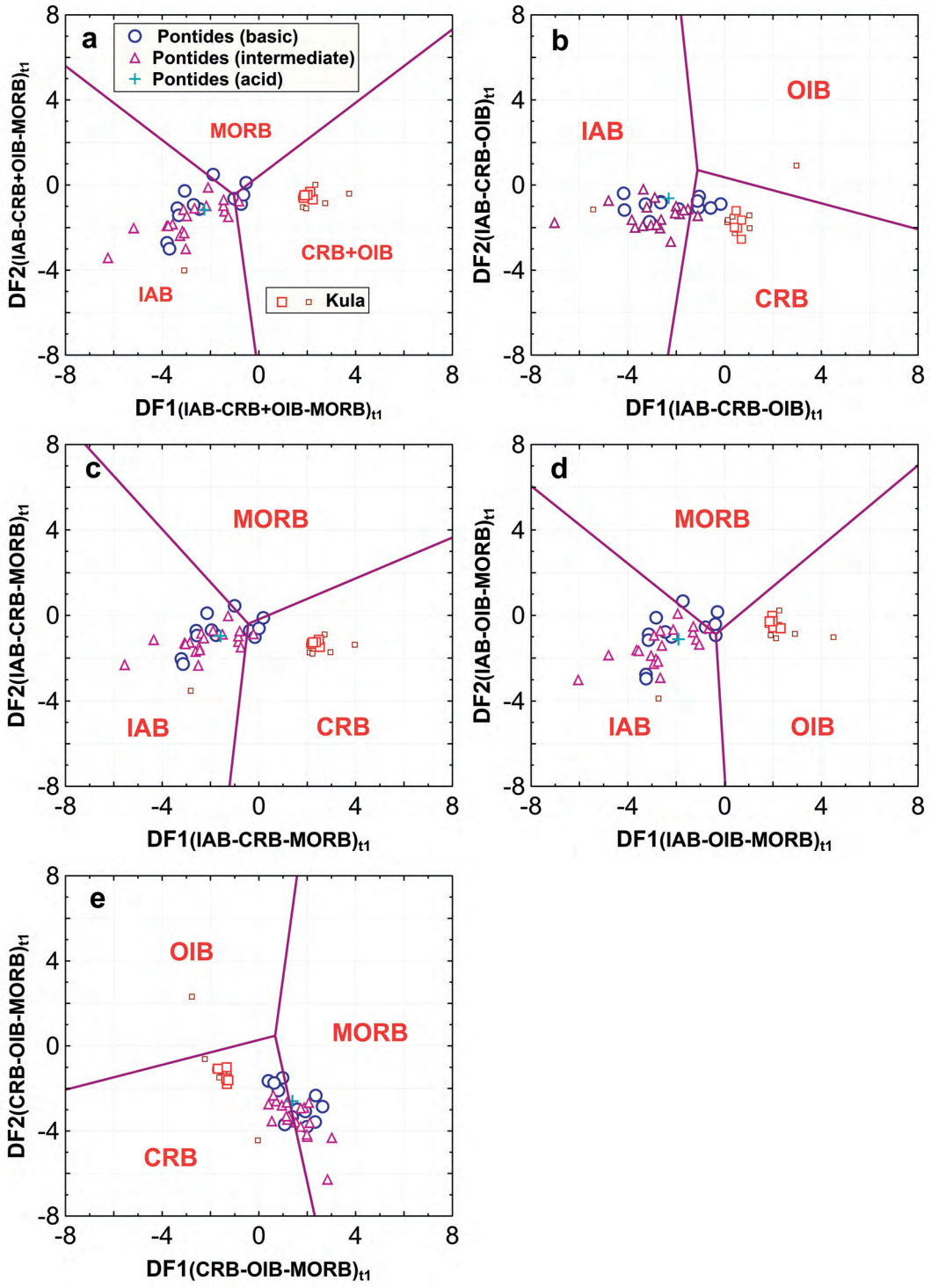

Figure 18. Statistical information of the application of the set of five discrimination diagrams based on natural logarithm transformation of trace-element ratios discriminant function DF1-DF2 (Agrawal *et al.* 2008) for island arc basalt (IAB), continental rift basalt (CRB), ocean-island basalt (OIB) and mid-ocean ridge basalt (MORB), to two areas of Turkey (Kula volcanics: Tokcaer *et al.* 2005; and Eastern Pontides: Şen 2007, note basic and intermediate rocks were separately used for this application). Symbols are explained as inset in Figure 18a, except that large red squares are for data from Tokcaer *et al.* (2005) and smaller squares are for other sources. Statistical results are summarised in Table 18.

Table 17. Statistical information of the application of the set of five discrimination diagrams based on natural logarithm transformation of major-element ratios discriminant function DF1-DF2 (Verma *et al.* 2006) for island arc basalt (IAB), continental rift basalt (CRB), ocean-island basalt (OIB) and mid-ocean ridge basalt (MORB), to three areas of Turkey.

Tectonic setting	Total samples	Number of discriminated samples (%)			
		IAB	CRB	OIB	MORB
Kula volcanics (Tokcaer *et al.* 2005)					
IAB-CRB-OIB-MORB	10 (100)	0 (0)	**8** (80)	2 (20)	0 (0)
IAB-CRB-OIB	10 (100)	0 (0)	**10** (100)	0 (0)	–
IAB-CRB-MORB	10 (100)	0 (0)	**10** (100)	–	0 (0)
IAB-OIB-MORB *	10 (100)	–	–	–	–
CRB-OIB-MORB	10 (100)	–	**10** (100)	0 (0)	0 (0)
Kula volcanics (other data – see text for details)					
IAB-CRB-OIB-MORB	190 (100)	3 (1.6)	**168** (88.4)	17 (8.9)	2 (1.1)
IAB-CRB-OIB	190 (100)	8 (4.2)	**182** (95.8)	0 (0)	–
IAB-CRB-MORB	190 (100)	2 (1.1)	**183** (96.3)	–	5 (2.6)
IAB-OIB-MORB *	190 (100)	–	–	–	–
CRB-OIB-MORB	190 (100)	–	**187** (98.4)	1 (0.5)	2 (1.1)
Eastern Pontides (basic)					
IAB-CRB-OIB-MORB	12 (100)	5 (42)	**6** (50)	0 (0)	1 (8)
IAB-CRB-OIB	12 (100)	3 (25)	**9** (75)	0 (0)	–
IAB-CRB-MORB	12 (100)	4 (33)	**7** (58)	–	1 (8)
IAB-OIB-MORB *	12 (100)	–	–	–	–
CRB-OIB-MORB	12 (100)	–	**10** (83)	0 (0)	2 (17)
Dikes in Lycian ophiolites (basic)					
IAB-CRB-OIB-MORB	16 (100)	7 (44)	0 (0)	0 (0)	9 (56)
IAB-CRB-OIB	16 (100)	8 (50)	4 (25)	4 (25)	–
IAB-CRB-MORB	16 (100)	7 (44)	0 (0)	–	9 (56)
IAB-OIB-MORB	16 (100)	7 (44)	–	2 (12)	7 (44)
CRB-OIB-MORB	16 (100)	–	0 (0)	2 (12)	14 (88)

* Unwanted diagram for this application (should not be used for the tectonic interpretion of these data).

example to highlight the application of discriminant function diagrams to an area of complex or controversial tectonic setting, with alteration effects superimposed on them.

In this example alteration effects might play a significant role in the interpretation of major element based diagrams (Figure 17; Table 17). From major elements of only basic rocks from the Pontides area (Figure 17), probably affected by alteration, it appears that a rift setting is more likely than an arc setting. However, using both basic and intermediate rocks in the trace element based diagrams (Figure 18; Table 18), a subduction-related or arc setting is more likely. Because these diagrams are for basic and ultrabasic rocks, the use of intermediate rocks is not generally recommended. I suggest that the conclusion of immobile trace-element based diagrams (Agrawal *et al.* 2008) should be regarded as valid. This inference could, in future, be further tested from the still newer diagrams currently under investigation (Verma & Agrawal, in preparation).

Table 18. Statistical information of the application of the set of five discrimination diagrams based on natural logarithm transformation of trace-element ratios discriminant function DF1-DF2 (Agrawal *et al.* 2008) for island arc basalt (IAB), continental rift basalt (CRB), ocean-island basalt (OIB) and mid-ocean ridge basalt (MORB), to two areas of Turkey.

Tectonic setting	Total samples	Number of discriminated samples (%)				
		IAB	Within-plate			MORB
			CRB+OIB	CRB	OIB	
Kula volcanics (Tokcaer *et al.* 2005)						
IAB-CRB-OIB-MORB	5 (100)	0 (0)	**5** (100)	–	–	0 (0)
IAB-CRB-OIB	5 (100)	0 (0)	–	**5** (100)	0 (0)	–
IAB-CRB-MORB	5 (100)	0 (0)	–	**5** (100)	–	0 (0)
IAB-OIB-MORB *	5 (100)	–	–	–	–	–
CRB-OIB-MORB	5 (100)	–	–	**5** (100)	0 (0)	0 (0)
Kula volcanics (other data – see text for details)						
IAB-CRB-OIB-MORB	17 (100)	1 (6)	**16** (94)	–	–	0 (0)
IAB-CRB-OIB	17 (100)	1 (6)	–	**15** (88)	1 (6)	–
IAB-CRB-MORB	17 (100)	1 (6)	–	**16** (94)	–	0 (0)
IAB-OIB-MORB *	17 (100)	–	–	–	–	–
CRB-OIB-MORB	17 (100)	–	–	**16** (94)	1 (0)	0 (0)
Eastern Pontides (basic)						
IAB-CRB-OIB-MORB	12 (100)	**8** (66)	2 (17)	–	–	2 (17)
IAB-CRB-OIB	12 (100)	**7** (58)	–	5 (42)	0 (0)	–
IAB-CRB-MORB	12 (100)	**7** (58)	–	4 (33)	–	1 (8)
IAB-OIB-MORB	12 (100)	**9** (75)	–	–	0 (0)	3 (25)
CRB-OIB-MORB *	12 (100)	–	–	–	–	–
Eastern Pontides (intermediate **)						
IAB-CRB-OIB-MORB	19 (100)	**18** (95)	1 (5)	–	–	–
IAB-CRB-OIB	19 (100)	**18** (95)	–	1 (5)	0 (0)	–
IAB-CRB-MORB	19 (100)	**18** (95)	–	1 (5)	–	1 (5)
IAB-OIB-MORB	19 (100)	**18** (95)	–	–	0 (0)	1 (5)
CRB-OIB-MORB *	19 (100)	–	–	9 (47)	0 (0)	10 (53)

* Unwanted diagram for this application (should not be used for the tectonic interpretion of these data).
** One dacite sample also reported by Şen (2007) consistenly plotted in the IAB field (see Figure 18).

Dykes from Tauride Belt Ophiolites, SW Turkey (Çelik & Chiaradia 2008)

These authors presented geochemical data from dolerite and gabbroic dykes cutting Lycian ophiolites in the western Taurides and suggested that all dykes, whether metamorphosed or not, have the same subduction-related origin. They used two conventional bivariate and two ternary diagrams (Pearce & Cann 1973; Pearce & Norry 1979; Shervais 1982; Meschede 1986), all of which indicated that the rocks plotted in the overlap regions of IAB and MORB. Thus, from radiogenic isotope data and other evidence including discrimination diagrams, Çelik & Chiaradia (2008) concluded a subduction-related setting for the dykes emplaced in this area.

The results of the application of the major element based diagrams (Figure 17; Table 17) are ambiguous; both arc and mid-ocean ridge settings are indicated. The samples distribute about equally between these two settings (with somewhat greater indication of MORB setting), but alteration effects of major elements in these diagrams cannot be evaluated. Unfortunately, complete trace element datasets were not presented by these authors; Th is missing from the data presented by Çelik & Chiaradia (2008). Therefore, the trace element based

diagrams (Agrawal *et al.* 2008) could not be applied to this area. Interestingly, the geochemical data presented by these authors could be used, in future, to apply the newer (2010) discriminant function diagrams currently under preparation (see the next section).

Discussion

Most existing and widely used bivariate and ternary discrimination diagrams evaluated in this work are shown to perform either unsatisfactorily or less efficiently (with smaller success rates) than the discriminant function diagrams, especially the newer ones proposed during 2004–2008. A major problem with bivariate and ternary diagrams is that they probably represent too few chemical variables to correctly handle the multivariate problem of tectonic discrimination. The closure and constant sum problem is another factor that requires the application of correct statistical treatment for handling of compositional data (Chayes 1960, 1978; Aitchison 1981, 1982, 1984, 1986, 1989; Aitchison *et al.* 2000, 2003; Egozcue *et al.* 2003; Aitchison & Egozcue 2005). Boundary lines, although listed by Rickwood (1989) for a better reproduction, were all based on the subjective judgement by eye fitting as practiced by the authors of discrimination diagrams before 2004 (Agrawal 1999; Agrawal *et al.* 2004). The representativeness of the initial datasets used for proposing these various diagrams may be another factor that affects their application (Verma *et al.* 2006; Agrawal & Verma 2007).

However, the proposal of combined (overlapping) fields for tectonic settings in some of the older diagrams (e.g., Pearce & Cann 1973; Pearce & Norry 1979; Pearce 1982) cannot be considered an advantage. This is because in the newer diagrams (2004–2008), mixing of sources, or transition of tectonic settings, will be shown by trends (sometimes linear if binary mixing of simple, homogeneous end-members is involved) that extend from the field of one tectonic setting to the other (see Agrawal *et al.* 2008). The advantage of these new diagrams (2004–2008) would be that the relative importance of the two (or more) tectonic settings could be visualized by the corresponding success rates for individual tectonic settings.

The problem of ternary diagrams is made even worse because the very construction of such diagrams introduces the closure effect. Futhermore, even for the older discriminant function diagrams, the boundaries were drawn by eye (Pearce 1976; Butler & Woronow 1986) and were not probability-based (Agrawal 1999).

Most, if not all, of these problems were overcome in recent diagrams by Verma *et al.* (2006) and Agrawal *et al.* (2008) as stressed by Agrawal & Verma (2007). A still newer set of such diagrams based on immobile elements –Ti, V, Y, Nb, and Zr– easily determinable by conventional x-ray fluorescence techniques is currently under investigation (Verma & Agrawal, manuscript in preparation). One final requirement implicit in LDA is that the natural logarithm transformed ratios used in this analysis should be normally distributed. Therefore, any statistical 'contamination' must be identified (Barnett & Lewis 1994; Verma & Quiroz-Ruiz 2006a, b, 2008; Verma 2008; Verma *et al.* 2008) before carrying out the discriminant analysis. The identification and treatment of discordant outliers is slowly becoming a standard practice for handling of experimental data (Verma 2005; Castrellon-Uribe *et al.* 2008; Díaz-González *et al.* 2008; Nagarajan *et al.* 2008; Obeidat *et al.* 2008; Palabiyik & Serpen 2008; Vattuone *et al.* 2008; Gómez-Arias *et al.* 2009; González-Ramírez *et al.* 2009; Madhavaraju & Lee 2009; Pandarinath 2009; Rodríguez-Ríos & Torres-Aguilera 2009; Verma *et al.* 2009a, b; Torres-Alvarado *et al.* 2010). The newer diagrams (2010) under preparation by Verma & Agrawal will also comply with this final recommendation for correctly applying LDA to compositional data.

Although a few discriminant function diagrams were proposed long ago, they have been little used, whereas simpler bivariate and ternary diagrams, shown here to perform worse than the former, are too frequently used, with thousands of references in the published literature. What could be the reason for this biased behaviour of the geological community? I guess the reason is the complexity of calculations of the discriminant functions required for the adequate use of these diagrams. That is the reason why for the newer diagrams (Agrawal *et al.* 2004, 2008; Verma *et al.* 2006), the authors have prepared Excel templates to facilitate their

application. The templates are likely to avoid frequent errors in the use of these diagrams and some discrepancies in the original papers, and thus make the application more reliable. These can be made available on request from the authors. In fact, a computer program is currently under preparation (by Verma and Rivera-Gómez) that would facilitate the use of all these complex discriminant-function based new diagrams for the discrimination of basic and ultrabasic magmas.

Finally, new diagrams are still required to discriminate other rock types, such as high-Mg, primitive magma varieties, or more differentiated intermediate types – a work yet to be done from representative databases and the above-mentioned correct statistical methodology. Discriminating primitive magmas from different tectonic settings would be a relatively easy task; the only problem might be to build a representative database. For intermediate rocks, on the other hand, it is not clear if such magma types could be well discriminated in new discrimination diagrams, although there are good indications from the recent work of Verma (2009a) that it should be possible to do so with relatively high success rates. Verma (2009a) has shown that both basic as well as intermediate magmas from island arcs and continental rifts are significantly different in their LILE/HFSE and LILE/LREE ratios (LILE–large ion lithophile elements; HFSE–high-field strength elements; LREE–light rare-earth elements). Some of these elements, particularly those designated as immobile elements, could thus be used to propose new discriminant function discrimination diagrams for intermediate magmas that should be useful for both complex as well as older terrains.

Conclusions

The statistical evaluation of a total of 28 bivariate, ternary and discriminant function discrimination diagrams indicated that only the more recent ones (2004–2008) could be totally recommended for use in future work. These newer diagrams (Verma *et al.* 2006; Agrawal *et al.* 2008) were proposed following exact statistical methodology of natural log-ratio transformation. Three application examples from Turkey also confirmed their usefulness, especially for areas of complex tectonic setting when geochemical data on relatively fresh rocks are available. Both sets of diagrams (major- and trace-element based) provided fully consistent results for Kula volcanic rocks. The trace element based diagrams are more useful for altered rocks or older terrains than the major element based diagrams, as confirmed by the application to the eastern Pontides area. The application to Lycian ophiolite area remains to be resolved by additional trace-element data (Th was missing from the dataset) or still newer diagrams. Work currently under progress should provide yet another set of immobile element based diagrams (Verma and Agrawal, in preparation) that would complement the existing set of trace-element based diagrams (Agrawal *et al.* 2008).

Acknowledgements

I am grateful to my Turkish friends, Tahir Öngür, Ümran Serpen, Cahit Helvacı, Reşat Ulusay, Zeynal Ergüler, among others, for inviting me to the 61st Geological Congress of Turkey, Ankara, March 2008, providing excellent hospitality both in Ankara and İstanbul and during the field trip. This short visit motivated me to expand on my presentation during this Congress with the outcome in the form of two papers –this paper and a second one coauthored by R. Rodríguez-Ríos and R. González-Ramírez, both of them being submitted to the prestigious Turkish Journal of Earth Sciences (TJES). I am also much grateful to the editor-in-chief Erdin Bozkurt for promptly and favourably deciding on the suitability of these manuscripts for their possible publication in TJES. I thank Samuele Agostini and an anonymous reviewer; both of them, while highly appreciating my work, provided numerous useful suggestions for improvement. Samuele Agostini is also further thanked for making his unpublished geochemical compilation on Turkey available to me for revising this manuscript. I am grateful to Alfredo Quiroz-Ruiz for computer maintainance and for help with the preparation of figures in their final form. John A. Winchester edited English of the final text and Yalçın Ersoy translated the abstract to Turkish.

References

Agostini, S. 2003. *Il magmatismo post-collisionale dell'Anatolia occidentale: caratteri geochimici e petrologici, distribuzione spazio-temporale, quadro geodinamico (Post-collisional Western Anatolia Magmatism: Geochemical and Petrologic Characters, Space-time Distribution, Geodynamic Framework)*. PhD Thesis, University of Pisa, Pisa-Italy.

Agrawal, S. 1999. Geochemical discrimination diagrams: a simple way of replacing eye-fitted boundaries with probability based classifier surfaces. *Journal of the Geological Society of India* **54**, 335–346.

Agrawal, S., Guevara, M. & Verma, S.P. 2004. Discriminant analysis applied to establish major-element field boundaries for tectonic varieties of basic rocks. *International Geology Review* **46**, 575–594.

Agrawal, S., Guevara, M. & Verma, S.P. 2008. Tectonic discrimination of basic and ultrabasic rocks through log-transformed ratios of immobile trace elements. *International Geology Review* **50**, 1057–1079.

Agrawal, S. & Verma, S.P. 2007. Comment on 'Tectonic classification of basalts with classification trees' by Pieter Vermeesch (2006). *Geochimica et Cosmochimica Acta* **71**, 3388–3390.

Ahmad, T., Deb, M., Tarney, J. & Raza, M. 2008. Proterozoic mafic volcanism in the Aravalli-Delhi orogen, northwestern India: Geochemistry and tectonic framework. *Journal of the Geological Society of India* **72**, 93–111.

Aitchison, J. 1981. A new approach to null correlations of proportions. *Mathematical Geology* **13**, 175–189.

Aitchison, J. 1982. The statistical analysis of compositional data. *Journal of the Royal Statistical Society* **44**, 139–177.

Aitchison, J. 1984. Reducing the dimensionality of compositional data set. *Mathematical Geology* **16**, 617–635.

Aitchison, J. 1986. *The Statistical Analysis of Compositional Data*. Chapman and Hall, London New York.

Aitchison, J. 1989. Measures of location of compositional data sets. *Mathematical Geology* **21**, 787–790.

Aitchison, J., Barceló-Vidal, C., Martín-Fernández, J.A. & Pawlowsky-Glahn, V. 2000. Logratio analysis and compositional distance. *Mathematical Geology* **32**, 271–275.

Aitchison, J. & Egozcue, J.J. 2005. Compositional data analysis: Where are we and where should we be heading? *Mathematical Geology* **37**, 829–850.

Aitchison, J., Mateau-Figueras, G. & Ng, K.W. 2003. Characterization of distributional forms for compositional data and associated distribution tests. *Mathematical Geology* **35**, 667–680.

Akal, C. 2003. Mineralogy and geochemistry of melilite leucitites, Balçıkhisar, Afyon (Turkey). *Turkish Journal of Earth Sciences* **12**, 215–239.

Alam, M.A., Chandrasekharam, D., Vaselli, O., Capaccioni, B., Manetti, P. & Santo, P.B. 2004. Petrology of the prehistoric lavas and dyke of the Barren island, Andaman Sea, Indian Ocean. *Proceedings of the Indian Academy of Sciences (Earth and Planetary Sciences)* **113**, 715–722.

Aldanmaz, E. 2006. Mineral-chemical constraints on the Miocene calc-alkaline and shoshonitic volcanic rocks of western Turkey: disequilibrium phenocryst assemblages as indicators of magma storage and mixing conditions. *Turkish Journal of Earth Sciences* **15**, 47–73.

Aldanmaz, E., Pearce, J.A., Thirlwall, M.F. & Mitchell, J.G. 2000. Petrogenetic evolution of late Cenozoic, post-collision volcanism in western Anatolia, Turkey. *Journal of Volcanology and Geothermal Research* **102**, 67–95.

Alici, P., Temel, A. & Gourgaud, A. 2002. Pb-Nd-Sr isotope and trace element geochemistry of Quaternary extension-related alkaline volcanism: a case study of Kula region (western Anatolia, Turkey). *Journal of Volcanology and Geothermal Research* **115**, 487–510.

Aoki, K.-I., Yoshida, T., Yusa, K. & Nakamura, Y. 1985. Petrology and geochemistry of the Nyamuragira volcano, Zaire. *Journal of Volcanology and Geothermal Research* **25**, 1–28.

Appelquist, K., Cornell, D. & Brander, L. 2008. Age, tectonic setting and petrogenesis of the Habo Volcanic Suite: evidence for an active continental margin setting for the TransScandinavian Igneous Belt. *GFF* (Part 3) **130**, 123–138.

Arculus, R.J. 1976. Geology and geochemistry of the alkali basalt-andesite association of Grenada, Lesser Antilles island arc. *Geological Society of America Bulletin* **87**, 612–624.

Armstrong-Altrin, J.S. & Verma, S.P. 2005. Critical evaluation of six tectonic setting discrimination diagrams using geochemical data of Neogene sediments from known tectonic settings. *Sedimentary Geology* **177**, 115–129.

Auchapt, A., Dupuy, C., Dostal, J. & Kanika, M. 1987. Geochemistry and petrogenesis of rift-related volcanic rocks from South Kivi (Zaire). *Journal of Volcanology and Geothermal Research* **31**, 33–46.

Ayalew, D., Ebinger, C., Bourdon, E., Wolfenden, E., Yirgu, G. & Grassingeau, N. 2006. Temporal compositional variation of syn-rift rhyolites along the western margin of the southern Red Sea and northern Main Ethiopian Rift. *In*: Yirgu, G., Ebinger, C. & Maguire, P.K.H. (eds), *The Afar Volcanic Province within the East African Rift System.* Geological Society, London, Special Publications **259**, 121–130.

Bach, W., Erzinger, J., Dosso, L., Bollinger, C., Bougault, H., Etoubleau, J. & Sauerwein, J. 1996. Unusually large Nb-Ta depletions in North Chile ridge basalts at 36°50' to 38°56' S: major element, trace element, and isotopic data. *Earth and Planetary Science Letters* **142**, 223–240.

Bach, W., Hegner, E., Erzinger, J. & Satir, M. 1994. Chemical and isotopic variations along the superfast spreading East Pacific Rise from 6 to 30°S. *Contributions to Mineralogy and Petrology* **116**, 365–380.

Bağci, U., Parlak, O. & Höck, V., 2008. Geochemistry and tectonic environment of diverse magma generations forming the crustal units of the Kızıldağ (Hatay) ophiolite, southern Turkey. *Turkish Journal of Earth Sciences* **17**, 43–71.

Barberi, F., Ferrara, G., Santacroce, R., Treuil, M. & Varet, J. 1975. A transitional basalt-pantellerite sequence of fractional crystallization, the Boina centre (Afar rift, Ethiopia). *Journal of Petrology* **16**, 22–56.

Barboza-Gudiño, J.R., Orozco-Esquivel, M.T., Gómez-Anguiano, M. & Zavala-Monsiváis, A. 2008. The early Mesozoic volcanic arc of western North America in northeastern Mexico. *Journal of South American Earth Sciences* **25**, 49–63.

Barling, J., Goldstein, S.L. & Nicholls, I.A. 1994. Geochemistry of Heard Island (southern Indian Ocean): characterization of an enriched mantle component and implication for enrichment of the Sub-Indian ocean mantle. *Journal of Petrology* **35**, 1017–1053.

Barnett, V. & Lewis, T. 1994. *Outliers in Statistical Data*. John Wiley & Sons, Chichester.

Barrat, J.A., Joron, J.L., Taylor, R.N., Fourcade, S., Nesbitt, R.W. & Jahn, B.M. 2003. Geochemistry of basalts from Manda Hararo, Ethiopia: LREE-depleted basalts in Central Afar. *Lithos* **69**, 1–13.

Barsdell, M. 1988. Petrology and petrogenesis of clinopyroxene-rich tholeiitic lavas, Merelava volcano, Vanuatu. *Journal of Petrology* **29**, 927–964.

Barsdell, M. & Berry, R.F. 1990. Origin and evolution of primitive island arc ankaramites from western Epi, Vanuatu. *Journal of Petrology* **31**, 747–777.

Basu, A.R., Junwen, W., Wankang, H., Guanghong, X. & Tatsumoto, M. 1991. Major element, REE, and Pb, Nd and Sr isotopic geochemistry of Cenozoic volcanic rocks of eastern China: implications for their origin from suboceanic-type mantle reservoirs. *Earth and Planetary Science Letters* **105**, 149–169.

Bau, M. & Knittel, U. 1993. Significance of slab-derived partial melts and aqueous fluids for the genesis of tholeiitic and calc-alkaline island-arc basalts: evidence from Mt. Arayat, Philippines. *Chemical Geology* **105**, 233–251.

Bell, K. & Peterson, T. 1991. Nd and Sr isotopic systematics of Shombole volcano, East Africa, and the links between nephelinites, phonolites, and carbonatites. *Geology* **19**, 582–585.

Benito, R., López-Ruiz, J., Cebriá, J.M., Hertogen, J., Doblas, M., Oyarzum, R. & Demaiffe, D. 1999. Sr and O isotope constraints on source and crustal contamination in the high-K calc-alkaline and shoshonitic Neogene volcanic rocks of SE Spain. *Lithos* **46**, 773–802.

Bergmanis, E.C., Sinton, J.M. & Trusdell, F.A. 2000. Rejuvenated volcanism along the southwest rift zone, East Maui, Hawaii. *Bulletin Volcanologique* **62**, 239–255.

Bertrand, H. 1991. The Mesozoic tholeiitic province of northwest Africa: a volcano-tectonic record of the early opening of Central Atlantic. *In*: Kampunzu, A.B. & Lubala, R.T. (eds), *Magmatism in Extensional Structural Settings*. Springer Verlag, Berlin, Germany, 147–188.

Bhatia, M.R. 1983. Plate tectonics and geochemical composition of sandstones. *Journal of Geology* **91**, 611–627.

Binard, N., Maury, R.C., Guille, G., Talandier, J., Gillot, P.Y. & Cotten, J. 1993. Mehetia island, South Pacific: geology and petrology of the emerged part of the Society hot spot. *Journal of Volcanology and Geothermal Research* **55**, 239–260.

Birkenmajer, K., Pecskay, Z., Grabowski, J., Lorenc, M.W. & Zagozdzon, P.P. 2007. Radiometric dating of the Tertiary volcanics in lower Silesia, Poland. V. K-Ar and palaeomagnetic data from late Oligocene to early Miocene basaltic rocks of the north-sudetic depression. *Annales Societatis Geologorum Poloniae* **77**, 1–16.

Bloomer, S.H., Stern, R.J., Fisk, E. & Geschwind, C.H. 1989. Shoshonitic volcanism in the northern Mariana arc. 1. Mineralogic and major and trace element characteristics. *Journal of Geophysical Research* **94**, 4469–4496.

Blum, N., Halbach, P. & Münch, U. 1996. Geochemistry and mineralogy of alkali basalts from Tropic Seamount, central Atlantic Ocean. *Marine Geology* **136**, 1–19.

Bohrson, W.A. & Reid, M.R. 1995. Petrogenesis of alkaline basalts from Socorro Island, Mexico: Trace element evidence for contamination of ocean-island basalt in the shallow ocean crust. *Journal of Petrology* **100**, 24555–24576.

Bonev, N. & Stampfli, G. 2008. Petrology, geochemistry and geodynamic implications of Jurassic island arc magmatism as revealed by mafic volcanic rocks in the Mesozoic low-grade sequence, eastern Rhodope, Bulgaria. *Lithos* **100**, 210–233.

Borisova, A.Y., Nikogosian, I.K., Scoates, J.S., Weis, D., Damasceno, D., Shimizu, N. & Touret, J.L.R. 2002. Melt, fluid and crystal inclusions in olivine phenocrysts from Kerguelen plume-derived picritic basalts: evidence for interaction with the Kerguelen plateau lithosphere. *Chemical Geology* **183**, 195–220.

Borsi, S., Ferrara, G., Innocenti, F. & Mazzuoli, R. 1972. Geochronology and petrology of recent volcanics in the eastern Aegean Sea (Western Anatolia and Lesbos island). *Bulletin Volcanologique* **36**, 473–496.

Bougault, H., Dmitriev, L., Schilling, J.G., Sobolev, A., Joron, J.L. & Needham, H.D. 1988. Mantle heterogeneity from trace elements: MAR triple junction near 14°N. *Earth and Planetary Science Letters* **88**, 27–36.

Boztuğ, D. 2008. Petrogenesis of the Kösedağ Pluton, Suşehri-NE Sivas, East-Central Pontides, Turkey. *Turkish Journal of Earth Sciences* **17**, 241–262.

Boztuğ, D., Yağmur, M., Otlu, N., Tatar, S. & Yeşiltaş, A. 1998. Petrology of the post-collisional, within-plate Yıldızdağ gabbroic pluton, Yıldızeli-Sivas region, central Anatolia, Turkey. *Turkish Journal of Earth Sciences* **7**, 37–51.

Brophy, J.G. 1986. The Cold Bay volcanic center, Aleutian volcanic arc. I. Implications for the origin of hi-alumina arc basalt. *Contributions to Mineralogy and Petrology* **93**, 368–380.

Brown, G.M., Holland, J.G., Sigurdsson, H., Tomblin, J.F. & Arculus, R.J. 1977. Geochemistry of the Lesser Antilles volcanic island arc. *Geochimica et Cosmochimica Acta* **41**, 785–801.

Bruni, S., D'Orazio, M., Haller, M.J., Innocenti, F., Manetti, P., Pecskay, Z. & Tonarini, S. 2008. Time-evolution of magma sources in a continental back-arc setting: the Cenozoic basalts from Sierra de San Bernardo (Patagonia, Chubut, Argentina). *Geological Magazine* **145**, 714–732.

Bryan, W.B., Stice, G.D. & Ewart, A. 1972. Geology, petrography, and geochemistry of the volcanic islands of Tonga. *Journal of Geophysical Research* **77**, 1566–1585.

Bryan, W.B., Thompson, G. & Ludden, J.N. 1981. Compositional variation in normal MORB from 22°–25°N: mid-Atlantic ridge and Kane fracture zone. *Journal of Geophysical Research* **86**, 11815–11836.

Buket, E. & Temel, A. 1998. Major-element, trace-element, and Sr-Nd isotopic geochemistry and genesis of Varto (Muş) volcanic rocks, Eastern Turkey. *Journal of Volcanology and Geothermal Research* **85**, 405–422.

Butler, J.C. & Woronow, A. 1986. Discrimination among tectonic settings using trace element abundances of basalts. *Journal of Geophysical Research* **91**, 10289–10300.

Cabanis, B. & Lecolle, M. 1989. Le diagramme La/10-Y/15-Nb/8: un outil pour la discrimination des séries volcaniques et la mise en évidence des processus de mélange et/ou de contamination crustale. *Comptes Rendus Academie de Sciences Paris Serie II* **309**, 2023–2029.

Camp, V.E., Roobol, M.J. & Hooper, P.R. 1991. The Arabian continental alkali basalt province: part II. Evolution of Harrats Khaybar, Ithnayn, and Kura, Kingdom of Saudi Arabia. *Geological Society of America Bulletin* **103**, 363–391.

Cassinis, G., Cortesogno, L., Gaggero, L., Perotti, C.R. & Buzzi, L. 2008. Permian to Triassic geodynamic and magmatic evolution of the Brescian Prealps (eastern Lombardy, Italy). *Bollettino della Societa Geologica Italiana* **127**, 501–518.

Castillo, P.R. & Newhall, C.G. 2004. Geochemical constraints on possible subduction components in lavas of Mayon and Taal volcanoes, southern Luzon, Philippines. *Journal of Petrology* **45**, 1089–1108.

Castrellon-Uribe, J., Cuevas-Arteaga, C. & Trujillo-Estrada, A. 2008. Corrosion monitoring of stainless steel 304L in lithium bromide aqueous solution using transmittance optical detection technique. *Optics and Lasers in Engineering* **46**, 469–476.

Çelik, O.F. 2008. Detailed geochemistry and K-Ar geochronology of the metamorphic sole rocks and their mafic dykes from the Mersin ophiolite, southern Turkey. *Turkish Journal of Earth Sciences* **17**, 685–708.

Çelik, O.F. & Chiaradia, M. 2008. Geochemical and petrological aspects of dike intrusions in the Lycian ophiolites (SW Turkey): a case study for the dike emplacement along the Tauride Belt Ophiolites. *International Journal of Earth Sciences* **97**, 1151–1164.

Chauvel, C. & Jahn, B.-M. 1984. Nd-Sr isotope and REE geochemistry of alkali basalts from the Massif Central, France. *Geochimica et Cosmochimica Acta* **48**, 93–110.

Chayes, F. & Velde, D. 1965. On distinguishing basaltic lavas of circumoceanic and oceanic-island type by means of discriminant functions. *American Journal of Science* **263**, 206–222.

Chayes, F. 1960. On correlation between variables of constant sum. *Journal of Geophysical Research* **65**, 4185–4193.

Chayes, F. 1965. Classification in a ternary-diagram by means of discriminant functions. *American Mineralogist* **50**, 1618–1633.

Chayes, F. 1978. *Ratio Correlation. A Manual for Students of Petrology and Geochemistry*. The University of Chicago Press, Chicago and London.

Chen, C.-Y., Frey, F.A. & Garcia, M.O. 1990. Evolution of alkalic lavas at Heleakala volcano, east Maui, Hawaii. *Contributions to Mineralogy and Petrology* **105**, 197–218.

Chen, C.Y., Frey, F.A., Garcia, M.O., Dalrymple, G.B. & Hart, S.R. 1991. The tholeiite to alkalic basalt transition at Haleakala volcano, Maui, Hawaii. *Contributions to Mineralogy and Petrology* **106**, 183–200.

Cheng, Q.C., MacDougall, J.D. & Lugmair, G.W. 1993. Geochemical studies of Tahiti, Teahitia and Mahetia, Society Island Chain. *Journal of Volcanology and Geothermal Research* **55**, 155–184.

Chung, S.L., Jahn, B.M., Chen, S.J., Lee, T. & Chen, C.-H. 1995. Miocene basalts in northwestern Taiwan: evidence for EM-type mantle sources in the continental lithosphere. *Geochimica et Cosmochimica Acta* **59**, 549–555.

Chung, S.-L., Sun, S.S., Tu, K., Chen-Hong, C. & Lee, C.L. 1994. Late Cenozoic basaltic volcanism around the Taiwan Strait, SE China: product of lithosphere-asthenosphere interaction during continental extension. *Chemical Geology* **112**, 1–20.

Churikova, T., Dorendorf, F. & Wörner, G. 2001. Sources and fluids in the mantle wedge below Kamchatka, evidence from across-arc geochemical variation. *Journal of Petrology* **42**, 1567–1593.

Class, C., Altherr, R., Volker, F., Eberz, G. & McCulloch, M.T. 1994. Geochemistry of Pliocene to Quaternary alkali basalts from the Huri Hills, northern Kenya. *Chemical Geology* **113**, 1–22.

Class, C. & Goldstein, S.L. 1997. Plume-lithosphere interactions in the ocean basins: constraints from the source mineralogy. *Earth and Planetary Science Letters* **150**, 245–260.

Class, C., Goldstein, S.L., Altherr, R. & Bachèlery, P. 1998. The process of plume-lithosphere interactions in the ocean basins – the case of Grande Comore. *Journal of Petrology* **39**, 881–903.

Claude-Ivanaj, C., Bourdon, B. & Allègre, C.J. 1998. Ra-Th-Sr isotope systematics in Grande Comore Island: a case study of plume-lithosphere interaction. *Earth and Planetary Science Letters* **164**, 99–117.

Cole, J.W. 1981. Genesis of lavas of the Taupo volcanic zone, North island, New Zealand. *Journal of Volcanology and Geothermal Research* **10**, 317–337.

Dampare, S.B., Shibata, T., Asiedu, D.K., Osae, S. & Banoeng-Yakubo, B. 2008. Geochemistry of Paleoproterozoic metavolcanic rocks from the southern Ashanti volcanic belt, Ghana: petrogenetic and tectonic setting implications. *Precambrian Research* **162**, 403–423.

Dautria, J.M. & Girod, M.M. 1991. Relationships between Cainozoic magmatism and upper mantle heterogeneities as exemplified by the Hoggar volcanic area (Central Sahara, southern Algeria). *In*: Kampunzu, A.B. & Lubala, R.T. (eds), *Magmatism in Extensional Structural Settings*. Springer Verlag, Berlin, Germany, 250–268.

Davidson, J.P. & Wilson, I.R. 1989. Evolution of an alkali basalt-trachyte suite from Jebel Marra volcano, Sudan, through assimilation and fractional crystallization. *Earth and Planetary Science Letters* **95**, 141–160.

De Moor, J.M., Fischer, T.P., Hilton, D.R., Hauri, E., Jaffe, L.A. & Camacho, J.T. 2005. Degassing at Anathan volcano during the May 2003 eruption: implications from petrology, ash leachates, and SiO_2 emissions. *Journal of Volcanology and Geothermal Research* **146**, 117–138.

De Mulder, M., Hertogen, J., Deutsch, S. & André, L. 1986. The role of crustal contamination in the potassic suite of the Karisimbi volcano (Virunga, African Rift Valley). *Chemical Geology* **57**, 117–136.

Defant, M.J., Jacques, D., Maury, R.C., De Boer, J. & Joron, J.-L. 1989. Geochemistry and tectonic setting of the Luzon arc, Philippines. *Geological Society of America Bulletin* **101**, 663–672.

Defant, M.J., Maury, R.C., Ripley, E.M., Feigenson, M.D. & Jacques, D. 1991. An example of island-arc petrogenesis: goechemistry and petrology of the southern Luzon arc, Philippines. *Journal of Petrology* **32**, 455–500.

Defant, M.J., Sherman, S., Maury, R.C., Bellon, H., De Boer, J., Davidson, J. & Kepezhinskas, P. 2001. The geology, petrology, and petrogenesis of Saba Island, Lesser Antilles. *Journal of Volcanology and Geothermal Research* **107**, 87–111.

Deniel, C., Vidal, P., Coulon, C., Vellutini, P. & Piguet, P. 1994. Temporal evolution of mantle sources during continental rifting: the volcanism of Djibouti (Afar). *Journal of Geophysical Research* **99**, 2853–2869.

Déruelle, B., Moreau, C., Nkoumbou, C., Kambou, R., Lissom, J., Njonfang, E., Ghogomu, R.T. & Nono, A. 1991. The Cameron line: a review. *In*: Kampunzu, A.B. & Lubala, R.T. (eds), *Magmatism in Extensional Structural Settings*. Springer Verlag, Berlin, Germany, 274–327.

Devine, J.D. 1995. Petrogenesis of the basalt-andesite-dacite association of Grenada, Lesser Antilles island arc, revisited. *Journal of Volcanology and Geothermal Research* **69**, 1–33.

Díaz-González, L., Santoyo, E. & Reyes-Reyes J. 2008. Tres nuevos geotermómetros mejorados de Na/K usando herramientas computacionales y geoquimiométricas: aplicación a la predicción de temperaturas de sistemas geotérmicos. *Revista Mexicana de Ciencias Geológicas* **25**, 465–482.

Dixon, T.H., Batiza, R., Futa, K. & Martin, D. 1984. Petrochemistry, age and isotopic composition of alkali basalts from Ponape island, western Pacific. *Chemical Geology* **43**, 1–28.

Dorendorf, F., Churikova, T., Koloskov, A. & Wörner, G. 2000. Late Pliocene to Holocene activity at Bakening volcano and surrounding monogenetic centers (Kamchatka): volcanic geology and geochemical evolution. *Journal of Volcanology and Geothermal Research* **104**, 131–151.

Dosso, L., Bougault, H. & Joron, J.-L. 1993. Geochemical morphology of the north Mid-Atlantic Ridge, 10°–24°N: trace element-isotope complementarity. *Earth and Planetary Science Letters* **120**, 443–462.

Dosso, L., Bougault, H., Beuzart, P., J.-Y., C. & Joron, J.-L. 1988. The geochemical structure of the South-East Indian Ridge. *Earth and Planetary Science Letters* **88**, 47–59.

Doucelance, R., Escrig, S., Moreira, M., Gariépy, C. & Kurz, M.D. 2003. Pb-Sr-He isotope and trace element geochemistry of the Cape Verde archipelago. *Geochimica et Cosmochimica Acta* **67**, 3717–3733.

Doucet, S., Weis, D., Scoates, J.S., Debaille, V. & Giret, A. 2004. Geochemical and Hf-Pb-Sr-Nd isotopic constraints on the origin of the Amsterdam-St Paul (indian Ocean) hotspot basalts. *Earth and Planetary Science Letters* **218**, 179–195.

Duncker, K.E., Wolff, J.A., Harmon, R.S., Leat, P.T., Dickin, A.P. & Thompson, R.N. 1991. Diverse mantle and crustal components in lavas of the NW Cerros del Rio volcanic field, Rio Grande Rift, New Mexico. *Contributions to Mineralogy and Petrology* **108**, 331–345.

Dupuy, C., Barsczus, H.G., Dostal, J., Vidal, P. & Liotard, J.-M. 1989. Subducted and recycled lithosphere as the mantle source of ocean-island basalts from southern Polynesia, central Pacific. *Chemical Geology* **77**, 1–18.

Dupuy, C., Barsczus, H.G., Liotard, J.M. & Dostal, J. 1988. Trace element evidence for the origin of ocean-island basalts: an example from the Austral Islands (French Polynesia). *Contributions to Mineralogy and Petrology* **98**, 293–302.

Dupuy, C., Dostal, J., Marcelot, G., Bougault, H., Joron, J.L. & Treuil, M. 1982. Geochemistry of basalts from central and southern New Hebrides arc: implication for their source rock composition. *Earth and Planetary Science Letters* **60**, 207–225.

Edwards, C.M.H., Menzies, M.A., Thirlwall, M.F., Morris, J.D., Leeman, W.P. & Harmon, R.S. 1994. The transition to potassic alkaline volcanism in island arcs: the Ringgit-Beser complex, east Java, Indonesia. *Journal of Petrology* **35**, 1557–1595.

Egozcue, J.J., Pawlowsky-Glahn, V., Mateu-Figueras, G. & Barceló-Vidal, C. 2003. Isometric logratio transformations for compositional data analysis. *Mathematical Geology* **35**, 279–300.

Elliott, T., Plank, T., Zindler, A., White, W.M. & Bourdon, B. 1997. Element transport from slab to volcanic front at the Mariana arc. *Journal of Geophysical Research* **102**, 14991–15019.

Ercan, T. 1981. *Kula Yöresinin Jeolojisi ve Volkanitlerin Petrolojisi [Geology of Kula Region and Petrology of Volcanics]*. PhD Thesis, İstanbul Üniversitesi, Turkey [in Turkish with English abstract, unpublished].

Ercan, T., Satir, M., Sevin, D. & Türkecan, A. 1996. Batı Anadolu'daki Tersiyer ve Kuvaterner yaşlı volkanik kayaçlarda yeni yapılan radyometrik yaş ölçümlerinin yorumu [Some new radiometric ages from Tertiary to Quaternary volcanic rocks from Western Anatolia (Turkey) and their significance]. *Maden Tetkik Arama Dergisi* **119**, 103–112.

Ercan, T., Satir, M., Türkecan, A., Akyürek, B., Çevikbaş, A., Günay, E., Ateş, M. & Can, B. 1985. Batı Anadolu Senozoyik volkanitlerine ait yeni kimyasal, izotopik ve radyometrik verilerin yorumu [Interpretation of new chemical, Isotopic and radiometric data on Cenozoic volcanics of western Anatolia]. *Geological Society of Turkey Bulletin* **28**, 121–136.

Ersoy, Y. & Helvaci, C. 2007. Stratigraphy and geochemical features of the Early Miocene bimodal (ultrapotassic and calc-alkaline) volcanic activity within the NE-trending Selendi Basin, western Anatolia, Turkey. *Turkish Journal of Earth Sciences* **16**, 117–139.

Ewart, A. & Bryan, W.B. 1972. Petrography and geochemistry of the igneous rocks from EUA, Tongan islands. *Geological Society of America Bulletin* **83**, 3281–3298.

Ewart, A., Brothers, R.N. & Mateen, A. 1977. An outline of the geology and geochemistry, and the possible petrogenetic evolution of the volcanic rocks of the Tonga-Kermadec-New Zealand island arc. *Journal of Volcanology and Geothermal Research* **2**, 205–270.

Fan, Q. & Hooper, P.R. 1991. The Cenozoic basaltic rocks of eastern China: petrology and chemical composition. *Journal of Petrology* **32**, 765–810.

Femenias, O., Berza, T., Tatu, M., Diot, H. & Demaiffe, D. 2008. Nature and significance of a Cambro–Ordovician high-K, calc-alkaline sub-volcanic suite: the late- to post-orogenic Motru Dyke Swarm (Southern Carpathians, Romania). *International Journal of Earth Sciences* **97**, 479–496.

Feuerbach, D.L., Smith, E.I., Walker, J.D. & Tangeman, J.A. 1993. The role of the mantle during crustal extension: constraints from geochemistry of volcanic rocks in the Lake Mead area, Nevada and Arizona. *Geological Society of America Bulletin* **105**, 1561–1575.

Fitton, J.G., James, D. & Leeman, W.P. 1991. Basic magmatism associated with Late Cenozoic extension in the western United States: compositional variations in space and time. *Journal of Geophysical Research* **96**, 13693–13711.

Floyd, P.A. 1993. Geochemical discrimination and petrogenesis of alkalic basalt sequences in part of the Ankara melange, central Turkey. *Journal of the Geological Society, London* **150**, 541–550.

Floyd, P.A., Helvaci, C. & Mittwede, S.K. 1998. Geochemical discrimination of volcanic rocks associated with borate deposits: an exploration tool? *Journal of Geochemical Exploration* **60**, 185–205.

Foden, J.D. & Varne, R. 1980. The petrology and tectonic setting of Quaternary–Recent volcanic centres of Lombok and Sumbawa, Sunda arc. *Chemical Geology* **30**, 201–226.

Förster, H.-J., Tischendorf, G. & Trumbull, R.B. 1997. An evaluation of the Rb vs. (Y+Nb) discrimination diagram to infer tectonic setting of silicic igneous rocks. *Lithos* **40**, 261–293.

Fretzdorff, S. & Haase, K.M. 2002. Geochemistry and petrology of lavas from the submarine flanks of Réunion island (western Indian Ocean): implications for magma genesis and the mantle source. *Mineralogy and Petrology* **75**, 153–184.

Frey, F.A., Garcia, M.O. & Roden, M.F. 1994. Geochemical characteristics of Koolau volcano: implications of intershield geochemical differences among Hawaiian volcanoes. *Geochimica et Cosmochimica Acta* **58**, 1441–1462.

Furman, T., Btyce, J.G., Karson, J. & Iotti, A. 2004. East African rift system (EARS) plume structure: insights from Quaternary mafic lavas of Turkana, Kenya. *Journal of Petrology* **45**, 1069–1088.

Gamble, J.A., Smith, I.E.M., McCulloch, M.T., Graham, I.J. & Kokelaar, B.P. 1993. The geochemistry and petrogenesis of basalts from the Taupo volcanic zone and Kermadec Island arc, S.W. Pacific. *Journal of Volcanology and Geothermal Research* **54**, 265–290.

Gamble, J.A., Wright, I.C., Woodhead, J.D. & McCulloch, M.T. 1995. Arc and back-arc geochemistry in the southern Kermadec arc – Ngatoro basin and offshore Taupo volcanic zone, SW Pacific. *In*: Smellie, J.L. (ed), *Volcanism Associated with Extension at Consuming Plate Margins*. Geological Society, London, Special Publications **81**, 193–212.

Garcia, M.O., Rhodes, J.M., Wolfe, E.W., Ulrich, G.E. & Ho, R.A. 1992. Petrology of lavas from episodes 2–47 of the Puu Oo eruption of Kilauea Volcano, Hawaii: evaluation of magmatic processes. *Bulletin of Volcanology* **55**, 1–16.

Geist, D.J., Mcbirney, A.R. & Duncan, R.A. 1986. Geology and petrogenesis of lavas from San Cristobal Islands, Galapos Archipelago. *Geological Society of America Bulletin* **97**, 555–566.

Geldmacher, J. & Hoernle, K. 2000. The 72 Ma geochemical evolution of the Medeira hotspot (eastern North Atlantic): recycling of Paleozoic (≤500 Ma) oceanic lithosphere. *Earth and Planetary Science Letters* **183**, 73–92.

Ghosh, B., Mahoney, J. & Ray, J. 2007. Mayodia ophiolites of Arunachal Pradesh, northeastern Himalaya. *Journal of the Geological Society of India* **70**, 595–604.

Gibson, S.A., Thompson, R.N., Leat, P.T., Dickin, A.P., Morrison, M.A., Hendry, G.L. & Mitchell, J.G. 1992. Asthenosphere-derived magmatism in the Rio Grande rift, western USA: implications for continental break-up. *In*: Storey, B.C., Alabaster, T. & Pankhurst, R.J. (eds), *Magmatism and the Causes of Continental Break-up*. Geological Society, London, Special Publications **68**, 61–89.

Gómez-Arias, E., Andaverde, J., Santoyo, E. & Urquiza, G. 2009. Determinación de la viscosidad y su incertidumbre en fluidos de perforación usados en la construcción de pozos geotérmicos: aplicación en el campo de Los Humeros, Puebla, México [Determination of viscosity and its uncertainty in drilling fluids used in the construction of geothermal wells: application in the Los Humeros field, Puebla, Mexico]. *Revista Mexicana de Ciencias Geológicas* **26**, 516–529.

González-Ramírez, R., Díaz-González., L. & Verma, S.P. 2009. Eficiencia relativa de las 33 pruebas de discordancia para valores desviados basada en datos geoquímicos de materiales de referencia [Relative efficiency of 33 discordancy tests for discordant outliers based on geochemical data for referente materials]. *Revista Mexicana de Ciencias Geológicas* **26**, 501–515.

Gorton, M.P. & Schandl, E.S. 2000. From continents to island arcs: a geochemical index of tectonic setting for arc-related and within-plate felsic to intermediate volcanic rocks. *Canadian Mineralogist* **38**, 1065–1073.

Greiling, R.O., Grimmer, J.C., De Wall, H. & Bjork, L. 2007. Mesoproterozoic dyke swarms in foreland and nappes of the central Scandinavian Caledonides: structure, magnetic fabric, and geochemistry. *Geological Magazine* **144**, 525–546.

Gribble, R.F., Stern, R.J., Newman, S., Bloomer, S.H. & O´Hearn, T. 1998. Chemical and isotopic composition of lavas from the northern Marianas trough: implications for magma genesis in back-arc basins. *Journal of Petrology* **39**, 125–154.

Güleç, N. 1991. Crust-mantle interaction in western Turkey: implications from Sr and Nd isotope geochemistry of Tertiary and Quaternary volcanics. *Geological Magazine* **128**, 417–435.

Haase, K.M., Devey, C.W., Mertz, D.F., Stoffers, P. & Dieter, G.-S. 1996. Geochemistry of lavas from Mohns Ridge, Norwegian-Greenland Sea: implications for melting conditions and magma sources near Jan Mayen. *Contributions to Mineralogy and Petrology* **123**, 223–237.

Haase, K.M., Goldschmidt, B. & Garbe-Schönberg, C.-D. 2004. Petrogenesis of Tertiary continental intra-plate lavas from the Westerwald region, Germany. *Journal of Petrology* **45**, 883–905.

Haase, K.M., Worthington, T.J., Stoffers, P., Garbe-Schönberg, D. & Wright, I. 2002. Mantle dynamics, element recycling, and magma genesis beneath the Kermadec arc-Havre Trough. *Geochemistry Geophysics Geosystems* **3**, 1071, doi:10.1029/2002GC00035.

Han, B.-F., Wang, S.-G. & Kagami, H. 1999. Trace element and Nd-Sr isotope constraints on origin of the Chifeng flood basalts, North China. *Chemical Geology* **155**, 187–199.

Harpp, K.S., Fornari, D.J., Geist, D.J. & Kurz, M.D. 2003. Genovesa submarine ridge: a manifestation of plume-ridge interaction in the northern Galápagos islands. *Geochemistry Geophysics Geosystems* **4**, 10.1029/2003GC000531.

Hart, S.R., Blusztajn, J. & Craddock, C. 1995. Cenozoic volcanism in Antarctica: Jones mountains and Peter I island. *Geochimica et Cosmochimica Acta* **59**, 3379–3388.

Hart, S.R., Coetzee, M., Workman, R.K., Blusztajn, J., Johnson, K.T.M., Sinton, J.M., Steinberger, B. & Hawkins, J.W. 2004. Genesis of the western Samoa seamount province: age, geochemical fingerprint and tectonics. *Earth and Planetary Science Letters* **227**, 37–56.

Hart, W.K., Woldegabriel, G., Walter, R.C. & Mertzman, S.A. 1989. Basaltic volcanism in Ethiopia: constraints on continental rifting and mantle interactions. *Journal of Geophysical Research* **94**, 7731–7748.

Hauri, E.H. & Hart, S.R. 1997. Rhenium abundances and systematics in oceanic basalts. *Chemical Geology* **139**, 185–205.

Hegner, E. & Smith, I.E.M. 1992. Isotopic compositions of late Cenozoic volcanics from southeast Papua New Guinea: evidence for multi-component sources in arc and rift environments. *Chemical Geology* **97**, 233–249.

Hekinian, R., Cheminée, J.L., Dubois, J., Stoffers, P., Scott, S., Guivel, C., Garbe-Schönberg, D., Devey, C., Bourdon, B., Lackschewitz, K., Mcmurtry, G. & Le Drezen, E. 2003. The Pitcairn hotspot in the South Pacific: distribution and composition of submarine volcanic sequences. *Journal of Volcanology and Geothermal Research* **121**, 219–245.

Hekinian, R., Francheteau, J., Armijo, R., Cogné, J.P., Constantin, M., Girardeau, J., Hey, R., Naar, D.F. & Searle, R. 1996. Petrology of the Easter microplate region in the South Pacific. *Journal of Volcanology and Geothermal Research* **72**, 259–289.

Hémond, C., Devey, C.W. & Chauvel, C. 1994. Source compositions and melting processes in the Society and Austral plumes (South Pacific ocean): element and isotope (Sr, Nd, Pb, Th) geochemistry. *Chemical Geology* **115**, 7–45.

Hildreth, W., Fierstein, J., Siems, D.F., Budahn, J.R. & Ruíz, J. 2004. Rear-arc vs. arc-front volcanoes in the Katmai reach of the Alaska peninsula: a critical appraisal of across-arc compositional variation. *Contributions to Mineralogy and Petrology* **147**, 243–275.

Hirotani, S. & Ban, M. 2006. Origin of silicic magma and magma feeding system of the Shirataka volcano, NE Japan. *Journal of Volcanology and Geothermal Research* **156**, 229–251.

Ho, K.-S., Chen, J.-C. & Juang, W.-S. 2000. Geochronology and geochemistry of late Cenozoic basalts from Leiqiong area, southern China. *Journal of Asian Earth Sciences* **18**, 307–324.

Hole, M.J., Saunders, A.D., Marriner, G.F. & Tarney, J. 1984. Subduction of pelagic sediments: implications for the origin of Ce-Anomalous basalts from the Marianas Islands. *Journal of the Geological Society, London* **141**, 453–472.

Holm, P.E. 1982. Non-recognition of continental tholeiites using the Ti-Y-Zr diagram. *Contributions to Mineralogy and Petrology* **79**, 308–310.

Holm, P.M., Wilson, J.R., Christensen, B.P., Hansen, L., Hansen, S.L., Hein, K.M., Mortensen, A.K., Pedersen, R.B., Plesner, S. & Runge, M.K. 2006. Sampling of Cape Verde mantle plume: evolution of melt compositions on Santo Antao, Cape Verde Islands. *Journal of Petrology* **47**, 145–189.

Hoogewerff, J.A., Van Bergen, M.J., Vroon, P.Z., Hertogen, J., Wordel, R., Sneyers, A., Nasution, A., Varekamp, J.C., Moens, H.L.E. & Mouchel, D. 1997. U-series, Sr-Nd-Pb isotope and trace-element systematics across an active island arc-continent collision zone: implications for element transfer at the slab-wedge interface. *Geochimica et Cosmochimica Acta* **61**, 1057–1072.

Hsu, C.-N., Chen, J.-C. & Ho, K.-S. 2000. Geochemistry of Cenozoic volcanic rocks from Kirin Province, northeast China. *Geochemical Journal* **34**, 33–58.

Innocenti, F., Agostini, S., Di Vincenzo, G., Doglioni, C., Manetti, P., Savaşcin, M.Y. & Tonarini, S. 2005. Neogene and Quaternary volcanism in Western Anatolia: magma sources and geodynamic evolution. *Marine Geology* **221**, 397–421.

Ishikawa, T., Tera, F. & Nakazawa, T. 2001. Boron isotope and trace element systematics of the three volcanic zones in the Kamchatka arc. *Geochimica et Cosmochimica Acta* **65**, 4523–4537.

Ishizuka, O., Taylor, R.N., Milton, J.A., Nesbitt, R.W., Yuasa, M. & Sakamoto, I. 2006. Variation in the mantle sources of the northern Izu arc with time and space – constraints from high-precision Pb isotopes. *Journal of Volcanology and Geothermal Research* **156**, 266–290.

Izbekov, P.E., Eichelberger, J.C. & Ivanov, B.V. 2004. The 1996 eruption of Karymsky volcano, Kamchatka: historical record of basaltic replenishment of an andesite reservoir. *Journal of Petrology* **45**, 2325–2345.

Jafarzadeh, M. & Hosseini-Barzi, M. 2008. Petrography and geochemistry of Ahwaz Sandstone Member of Asmari Formation, Zagros, Iran: implications on provenance and tectonic setting. *Revista Mexicana de Ciencias Geológicas* **25**, 247–260.

Jarrar, G.H., Manton, W.I., Stern, R.J. & Zachmann, D. 2008. Late Neoproterozoic A-type granites in the northernmost Arabian-Nubian Shield formed by fractionation of basaltic melts. *Chemie Der Erde-Geochemistry* **68**, 295–312.

Johnson, C.M. & Lipman, P.W. 1988. Origin of metaluminous and alkaline volcanic rocks of the Latir volcanic field, northern Rio Grande rift, New Mexico. *Contributions to Mineralogy and Petrology* **100**, 107–128.

Jørgensen, J.O. & Holm, P.M. 2002. Temporal variation and carbonatite contamination in primitive ocen island volcanics from São Vicente, Cape Verde islands. *Chemical Geology* **192**, 249–267.

Kabeto, K., Sawada, Y., Iizumi, S. & Wakatsuki, T. 2001. Mantle sources and magma-crust interactions in volcanic rocks from northern Kenya rift: geochemical evidence. *Lithos* **56**, 111–136.

Kampunzu, A.B. & Mohr, P. 1991. Magmatic evolution and petrogenesis in the East African rift system. *In*: Kampunzu, A.B. & Lubala, R.T. (eds), *Magmatism in Extensional Structural Settings*. Springer Verlag, Berlin, Germany, 85–136.

Kay, S.M. & Kay, R.W. 1994. Aleutian magmas in space and time. *In*: Plafker, G. & Berg, H.C. (eds), *The Geology of North America*. Geological Society of America, USA, **G-1**, 687–722.

Kay, S.M., Kay, R.W. & Citron, G.P. 1982. Tectonic controls on tholeiitic and calc-alkaline magmatism in the Aleutian arc. *Journal of Geophysical Research* **87**, 4051–4072.

Kela, J.M., Stakes, D.S. & Duncan, R.A. 2007. Geochemical and age constraints on the formation of the Gorda escarpment and Mendocino Ridge of the Mendocino transform fault in the NE Pacific. *Geological Society of America Bulletin* **119**, 88–100.

Kempton, P.D., Fitton, J.G., Hawkesworth, C.J. & Ormerod, D.S. 1991. Isotopic and trace element constraints on the composition and evolution of the lithosphere beneath the Southwestern United States. *Journal of Geophysical Research* **96**, 13713–13735.

Kepezhinskas, P., Mcdermott, F., Defant, M.J., Hochstaedter, A., Drummond, M.S., Hawkesworth, C.J., Koloskov, A., Maury, R.C. & Bellon, H. 1997. Trace element and Sr-Nd-Pb isotopic constraints on a three-component model of Kamchatka arc petrogenesis. *Geochimica et Cosmochimica Acta* **61**, 577–600.

Keskin, M., Genç, Ş.C. & Tüysüz, O. 2008. Petrology and geochemistry of post-collisional Middle Eocene volcanic units in North-Central Turkey: evidence for magma generation by slab breakoff following the closure of the Northern Neotethys Ocean. *Lithos* **104**, 267–305.

Kimura, J.-I. & Yoshida, T. 2006. Contributions of slab fluid, mantle wedge and crust to the origin of Quaternary lavas in the NE Japan arc. *Journal of Petrology* **47**, 2185–2232.

Kimura, J.-I., Manton, W.I., Sun, C.-H., Iizumi, S., Yoshida, T. & Stern, R.J. 2002. Chemical diversity of the Ueno basalts, Central Japan: identification of mantle and crustal contributions to arc basalts. *Journal of Petrology* **43**, 1923–1946.

Kita, I., Yamamoto, M., Asakawa, Y., Nakagawa, M., Taguchi, S. & Hasegawa, H. 2001. Contemporaneous ascent of within-plate type and island-arc type magmas in the Beppu-Shimabara graben system, Kyushu island, Japan. *Journal of Volcanology and Geothermal Research* **111**, 99–109.

Knittel, U., Hegner, E., Bau, M. & Satir, M. 1997. Enrichment processes in the sub-arc mantle: a Sr-Nd-Pb isotopic and REE study of primitive arc basalts from the Philippines. *The Canadian Mineralogist* **35**, 327–346.

Koçak, K. 2008. Mineralogy, geochemistry, and Sr-Nd isotopes of the Cretaceous leucogranite from Karamadaz (Kayseri), central Turkey: implications for their sources and geological setting. *Canadian Journal of Earth Sciences* **45**, 949–968.

Kumar, K.V. & Rathna, K. 2008. Geochemistry of the mafic dykes in the Prakasam Alkaline Province of Eastern Ghats Belt, India: implications for the genesis of continental rift-zone magmatism. *Lithos* **104**, 306–326.

Kurt, H., Asan, K. & Ruffet, G. 2008. The relationship between collision-related calcalkaline, and within-plate alkaline volcanism in the Karacadağ area (Konya-Turkiye, Central Anatolia). *Chemie Der Erde-Geochemistry* **68**, 155–176.

Lassiter, J.C., Blichert-Toft, J. & Hauri, E.H. 2003. Isotope and trace element variations in lavas from Raivavae and Rapa, Cook-Austral islands: constraints on the nature of HIMU- and EM-mantle and the origin of mid-plate volcanism in French Polynesia. *Chemical Geology* **202**, 115–138.

Le Bas, M.J. 2000. IUGS reclassification of the high-Mg and picritic volcanic rocks. *Journal of Petrology* **41**, 1467–1470.

Le Bas, M.J., Le Maitre, R.W., Streckeisen, A. & Zanettin, B. 1986. A chemical classification of volcanic rocks based on the total alkali-silica diagram. *Journal of Petrology* **27**, 745–750.

Le Maitre, R.W. 1976. Some problems of the projection of chemical data into mineralogical classifications. *Contributions to Mineralogy and Petrology* **56**, 181–189.

Le Maitre, R.W., Streckeisen, A., Zanettin, B., Le Bas, M.J., Bonin, B., Bateman, P., Bellieni, G., Dudek, A., Schmid, R., Sorensen, H. & Woolley, A.R. 2002. *Igneous Rocks. A Classification and Glossary of Terms: Recommendations of the International Union of Geological Sciences Subcommission of the Systematics of Igneous Rocks*. Cambridge University Press, Cambridge.

Le Roex, A.P. & Dick, H.J.B. 1981. Petrography and geochemistry of basaltic rocks from the Conrad fracture zone on the America-Antarctica Ridge. *Earth and Planetary Science Letters* **54**, 117–138.

Le Roex, A.P. & Erlank, A.J. 1982. Quantitative evaluation of fractional crystallization in Bouvet Island lavas. *Journal of Volcanology and Geothermal Research* **13**, 309–338.

Le Roex, A.P., Dick, H.J.B., Gulen, L., Reid, A.M. & Erlank, A.J. 1987. Local and regional heterogeneity in MORB from the Mid-Atlantic Ridge between 54.5°S and 51°S: evidence for geochemical enrichment. *Geochimica et Cosmochimica Acta* **51**, 541–555.

Le Roex, A.P., Späth, A. & Zartman, R.E. 2001. Lithospheric thickness beneath the southern Kenya rift: implications from basalt geochemistry. *Contributions to Mineralogy and Petrology* **142**, 89–106.

Le Roux, P.J., Le Roux, A.P. & Schilling, J.-G. 2002a. Crystallization process beneath the southern Mid-Atlantic Ridge (40–55°S), evidence for high pressure initiation of crystallization. *Contributions to Mineralogy and Petrology* **142**, 582–602.

Le Roux, P.J., Le Roux, A.P., Schilling, J.-G., Shimizu, N., Perkins, W.W. & Pearce, N.J.G. 2002b. Mantle heterogeneity beneath the southern Mid-Atlantic Ridge: trace element evidence for contamination of ambient asthenospheric mantle. *Earth and Planetary Science Letters* **203**, 479–498.

Leat, P.T., Thompson, R.N., Dickin, A.P., Morrison, M.A. & Hendry, G.L. 1989. Quaternary volcanism in northwestern Colorado: implications for the roles of asthenosphere and lithosphere in the genesis of continental basalts. *Journal of Volcanology and Geothermal Research* **37**, 291–310.

Lee, D.-C., Halliday, A.N., Fitton, J.G. & Poli, G. 1994. Isotopic variations with distance and time in the volcanic islands of the Cameroon line: evidence for a mantle plume origin. *Earth and Planetary Science Letters* **123**, 119–138.

Lindsay, J.M., Trumbull, R.B. & Siebel, W. 2005. Geochemistry and petrogenesis of late Pleistocene to Recent volcanism in Southern Dominica, Lesser Antilles. *Journal of Volcanology and Geothermal Research* **148**, 253–394.

Liotard, J.M., Barsczus, H.G., Dupuy, C. & Dostal, J. 1986. Geochemistry and origin of basaltic lavas from Marquesas Archipelago, French Polynesia. *Contributions to Mineralogy and Petrology* **92**, 260–268.

Lipman, P.W., Rhodes, R.M. & Dalrymple, G.B. 1990. The Ninole Basalt – implications for the structural evolution of Mauna Loa volcano, Hawaii. *Bulletin of Volcanology* **53**, 1–19.

Liu, C.-Q., Masuda, A. & Xie, G.-H. 1992. Isotope and trace-element geochemistry of alkali basalts and associated megacrysts from the Huangyishan volcano, Kuandian, Liaoning, NE China. *Chemical Geology* **97**, 219–231.

Liu, C.-Q., Masuda, A. & Xie, G.-H. 1994. Major- and trace-element compositions of Cenozoic basalts in eastern China: petrogenesis and mantle source. *Chemical Geology* **114**, 19–42.

Lloyd, F.E., Huntingdon, A.T., Davies, G.R. & Nixon, P.H. 1991. Phanerozoic volcanism of southern Uganda: a case for regional K and LILE enrichment of the lithosphere beneath a domed and rifted continental plate. *In*: Kampunzu, A.B. & Lubala, R.T. (eds), *Magmatism in Extensional Structural Settings*. Springer Verlag, Berlin, Germany, 23–72.

Lonsdale, P., Blum, N. & Puchelt, H. 1992. The RRR triple junction at the southern end of the Pacific-Cocos East Pacific Rise. *Earth and Planetary Science Letters* **109**, 73–85.

Luhr, J.F. & Haldar, D. 2006. Barren island volcano (NE Indian ocean): island-arc high-alumina basalts produced by troctolite contamination. *Journal of Volcanology and Geothermal Research* **149**, 177–212.

Luhr, J.F., Aranda-Gómez, J.J. & Housh, T.B. 1995. San Quintín volcanic field, Baja California Norte, México: geology, petrology, and geochemistry. *Journal of Geophysical Research* **100**, 10353–10380.

Lum, C.C.L., Leeman, W.P., Foland, K.A., Kargel, J.A. & Fitton, J.G. 1989. Isotopic variations in continental basaltic lavas as indicators of mantle heterogeneity: examples from the western U.S. Cordillera. *Journal of Geophysical Research* **94**, 7871–7884.

Maaløe, S., James, D., Smedley, P., Petersen, S. & Germann, L.B. 1992. The Koloa volcanic suite of Kauai, Hawaii. *Journal of Petrology* **33**, 761–784.

MacDonald, R., Davies, G.R., Upton, B.G.J., Denkley, P.N., Smith, M. & Leat, P.T. 1995. Petrogenesis of Silali volcano, Gregory rift, Kenya. *Journal of the Geological Society, London* **152**, 703–720.

MacDonald, R., Rogers, N.W., Fitton, J.G., Black, S. & Smith, M. 2001. Plume-lithosphere interactions in the generation of the basalts of the Kenya rift, East Africa. *Journal of Petrology* **42**, 877–900.

Madhavaraju, J. & Lee, Y.I. 2009. Geochemistry of the Dalmiapuram Formation of the Uttatur Group (Early Cretaceous), Cauvery Basin, Southeastern India: implications on Provenance and Paleo-redox conditions. *Revista Mexicana de Ciencias Geológicas* **26**, 516–529.

Mahoney, J., Le Roex, A.P., Peng, Z., Fisher, R.L. & Natland, J.H. 1992. Southwestern limits of Indian Ocean ridge mantle and the origin of low $^{206}Pb/^{204}Pb$ Mid-Ocean Ridge Basalt: isotope systematics of the central southwestern Indian Ridge (17°–50°E). *Journal of Geophysical Research* **97**, 19771–19790.

Maldonado, F., Budahn, J.R., Peters, L. & Unruh, D.M. 2006. Geology, geochronology, and geochemistry of basaltic flows of the Cat Hills, Cat Mesa, Wind Mesa, Cerro Verde, and Mesita Negra central New Mexico. *Canadian Journal of Earth Sciences* **43**, 1251–1268.

McMillan, N.J., Dickin, A.P. & Haag, D. 2000. Evolution of magma source regions in the Rio Grande rift, southern New Mexico. *Geological Society of America Bulletin* **112**, 1582–1593.

Meschede, M. 1986. A method of discriminating between different types of mid-ocean ridge basalts and continental tholeiites with the Nb-Zr-Y diagram. *Chemical Geology* **56**, 207–218.

Middlemost, E.A.K. 1989. Iron oxidation ratios, norms and the classification of volcanic rocks. *Chemical Geology* **77**, 19–26.

Monzier, M., Robin, C., Eissen, J.-P. & Cotten, J. 1997. Geochemistry vs. seismo-tectonics along the volcanic New Hebrides Central Chain (Southwest Pacific). *Journal of Volcanology and Geothermal Research* **78**, 1–29.

Moriguti, T., Shibata, T. & Nakamura, E. 2004. Lithium, boron and lead isotope and trace element systematics of Quaternary basaltic volcanic rocks in northeastern Japan: mineralogical controls on slab-derived fluid composition. *Chemical Geology* **212**, 81–100.

Moyer, T.C. & Esperança, S. 1989. Geochemical and isotopic variations in a bimodal magma system: the Kaiser Spring volcanic field, Arizona. *Journal of Geophysical Research* **94**, 7841–8759.

Mullen, E.D. 1983. $MnO/TiO_2/P_2O_5$: a minor element discrimination for basaltic rocks of oceanic environments and its implications for petrogenesis. *Earth and Planetary Science Letters* **62**, 53–62.

Myers, J.D., Marsh, B.D. & Sinha, A.K. 1985. Strontium isotopic and selected trace element variations between two Aleutian volcanic centers (Adak and Atka): implications for the development of arc volcanic plumbing systems. *Contributions to Mineralogy and Petrology* **91**, 221–234.

Myers, J.D., Marsh, B.D., Frost, C.D. & Linton, J.A. 2002. Petrologic constraints on the spatial distribution of crustal magma chambers, Atka volcanic center, central Aleutian arc. *Contributions to Mineralogy and Petrology* **143**, 567–586.

Nagarajan, R., Sial, A.N., Armstrong-Altrin, J.S., Madhavaraju, J. & Nagendra, R. 2008. Carbon and oxygen isotope geochemistry of Neoproterozoic limestones of the Shahabad Formation, Bhima basin, Karnataka, southern India. *Revista Mexicana de Ciencias Geológicas* **25**, 225–235.

Nakada, S., Matsushima, T., Yoshimoto, M., Sugimoto, T., Kato, T., Watanabe, T., Chong, R. & Camacho, J.T. 2005. Geological aspects of the 2003–2004 eruptions of Anathan volcano, northern Mariana Islands. *Journal of Volcanology and Geothermal Research* **146**, 226–240.

Nakagawa, M., Ishizuka, Y., Kudo, T., Yoshimoto, M., Hirose, W., Ishizaki, Y., Gouchi, N., Katsui, Y., Solovyow, A.W., Steinberg, G.S. & Abdurakhmanov, A.I. 2002. Tyatya volcano, southwestern Kuril arc: recent eruptive activity inferred from widespread tephra. *Island Arc* **11**, 236–254.

Nardi, L.V.S., Pla-Cid, J., Bitencourt, M.D. & Stabel, L.Z. 2008. Geochemistry and petrogenesis of post-collisional ultrapotassic syenites and granites from southernmost Brazil: the Piquiri Syenite Massif. *Anais da Academia Brasileira de Ciencias* **80**, 353–371.

Nye, C.J. & Reid, M.R. 1986. Geochemistry of primary and least fractionated lavas from Okmok volcano, central Aleutians: implications for arc magma genesis. *Journal of Geophysical Research* **91**, 10271–10287.

Obeidat, M.M., Ahmad, F.Y., Hamouri, N.A.A., Massadeh, A.M. & Athamneh, F.S. 2008. Assessment of Nitrate Contamination of Karst Springs, Bani Kanana, Northern Jordan. *Revista Mexicana de Ciencias Geológicas* **25**, 426–437.

Ohara, Y., Fujioka, K., Ishizuka, O. & Ishii, T. 2002. Peridotites and volcanics from the Yap arc system: implications for tectonics of the southern Philippine Sea plate. *Chemical Geology* **189**, 35–53.

Önal, A., Boztuğ, D., Arslan, M., Spell, T.L. & Kurum, S. 2008. Petrology and ^{40}Ar-^{39}Ar Age of the bimodal Orduzu volcanics (Malatya) from the western end of the eastern Anatolian Neogene volcanism, Turkey. *Turkish Journal of Earth Sciences* **17**, 85–109.

Pal, T., Bandopadhyay, P.C., Mitra, S.K. & Raghav, S. 2007. The 2005 eruption of barren volcano: an explosive inner arc volcanism in Andaman Sea. *Journal of the Geological Society, India* **69**, 1195–1202.

Palabiyik, Y. & Serpen, U. 2008. Geochemical assessment of Simav geothermal field, Turkey. *Revista Mexicana de Ciencias Geológicas* **25**, 408–425.

Palacz, Z.A. & Saunders, A.D. 1986. Coupled trace element and isotope enrichment in the Cook-Austral-Samoa islands, southwest pacific. *Earth and Planetary Science Letters* **79**, 270–280.

Pallister, J.S., Truesdell, F.A., Brownfield, I.K., Siems, D.F., Budahn, J.R. & Sutley, S.F. 2005. The 2003 phreatomagmatic eruptions of Anathan volcano-textural and petrological features of deposits at an emergent island volcano. *Journal of Volcanology and Geothermal Research* **146**, 208–225.

Pandarinath, K. 2009. Clay minerals in SW Indian continental shelf sediments cores as indicators of provenance and paleomonsoonal conditions: a statistical approach. *International Geology Review* **51**, 145–165.

Panter, K.S., Hart, S.R., Kyle, P., Blusztanjn, J. & Witch, T. 2000. Geochemistry of late Cenozoic basalts from the Crary mountains: characterization of mantle sources in Marie Byrd land, Antarctica. *Chemical Geology* **165**, 215–241.

Park, S.-H., Lee, S.-M. & Arculus, R.J. 2006. Geochemistry from the Ayu Trough, equatorial western Pacific. *Earth and Planetary Science Letters* **248**, 700–714.

Parlak, O. 2000. Geochemistry and significance of mafic dyke swarms in the Pozantı-Karsantı ophiolite (southern Turkey). *Turkish Journal of Earth Sciences* **9**, 29–38.

Parlak, O., Kop, A., Ünlügenç, U.C. & Demirkol, C. 1998. Geochronology and geochemistry of basaltic rocks in the Karasu graben around Kırıkhan (Hatay), S. Turkey. *Turkish Journal of Earth Sciences* **7**, 53–61.

Paslick, C., Halliday, A., James, D. & Dawson, J.B. 1995. Enrichment of the continental lithosphere by OIB melts: isotopic evidence from the volcanic province of northern Tanzania. *Earth and Planetary Science Letters* **130**, 109–126.

Pearce, J.A. 1976. Statistical analysis of major element patterns in basalts. *Journal of Petrology* **17**, 15–43.

Pearce, J.A. 1982. Trace element characteristics of lavas from destructive plate boundaries. *In*: Thorpe, R.S. (ed), *Andesites*. John Wiley & Sons, Chichester, 525–548.

Pearce, J.A. 1983. Role of the sub-continental lithosphere in magma genesis at active continental margins. *In*: Hawkesworth, C.J. & Norry, M.J. (eds), *Continental Basalts and Mantle Xenoliths*. Shiva Publishing Company, Cheshire, U.K., 230–249.

Pearce, J.A. 2008. Geochemical fingerprinting of oceanic basalts with applications to ophiolite classification and the search for Archean oceanic crust. *Lithos* **100**, 14–48.

Pearce, J.A. & Cann, J.R. 1971. Ophiolite origin investigated by discriminant analysis using Ti, Zr and Y. *Earth and Planetary Science Letters* **12**, 339–349.

Pearce, J.A. & Cann, J.R. 1973. Tectonic setting of basic volcanic rocks determined using trace element analyses. *Earth and Planetary Science Letters* **19**, 290–300.

Pearce, J.A. & Gale, G.H. 1977. Identification of ore-deposition environment from trace-element geochemistry of associated igneous host rocks. *In: Volcanic Processes in Ore Genesis*. Geological Society, London, Special Publications **7**, 14–24.

Pearce, T.H., Gorman, B.E. & Birkett, T.C. 1977. The relationship between major element chemistry and tectonic environment of basic and intermediate volcanic rocks. *Earth and Planetary Science Letters* **36**, 121–132.

Pearce, J.A., Harris, N.B.W. & Tindle, A.G. 1984. Trace element discrimination diagrams for the tectonic interpretation of granitic rocks. *Journal of Petrology* **25**, 956–983.

Pearce, J.A. & Norry, M.J. 1979. Petrogenetic implications of Ti, Zr, Y, and Nb variations in volcanic rocks. *Contributions to Mineralogy and Petrology* **69**, 33–47.

Peate, D.W., Pearce, J.A., Hawkesworth, C.J., Colley, H., Edwards, C.M.H. & Hirose, K. 1997. Geochemical variations in Vanuatu arc lavas: the role of subducted material and a variable mantle wedge composition. *Journal of Petrology* **38**, 1331–1358.

Peccerillo, A., Barberio, M.R., Yirgu, G., Ayalew, D., Barbieri, M. & Wu, T.W. 2003. Relationships between mafic and peralkaline silicic magmatism in continental rift settings: a petrological, geochemical and isotopic study of the Gedemsa volcano, central Ethiopian rift. *Journal of Petrology* **44**, 2003–2032.

Peng, T.P., Wang, Y.J., Zhao, G.C., Fan, W.M., Peng, B.X. 2008. Arc-like volcanic rocks from the southern Lancangjiang zone, SW China: geochronological and geochemical constraints on their petrogenesis and tectonic implications. *Lithos* **102**, 358–373.

Peng, Z.C., Zartman, R.E., Futa, K. & Chen, D.G. 1986. Pb-, Sr- and Nd-isotopic systematics and chemical characteristics of Cenozoic basalts, eastern China. *Chemical Geology* **59**, 3–33.

Perry, F.V., Baldridge, W.S., Depaolo, D.J. & Shafiqullah, M. 1990. Evolution of a magmatic system during continental extension: the mount Taylor volcanic field, New Mexico. *Journal of Geophysical Research* **95**, 19327–19348.

Pilet, S., Hernandez, J., Sylvester, P. & Poujol, M. 2005. The metasomatic alternative for ocean-island basalt chemical heterogeneity. *Earth and Planetary Science Letters* **236**, 148–166.

Praegel, N.-O. & Holm, P.M. 2006. Lithosphere contributions to high-MgO basanites from the Cumbre Vieja volcano, La Palma, Canary Islands and evidence for temporal variation in plume influence. *Journal of Volcanology and Geothermal Research* **149**, 213–239.

Price, R.C., Gray, C.M. & Frey, F.A. 1997. Strontium isotopic and trace element heterogeneity in the plains basalts of the Newer Volcanic Province, Victoria, Australia. *Geochimica et Cosmochimica Acta* **61**, 171–192.

Price, R.C., Kennedy, A.K., Riggs-Sneeringer, M. & Frey, F.A. 1986. Geochemistry of basalts from the Indian Ocean triple junction: implications for the generation and evolution of Indian Ocean ridge basalts. *Earth and Planetary Science Letters* **78**, 379–396.

Rahmani, F., Noghreyan, M. & Khalili, M. 2007. Geochemistry of sheeted dikes in the Nain ophiolite (central Iran). *Ofioliti* **32**, 119–129.

Rajesh, H.M. 2007. The petrogenetic characterization of intermediate and silicic charnockites in high-grade terrains: a case study from southern India. *Contributions to Mineralogy and Petrology* **154**, 591–606.

Rao, D.R. & Rai, H. 2007. Permian komatiites and associated basalts from the marine sediments of Chhongtash Formation, southeast Karakoram, Ladakh, India. *Mineralogy and Petrology* **91**, 171–189.

Raos, A.M. & Crawford, A.J. 2004. Basalts from the Afate Island group, central section of the Vanuatu arc, SW Pacific: geochemistry and petrogenesis. *Journal of Volcanology and Geothermal Research* **134**, 35–64.

Raveggi, M., Giles, D., Foden, J. & Raetz, M. 2007. High Fe-Ti mafic magmatism and tectonic setting of the Paleoproterozoic Broken Hill Block, NSW, Australia. *Precambrian Research* **156**, 55–84.

Ray, D., Iyer, S.D., Banereje, R., Misra, S. & Widdowson, M. 2007. A petrogenetic model of basalts from the northern Central Indian Ridge: 3–11°S. *Acta Geologica Sinica* **81**, 99–112.

Raza, M., Khan, M.S., Azam, M.S. 2007. Plate-plume-accretion tectonics in Proterozoic terrain of northeastern Rajasthan, India: evidence from mafic volcanic rocks of north Delhi fold belt. *Island Arc* **16**, 536–552.

Ren, Z.-Y., Takahashi, E., Orihashi, Y. & Johnson, K.T.M. 2004. Petrogenesis of tholeiitic lavas from the submarine Hana ridge, Haleakala volcano, Hawaii. *Journal of Petrology* **45**, 2067–2099.

Richardson-Bunbury, J.M. 1996. The Kula volcanic field, western Turkey: the development of a Holocene alkali basalt province and the adjacent normal-faulting graben. *Geological Magazine* **133**, 275–283.

Rickwood, P.C. 1989. Boundary lines within petrologic diagrams which use oxides of major and minor elements. *Lithos* **22**, 247–263.

Rodríguez-Ríos, R. & Torres-Aguilera, J.M. 2009. Evolución petrológica y geoquímica de un vulcanismo bimodal oligocénico en el Campo Volcánico de San Luis Potosí, México [Petrological and geochemical evolution of Oligocene bimodal volcanism in the San Luis Potosí Volcanic Field, Mexico]. *Revista Mexicana de Ciencias Geológicas* **26**, 658–673.

Rollinson, H.R. 1993. *Using Geochemical Data: Evaluation, Presentation, Interpretation.* Longman Scientific Technical, Essex.

Romick, J.D., Perfit, M.R., Swanson, S.E. & Shuster, R.D. 1990. Magmatism in the eastern Aleutian arc: temporal characteristic of igneous activity on Akutan Island. *Contributions to Mineralogy and Petrology* **104**, 700–721.

Roser, B.P. & Korsch, R.J. 1986. Determination of tectonic setting of sandstone-mudstone suites using SiO_2 content and K_2O/Na_2O ratio. *Journal of Geology* **94**, 635–650.

Sakuyama, M. & Nesbitt, R.W. 1986. Geochemistry of the Quaternary volcanic rocks of the Northeast Japan arc. *Journal of Volcanology and Geothermal Research* **29**, 413–450.

Sano, T., Hasenaka, T., Shimaoka, A., Yonesawa, C. & Fukuoka, T. 2001. Boron contents of Japan trench sediments and Iwate basaltic lavas, northeastern Japan arc: estimation of sediment-derived fluid contribution in mantle wedge. *Earth and Planetary Science Letters* **186**, 187–198.

Schilling, J.-G., Kingsley, R.H. & Devine, J.D. 1982. Galapagos hot spot-spreading center system. 1. Spatial petrological and geochemical variations (83°W–101°W). *Journal of Geophysical Research* **87**, 5593–5610.

Schilling, J.-G., Zajac, M., Evans, R., Johnston, T., White, W., Devine, J.D. & Kingsley, R. 1983. Petrologic and geochemical variations along the Mid-Atlantic Ridge from 29°N to 73°N. *American Journal of Science* **283**, 510–586.

Schmitz, M.D. & Smith, I.E.M. 2004. The petrology of the Rotoiti eruption sequence, Taupo Volcanic Zone: an example of fractionation and mixing in a rhyolitic system. *Journal of Petrology* **45**, 2045–2066.

Schwarz, S., Klügel, A., Van Den Bogaard, P. & Geldmacher, J. 2005. Internal structure and evolution of a volcanic rift system in the eastern North Atlantic: the Desertas rift zone, Madeira archipelago. *Journal of Volcanology and Geothermal Research* **141**, 123–155.

Şen, C. 2007. Jurassic volcanism in the eastern Pontides: Is it rift related or subduction related? *Turkish Journal of Earth Sciences* **16**, 523–539.

Şen, C., Arslan, M. & Van, A. 1998. Geochemical and petrological characteristics of the eastern Pontide Eocene (?) alkaline volcanic province, NE Turkey. *Turkish Journal of Earth Sciences* **7**, 231–239.

Shahabpour, J. 2007. Island-arc affinity of the central Iranian volcanic belt. *Journal of Asian Earth Sciences* **30**, 652–665.

Shekhawat, L.S., Pandit, M.K. & Joshi, D.W. 2007. Geology and geochemistry of palaeoproterozoic low-grade metabasic volcanic rocks from Salumber area, Aravalli Supergroup, NW India. *Journal of Earth System Science* **116**, 511–524.

Shervais, J.W. 1982. Ti-V plots and the petrogenesis of modern and ophiolitic lavas. *Earth and Planetary Science Letters* **59**, 101–118.

Sheth, H.C. 2008. Do major oxide tectonic discrimination diagrams work? Evaluating new log-ratio and discriminant-analysis-based diagrams with Indian Ocean mafic volcanics and Asian ophiolites. *Terra Nova* **20**, 229–236.

Sheth, H.C., Torres-Alvarado, I.S. & Verma, S.P. 2002. What is the 'calc-alkaline rock series'? *International Geology Review* **44**, 686–701.

Shimizu, N. & Arculus, R.J. 1975. Rare earth element concentrations in a suite of basanitoids and alkali olivine basalts from Grenada, Lesser Antilles. *Contributions to Mineralogy and Petrology* **50**, 231–240.

Shinjo, R. 1998. Petrochemistry and tectonic significance of the emerged late Cenozoic basalts behind the Okinawa Trough Ryukyu arc system. *Journal of Volcanology and Geothermal Research* **80**, 39–53.

Shinjo, R. 1999. Geochemistry of high Mg andesites and the tectonic evolution of the Okinawa Trough-Ryukyu arc system. *Chemical Geology* **157**, 69–88.

Shinjo, R., Woodhead, J.D. & Hergt, J.M. 2000. Geochemical variation within the northern Ryukyu: magma source compositions and geodynamic implications. *Contributions to Mineralogy and Petrology* **140**, 263–282.

Shukuno, H., Tamura, Y., Tani, K., Chang, Q., Suzuki, T. & Fiske, R.S. 2006. Origin of silicic magmas and the compositional gap at Sumisu submarine caldera, Izu-Bonin arc, Japan. *Journal of Volcanology and Geothermal Research* **156**, 187–216.

Shuto, K., Hirahara, Y., Ishimoto, H., Aoki, A., Jinbo, A. & Goto, Y. 2004. Sr and Nd isotopic compositions of the magma source beneath north Hokkaido, Japan: comparison with the back-arc side in the NE Japan arc. *Journal of Volcanology and Geothermal Research* **134**, 57–75.

Sims, K.W.W., Blichert-Toft, J., Fornari, D.J., Perfit, M.R., Goldstein, S.J., Johnson, P., Depaolo, D.J., Hart, S.R., Murrell, M.T., Michael, P.J., Layne, G.D. & Ball, L.A. 2003. Aberrant youth: chemical and isotopic constraints on the origin of off-axis lavas from the East Pacific Rise, 9°–10°N. *Geochemistry Geophysics Geosystems* **4**, 10.1029/2002GC000443.

Singer, B.S. & Kudo, A.M. 1986. Assimilation-fractional crystallization of Polvadera Group rocks in the northwestern Jemez volcanic field, New Mexico. *Contributions to Mineralogy and Petrology* **94**, 374–386.

Singer, B.S., Myers, J.D. & Frost, C.D. 1992a. Mid–Pleistocene lavas from the Seguam volcanic center, central Aleutian arc: closed-system fractional crystallization of a basalt to rhyodacite eruptive suite. *Contributions to Mineralogy and Petrology* **110**, 87–112.

Singer, B.S., Myers, J.D. & Frost, C.D. 1992b. Mid–Pleistocene basalt from the Seguam volcanic center, central Aleutian arc, Alaska: local lithospheric structures and source variability in the Aleutian arc. *Journal of Geophysical Research* **97**, 4561–4578.

Slater, L., Jull, M., McKenzie, D. & Gronvöld, K. 1998. Deglaciation effects on mantle melting under Iceland: results from the northern volcanic zone. *Earth and Planetary Science Letters* **164**, 151–164.

Smellie, J.L. 1983. A geochemical overview of subduction-related igneous activity in the South Shetland islands, Lesser Antarctica. *In*: Oliver, R.L., James, P.R. & Jago, J.B. (eds), *Antarctic Earth Science*. Australian Academy of Sciences and Cambridge University Press, 352–356.

Smith, E.I., Sánchez, A., Walker, J.D. & Wang, K. 1999. Geochemistry of mafic magmas in the Hurricane Volcanic Field, Utah: implications of small- and large-scale chemical variability of the lithospheric mantle. *Journal of Geology* **107**, 433–448.

Smith, I.E.M., Stewart, R.B. & Price, R.C. 2003. The petrology of a large intra-oceanic silicic eruption: the Sandy Bay tephra, Kermadec arc, southwest Pacific. *Journal of Volcanology and Geothermal Research* **124**, 173–194.

Smith, T.E., Thirlwall, M.F. & MacPherson, C. 1996. Trace element and isotope geochemistry of the volcanic rocks of Bequia, Grenadine Islands, Lesser Antilles Arc: a study of subduction enrichment and intra-crustal contamination. *Journal of Petrology* **37**, 117–143.

Srivastava, R.K. & Rao, N.V.C. 2007. Petrology, geochemistry and tectonic significance of Palaeoproterozoic alkaline lamprophyres from the Jungel Valley, Mahakoshal supracrustal belt, Central India. *Mineralogy and Petrology* **89**, 189–215.

Srivastava, R.K. & Sinha, A.K. 2007. Nd and Sr isotope systematics and geochemistry of plume related early Cretaceous alkaline-mafic-ultramafic igneous complex from Jasra, Shillong Plateau, northeastern India. *In*: Foulger, G.R. & Jurdy, D.M. (eds), *The Origins of Melting Anomalies: Plates, Plumes, and Planetary Processes*. Geological Society of America Special Paper **430**, 815–830.

Stephenson, D. & Marshall, T.R. 1984. The petrology and mineralogy of Mt. Popa volcano and the nature of the late-Cenozoic Burma volcanic arc. *Journal of the Geological Society, London* **141**, 747–762.

Stolz, A.J., Varne, R., Davies, G.R., Wheller, G.E. & Fodon, J.D. 1990. Magma source components in an arc-continent collision zone: the Flores-Lembata sector, Sunda arc, Indonesia. *Contributions to Mineralogy and Petrology* **105**, 585–601.

Stolz, A.J., Varne, R., Wheller, G.E., Foden, J.D. & Abbott, M.J. 1988. The geochemistry and petrogenesis of K-rich alkaline volcanics from the Batu Tara volcano, eastern Sunda arc. *Contributions to Mineralogy and Petrology* **98**, 374–389.

Storey, M., Rogers, G., Saunders, A.D. & Terrell, D.J. 1989. San Quintín volcanic field, Baja California, Mexico: 'within plate' magmatism following ridge subduction. *Terra Nova* **1**, 195–202.

Storey, M., Saunders, A.D., Tarney, J., Leat, P., Thirlwall, M.F., Thompson, R.N., Menzies, M.A. & Marriner, G.F. 1988. Geochemical evidence for plume-mantle interactions beneath Kerguelen and Heard islands, Indian ocean. *Nature* **336**, 371–374.

Streck, M.J. 2002. Partial melting to produce high-silica rhyolites of a young bimodal suite: compositional constraints among rhyolites, basalts, and metamorphic xenoliths from the Harney Basin, Oregon. *International Journal of Earth Sciences* **91**, 583–593.

Streck, M.J. & Grunder, A.L. 1999. Enrichment of basalt and mixing of dacite in the rootzone of a large rhyolite chamber: inclusions and pumices from the Rattelsnake tuff, Oregon. *Contributions to Mineralogy and Petrology* **136**, 193–212.

Tamura, Y. 1994. Genesis of island arc magmas by mantle derived bimodal magmatism: evidence from the Shiraham group, Japan. *Journal of Petrology* **35**, 619–645.

Tamura, Y., Yuhara, M., Ishii, T., Irino, N. & Shukuno, H. 2003. Andesites and dacites from Daisen volcano, Japan: partial-to-total remelting of an andesite magma body. *Journal of Petrology* **44**, 2243–2260.

Tankut, A., Güleç, N., Wilson, M., Toprak, V., Savaşcin, Y. & Akiman, O. 1998. Alkali basalts from the Galatia volcanic complex, NW Central Anatolia, Turkey. *Turkish Journal of Earth Sciences* **7**, 269–274.

Tatar, O., Yurtmen, S., Temİz, H., Gürsoy, H., Koçbulut, F., Mescİ, B.L. & Guezou, J.C. 2007. Intracontinental Quaternary volcanism in the Niksar pull-apart basin, North Anatolian Fault Zone, Turkey. *Turkish Journal of Earth Sciences* **16**, 417–440.

Tatsumi, Y., Murasaki, M. & Nohda, S. 1992. Across-arc variation of lava chemistry in the Izu-Bonin arc: identification of subduction components. *Journal of Volcanology and Geothermal Research* **49**, 179–190.

Tatsumi, Y., Murasaki, M., Arsadi, E.M. & Nohda, S. 1991. Geochemistry of Quaternary lavas from NE Sulawesi: transfer of subduction components into the mantle wedge. *Contributions to Mineralogy and Petrology* **107**, 137–149.

Taylor, R.N. & Nesbitt, R.W. 1998. Isotopic characteristics of subduction fluids in an intra-oceanic setting, Izu-Bonin Arc, Japan. *Earth and Planetary Science Letters* **164**, 79–98.

Thirlwall, M.F. & Graham, A.M. 1984. Evolution of high-Ca, high-Sr C-series basalts from Grenada, Lesser Antilles: the effects of intra-crustal contamination. *Journal of the Geological Society, London* **141**, 427–445.

Thirlwall, M.F., Graham, A.M., Arculus, R.J., Harmon, R.S. & MacPherson, C.G. 1997. Resolution of the effects of crustal assimilation, sediment subduction, and fluid transport in island arc magmas: Pb-Sr-Nd-O isotope geochemistry of Grenada, Lesser Antilles. *Geochimica et Cosmochimica Acta* **60**, 4785–4810.

Togashi, S., Tanaka, T., Yoshida, T., Ishikawa, K.-I., Fujinawa, A. & Kurasawa, H. 1992. Trace elements and Nd-Sr isotopes of island arc tholeiites from frontal arc of northeast Japan. *Geochemical Journal* **26**, 261–277.

Tokcaer, M., Agostini, S. & Savaşcin, M.Y. 2005. Geotectonic setting and origin of the youngest Kula volcanics (western Anatolia), with a new emplacement model. *Turkish Journal of Earth Sciences* **14**, 145–166.

Torres-Alvarado, I.S., Smith, A.D. & Castillo-Román, J. 2010. Sr, Nd, and Pb isotopic and geochemical constraints for the origin of magmas in Popocatépetl volcano (Central Mexico) and their relationship with the adjacent volcanic fields. *International Geology Review* (in press).

Trua, T., Deniel, C. & Mazzuoli, R. 1999. Crustal control in the genesis of Plio–Quaternary bimodal magmatism of the Main Ethiopian Rift (MER): geochemical and isotopic (Sr, Nd, Pb) evidence. *Chemical Geology* **155**, 201–231.

Turner, S. & Foden, J. 2001. U, Th and Ra disequilibria, Sr, Nd and Pb isotope and trace element variations in Sunda arc lavas: predominance of a subducted sediment component. *Contributions to Mineralogy and Petrology* **142**, 43–57.

Turner, S., Foden, J., George, R., Evans, P., Varne, R., Elburg, M. & Jenner, G. 2003. Rates and processes of potassic magma evolution beneath Sangeang Api volcano, East Sunda arc, Indonesia. *Journal of Petrology* **44**, 491–515.

Ujike, O. & Stix, J. 2000. Geochemistry and origins of Ueno and Ontake basaltic to andesitic rocks (<3 Ma) produced by distinct contributions of subduction components, central Japan. *Journal of Volcanology and Geothermal Research* **95**, 49–64.

Van Bergen, M.J., Vroon, P.Z., Varekamp, J.C. & Poorter, R.P.E. 1992. The origin of the potassic rock suite from Batu Tara volano (East Sunda Arc, Indonesia). *Lithos* **28**, 261–282.

Varol, E., Temel, A. & Gourgaud, A. 2008. Textural and compositional evidence for magma mixing in the evolution of the Çamlıdere volcanic rocks (Galatean volcanic province), central Anatolia, Turkey. *Turkish Journal of Earth Sciences* **17**, 709–727.

Vasconcelos-F., M., Verma, S.P. & Rodríguez-G., J.F. 1998. Discriminación tectónica: nuevo diagrama Nb-Ba para arcos continentales, arcos insulares, 'rifts' e islas oceánicas en rocas máficas [Tectonic discrimination: new Nb-Ba diagram for mafic magmas from continental arcs, island arcs, rifts and ocean-islands]. *Boletín de la Sociedad Española de Mineralogía* **21**, 129–146.

Vasconcelos-F., M., Verma, S.P. & Vargas-B., R.C. 2001. Diagrama Ti-V: una nueva propuesta de discriminación para magmas básicos en cinco ambientes tectónicos [Ti-V diagram: a new proposal for discrimination of basic magmas from five tectonic settings]. *Revista Mexicana de Ciencias Geológicas* **18**, 162–174.

Vattuone, M.E., Leal, P.R., Crosta, S., Berbeglia, Y., Gallegos, E. & Martínez-Dopico, C. 2008. Paragénesis de zeolitas alcalinas en un afloramiento de basaltos olivínicos amigdaloides de Junín de Los Andes, Neuquén, Patagonia, Argentina. *Revista Mexicana de Ciencias Geológicas* **25**, 483–493.

Verma, S.P. 1996. Uso y abuso de los diagramas de discriminación (Use and abuse of discrimination diagrams). *Actas INAGEQ* **2**, 17–22.

Verma, S.P. 1997. Estado actual de los diagramas de clasificación magmática y de discriminación tectónica [Present state of magmatic classification and tectonic discrimination diagrams]. *Actas INAGEQ* **3**, 49–78.

Verma, S.P. 2000. Geochemistry of the subducting Cocos plate and the origin of subduction-unrelated mafic volcanism at the volcanic front of the central Mexican Volcanic Belt. *In*: Delgado-Granados, H., Aguirre-Díaz, G. & Stock, J.M. (eds), *Cenozoic Tectonics and volcanism of Mexico*. Geological Society of America Special Paper **334**, 195–222.

VERMA, S.P. 2002. Absence of Cocos plate subduction-related basic volcanism in southern Mexico: a unique case on Earth? *Geology* **30**, 1095–1098.

VERMA, S.P. 2005. *Estadística básica para el manejo de datos experimentales: aplicación en la Geoquímica (Geoquimiometría) [Basic Statistics for the Handling of Experimental Data: Application in Geochemistry (Geochemometrics)]*. Universidad Nacional Autónoma de México, México City.

VERMA, S.P. 2006. Extension related origin of magmas from a garnet-bearing source in the Los Tuxtlas volcanic field, Mexico. *International Journal of Earth Sciences* **95**, 871–901.

VERMA, S.P. 2008. New discriminant diagrams based on log-ratio transformation of data and discrimination of four tectonic settings (island arc, continental rift, ocean-island, and Mid-Ocean ridge). *Abstracts, 61th Geological Congress of Turkey*, Ankara, p. 11.

VERMA, S.P. 2009a. Continental rift setting for the central part of the Mexican Volcanic Belt: a statistical approach. *Open Geology Journal* **3**, 8–29.

VERMA, S.P. 2009b. Evaluation of polynomial regression models for the Student t and Fisher F critical values, the best interpolation equations from double and triple natural logarithm transformation of degrees of freedom up to 1000, and their applications to quality control in science and engineering. *Revista Mexicana de Ciencias Geológicas* **26**, 79–92.

VERMA, S.P., DÍAZ-GONZÁLEZ. L. & GONZÁLEZ-RAMÍREZ, R. 2009a. Relative efficiency of single-outlier discordancy tests for processing geochemical data on reference materials and application to instrumental calibrations by a weighted least-squares linear regression model. *Geostandards and Geoanalytical Research* **33**, 29–49.

VERMA, S.P., PANDARINATH, K., VELASCO-TAPIA, F. & RODRÍGUEZ-RÍOS, R. 2009b. Evaluation of the odd-even effect in limits of detection for electron microprobe analysis of natural minerals. *Analytica Chimica Acta* **638**, 126–132.

VERMA, S.P. & QUIROZ-RUIZ, A. 2006a. Critical values for six Dixon tests for outliers in normal samples up to sizes 100, and applications in science and engineering. *Revista Mexicana de Ciencias Geológicas* **23**, 133–161.

VERMA, S.P. & QUIROZ-RUIZ, A. 2006b. Critical values for 22 discordancy test variants for outliers in normal samples up to sizes 100, and applications in science and engineering. *Revista Mexicana de Ciencias Geológicas* **23**, 302–319.

VERMA, S.P. & QUIROZ-RUIZ, A. 2008. Critical values for 33 discordancy test variants for outliers in normal samples for very large sizes of 1,000 to 30,000 and evaluation of different regression models for the interpolation and extrapolation of critical values. *Revista Mexicana de Ciencias Geológicas* **25**, 369–381.

VERMA, S.P. & QUIROZ-RUIZ, A. & DÍAZ-GONZÁLEZ. L. 2008. Critical values for 33 discordancy test variants for outliers in normal samples up to sizes 1000, and applications in quality control in Earth Sciences. *Revista Mexicana de Ciencias Geológicas* **25**, 82–96.

VERMA, S.P. & SCHILLING, J.-G. 1982. Galapagos hot spot-spreading center system. 2. $^{87}Sr/^{86}Sr$ and large lithophile element variations (85°W–101°W). *Journal of Geophysical Research* **87**, 10838–10856.

VERMA, S.P., GUEVARA, M. & AGRAWAL, S. 2006. Discriminating four tectonic settings: five new geochemical diagrams for basic and ultrabasic volcanic rocks based on log-ratio transformation of major-element data. *Journal of Earth System Science* **115**, 485–528.

VERMA, S.P., RODRÍGUEZ-RÍOS, R. & GONZÁLEZ-RAMÍREZ, R. 2010. Statistical evaluation of classification diagrams for altered igneous rocks. *Turkish Journal of Earth Sciences* **19**, 239–265.

VERMA, S.P., TORRES-ALVARADO, I.S. & SOTELO-RODRÍGUEZ, Z.T. 2002. SINCLAS: standard igneous norm and volcanic rock classification system. *Computers & Geosciences* **28**, 711–715.

VERMA, S.P., TORRES-ALVARADO, I.S. & VELASCO-TAPIA, F. 2003. A revised CIPW norm. *Schweizerische Mineralogische und Petrographische Mitteilungen* **83**, 197–216.

VERMEESCH, P. 2006. Tectonic discrimination of basalts with classification trees. *Geochimica et Cosmochimica Acta* **70**, 1839–1848.

VERMEESCH, P. 2007. Reply to 'Comment on 'Tectonic classification of basalts with classification trees' by Pieter Vermeesch (2006)' by AGRAWAL and VERMA. *Geochimica et Cosmochimica Acta* **71**, 3392–3394.

VERWOERD, W.J., ERLANK, A.J. & KABLE, E.J.D. 1976. Geology and geochemistry of Bouvet island. *Proceedings of the Symposium on 'Andean and Antarctic Volcanology Problems'. International Association of Volcanology and Chemistry of the Earth's Interior, Santiago, Chile*, 201–237.

WADE, J.A., PLANK, T., STERN, R.J., TOLLSTRUP, D.L., GILL, J.B., O'LEARY, J.C., EILER, J.M., MOORE, R.B., WOODHEAD, J.D., TRUSDELL, F., FISCHER, T.P. & HILTON, D.R. 2005. The May 2003 eruption of Anatahan volcano, Mariana islands: geochemical evolution of a silicic island-arc volcano. *Journal of Volcanology and Geothermal Research* **146**, 139–170.

WANG, P. & GLOVER III, L. 1992. A tectonics test of the most commonly used geochemical discriminant diagrams and patterns. *Earth-Science Reviews* **33**, 111–131.

WEIS, D., FREY, F.A., LEYRIT, H. & GAUTIER, I. 1993. Kerguelen archipelago revisited: geochemical and isotopic study of the southeast province lavas. *Earth and Planetary Science Letters* **118**, 101–119.

WEST, H.B., GARCIA, M.O., GERLACH, D.C. & ROMERO, J. 1992. Geochemistry of tholeiites from Lanai, Hawaii. *Contributions to Mineralogy and Petrology* **112**, 520–542.

WHELLER, G.E., VARNE, R., FODEN, J.D. & ABBOTT, M.J. 1987. Geochemistry of Quaternary volcanism in the Sunda-Banda arc, Indonesia, and three-component genesis of island-arc basaltic magmas. *Journal of Volcanology and Geothermal Research* **32**, 137–160.

White, W.M., McBirney, A.R. & Duncan, R.A. 1993. Petrology and geochemistry of the Galápagos Islands: portrait of a pathological mantle plume. *Journal of Geophysical Research* **98**, 19533–19563.

Whitford, D.J., Nicholls, I.A. & Taylor, S.R. 1979. Spatial variations in the geochemistry of Quaternary lavas across the Sunda arc in Java and Bali. *Contributions to Mineralogy and Petrology* **70**, 341–356.

Wiszniewska, J., Krzeminska, E. & Dorr, W. 2007. Evidence of arc-related Svecofennian magmatic activity in the southwestern margin of the East European Craton in Poland. *Gondwana Research* **12**, 268–278.

Wood, D.A. 1980. The application of a Th-Hf-Ta diagram to problems of tectonomagmatic classification and to establishing the nature of crustal contamination of basaltic lavas of the British Tertiary volcanic province. *Earth and Planetary Science Letters* **50**, 11–30.

Wood, D.A., Joron, J.-L. & Treuil, M. 1979. A re-appraisal of the use of trace elements to classify and discriminate between magma series erupted in different tectonic settings. *Earth and Planetary Science Letters* **45**, 326–336.

Woodhead, J.D. 1988. The origin of geochemical variations in Mariana lavas: a general model for petrogenesis in intra-oceanic island arcs. *Journal of Petrology* **29**, 805–830.

Woodhead, J.D. & Johnson, R.W. 1993. Isotopic and trace-element profiles across the New Britain island arc, Papua New Guinea. *Contributions to Mineralogy and Petrology* **113**, 479–491.

Wright, I.C., Worthington, T.J. & Gamble, J.A. 2006. New multibeam and geochemistry of the 30°–35° S sector, and overview, of southern Kermadec arc volcanism. *Journal of Volcanology and Geothermal Research* **149**, 263–296.

Xu, Y.G., Lan, J.B., Yang, Q.J., Huang, X.L. & Qiu, H.N. 2008. Eocene break-off of the Neo-Tethyan slab as inferred from intraplate-type mafic dykes in the Gaoligong orogenic belt, eastern Tibet. *Chemical Geology* **255**, 439–453.

Yang, S.F., Li, Z.L., Chen, H.L., Santosh, M., Dong, C.W. & Yu, X. 2007. Permian bimodal dyke of Tarim Basin, NW China: geochemical characteristics and tectonic implications. *Gondwana Research* **12**, 113–120.

Yilmaz, S. & Boztuğ, D. 1998. Petrogenesis of the Çiçekdağ igneous complex, N of Kırşehir, central Anatolia, Turkey. *Turkish Journal of Earth Sciences* **7**, 185–199.

Zellmer, G., Turner, S. & Hawkesworth, C. 2000. Timescales of destructive plate margin magmatism: new insights from Santorini, Aegean volcanic arc. *Earth and Planetary Science Letters* **174**, 265–281.

Zellmer, G.F., Hawkesworth, C.J., Sparks, R.S.J., Thomas, L.E., Harford, C.L., Brewer, T.S. & Loughlin, S.C. 2003. Geochemical evolution of the Soufrière Hills volcano, Montserrat, Lesser Antilles volcanic arc. *Journal of Petrology* **44**, 1349–1374.

Zhang, M., Suddaby, P., Thompson, R.N., Thirlwall, M.F. & Menzies, M.A. 1995. Potassic volcanic rocks in NE China: geochemical constraints on mantle source and magma genesis. *Journal of Petrology* **36**, 1275–1303.

Zhi, X., Song, Y., Frey, F.A., Feng, J. & Zhai, M. 1990. Geochemistry of Hannuoba basalts, eastern China: constraints on the origin of continental alkalic and tholeiitic basalt. *Chemical Geology* **88**, 1–33.

Zhuravlev, D.Z., Tsvetkov, A.A., Zhuravlev, A.Z., Gladkov, N.G. & Chernysheva, I.V. 1987. $^{143}Nd/^{144}Nd$ and $^{87}Sr/^{86}Sr$ ratios in recent magmatic rocks of the Kurile Island Arc. *Chemical Geology* **66**, 227–243.

Zou, H., Reid, M.R., Liu, Y., Yao, Y., Xu, X. & Fan, Q. 2003. Constraints on the origin of historic potassic basalts from northeast China by U-Th disequilibrium data. *Chemical Geology* **200**, 189–201.

Zou, H., Zindler, A., Xisheng, X. & Qi, Q. 2000. Major, trace element, and Nd, Sr and Pb isotope studies of Cenozoic basalts in SE China: mantle sources, regional variations and tectonic significance. *Chemical Geology* **171**, 33–47.